OPTICAL ABSORPTION AND PLASMA REFLECTION STUDIES IN III - V ALLOY SEMICONDUCTORS

by

MATHEW B. THOMAS

Submitted in partial fulfillment of
the requirements for the degree of
Doctor of Philosophy

Department of Physics,
Faculty of Pure and Applied Science,
The University of Ottawa,
Ottawa, Canada

1969

ProQuest LLC
789 East Eisenhower Parkway
P.O. Box 1346
Ann Arbor, MI 48106-1346

ACKNOWLEDGEMENTS

First of all, I like to thank most sincerely my supervisor Prof. J.C. Woolley for his invaluable guidance and for the financial support provided during the course of my research work.

I have benefited from discussion with other Professors and my colleagues in the department.

The optial systems used in this work were largely built in the Physics Department workshop. Specifically I wish to thank Mr. Derek Kingswell. I deeply appreciate the assistance provided by the National Research Council for making some optical components.

Lastly, I wish to thank Mrs Lise Dorey and Miss Diane Dubé for typing the thesis.

STATEMENT OF ORIGINALITY

So far as the author is aware the following parts of the work are original

1. The determination of accurate values of room temperature energy gap for $Ga_xIn_{(1-x)}As$ alloys over the complete composition range.

2. Preparation of homogeneous bulk samples of the alloy system $GaAs_xSb_{(1-x)}$ in the ranges $0 < x < 0.34$ and $0.85 < x < 1.0$ and the determination of room temperature energy gap values.

3. Plasma reflection measurements on $Ga_xIn_{(1-x)}Sb$, $Ga_xIn_{(1-x)}As$ and $In\,As_xSb_{(1-x)}$ alloys over the complete composition range.

4. The extension of the expressions of Spitzer and Fan (57S1) for the dielectric constant to the case of general degeneracy in a Kane type band taking into account the lattice contribution to thd dielectric constant.

5. Determination of effective mass values at the bottom of the (000) band for the alloy systems $Ga_xIn_{(1-x)}Sb$, $Ga_xIn_{(1-x)}As$ and $In\,As_xSb_{(1-x)}$. Simultanously results were also obtained from Faraday rotation and magnetothermoelectric power measurements by other workers in the same laboratory. The variation of the high frequency dielectric constant as a function of molecular composition has also been determined for all the three alloy systems.

ABSTRACT

Room temperature optical energy gap values for $Ga_xIn_{(1-x)}As$ and $GaAs_xSb_{(1-x)}$ alloys have been determined from infrared transmission measurements. For $Ga_xIn_{(1-x)}As$ alloys Burstein effect was observed and the necessary correction to the energy gap was made by finding the Fermi energy from thermoelectric power data. For both the alloy systems value of C the bowing parameter has been obtained. These values show good agreement with the theoretical values of Van Vechten and Bergstresser.

Room temperature infrared reflectivity measurements near the plasma edge and high field Hall effect measurements have been made on polycrystalline n-type samples of $Ga_xIn_{(1-x)}Sb$, $Ga_xIn_{(1-x)}As$ and $InAs_xSb_{(1-x)}$ alloys. The Spitzer and Fan expressions for dielectric constant (57S1) applicable for degenerate case have been extended to the case of general degeneracy in a Kane type band, the effects of lattice contributions to the dielectric constant being included. This analysis has been applied to the experimental data to give values of effective mass at the bottom of the (000) conduction band minimum of the three alloy systems. These effective mass values show very good agreement with the values obtained by Faraday rotation and magnetothermoelectric power measurements.

TABLE OF CONTENTS

Chapter I : Review of the Band Theory

1.1 Historical note on semiconductors 1
1.2 Energy band theory of solids 3
1.3 Band structure representations 6
1.4 Band structure of Ge and Si of the group IV 8
1.5 Band structure of III - V Compounds 10
  a) Method of Band Calculation 10
  b) Kane's band calculation 11
1.6 Concept of effective mass 17
  a) Band Curvature effective mass 17
  b) Cyclotron effective mass 18
  c) Density of states effective mass 19
  d) Conductivity effective mass 20
1.7 Temperature dependence of the effective mass 24
1.8 Kane band model 25
  a) Kane equation for the conduction band 25
  b) Effective mass band gap 27

Chapter II: Preparation and Properties of III - V semiconductor alloys

2.1 Introduction 29
2.2 Virtual crystal model 31
2.3 Review of III - V semiconductor alloys 34

2.4 Present work

2.5 Method of Preparation of III - V alloys 39

- a) Gradient Freeze method 40
- b) Step Freeze method 42
- c) Travelling zone method 45
- d) Other possible methods 48

2.6 Alloys prepared 49

- a) $Ga_xIn_{(1-x)}Sb$ alloys 49
- b) $Ga_xIn_{(1-x)}As$ alloys 52
- c) $InAs_xSb_{(1-x)}$ alloys 55
- d) $GaAs_xSb_{(1-x)}$ alloys 58

Chapter III: Optical Absorption and Thermoelectric Power

3.1 Optical absorption in semiconductors 64

- a) Classical theory of free carrier absorption 66
- b) Interband absorption 69
- c) Burstein effect 72

3.2 Theory of Thermoelectric power 74

- a) Scattering mechanisms 75
- b) Expressions for Thermoelectric power 80

3.3 Energy gap variation in III - V alloys 84

3.4 Review on energy gap measurements 88

- a) $Ga_xIn_{(1-x)}As$ alloys 89
- b) $GaAs_xSb_{(1-x)}$ alloys 91

3.5 Equipment and experimental techniques 93
- a) The optical system 93
- b) The wavelength range 98
- c) Apparatus for thermoelectric power measurement 99
- d) Sample preparation 101
- e) Absorption measurements 102
- f) Thermoelectric power measurements 104

3.6 Data Analysis and Discussions 106
- a) $Ga_xIn_{(1-x)}As$ alloys 106
- b) $GaAs_xSb_{(1-x)}$ alloys 122

Chapter IV: Plasma Reflection

4.1 Introduction 128

4.2 Classical theory of infrared reflectivity 130
- a) Plasma reflection 130
- b) Lattice reflection 134

4.3 Statistical theory of free carrier reflection 136
- a) Free carrier susceptibility 136
- b) Carrier concentration 142
- c) Effective mass 143

4.4 Review of previous work on III - V materials 145

4.5 Reflectivity measurements 147
- a) Sample preparation 147
- b) Optical system 148
- c) Alignment procedure 152
- d) Measurement procedure 153

4.6 Hall effect measurements 155

a) Equipment 155

b) Measurement 155

4.7 Method of analysis of data 158

a) Degenerate case ie $E_F >> KT$ 159

b) Case of general degeneracy 161

c) Determination of τ, μ_{opt} and σ 165

4.8 Data , Result and Discussion 167

a) $Ga_xIn_{(1-x)}Sb$ alloys 167

b) $Ga_xIn_{(1-x)}As$ alloys 178

c) $InAs_xSb_{(1-x)}$ alloys 189

4.9 Estimation of error in the effective mass values 198

Chapter V : Summary and Conclusions

5.1 Summary of Results 201

5.2 Suggestions for future work 204

Reference

Appendix I

LIST OF FIGURES

Fig.(1:1) Brillouin zone for a diamond lattice 9

Fig.(1:2) Band structure of Germanium 9

Fig.(1:3) Schematic diagram of the band structure of InSb near the Γ point 15

Fig.(1:4) Band structure of GaAs 15

Fig.(2:1) Temperature profile of the step freeze furnace 43

Fig.(2:2) Temperature profile of the Travelling zone furnace 47

Fig.(2:3) Variation of composition along the length of the ingot for $Ga_xIn_{(1-x)}Sb$ alloys 51

Fig.(2:4) Variation of composition along the length of the ingot for $Ga_xIn_{(1-x)}As$ alloys 54

Fig.(2:5) Variation of composition along the length of the ingot for $InAs_xSb_{(1-x)}$ alloys 57

Fig.(2:6) T-x Phase diagram for $GaAs_xSb_{(1-x)}$ alloys 58

Fig.(2:7) Variation of composition along length of the ingot for $GaAs_xSb_{(1-x)}$ alloys 61

Fig.(3:1) Experimental layout used for absorption measurements 94

Fig.(3:2) Thermoelectric power apparatus 100

Fig.(3:3a) Variation of I_0/I with photon energy for $Ga_xIn_{(1-x)}As$ alloys 109

Fig.(3:3b) Variation of I_0/I with photon energy for $Ga_xIn_{(1-x)}As$ alloys 110

Fig.(3:4a) Variation of I_0/I with photon energy $h\nu$ for a typical sample showing the values of E_g for different criteria 111

Fig.(3:4b) Variation of α^2 with $h\nu$ for a typical sample 111

Fig.(3:5) Values of E_g for different criteria plotted as a function of x 113

Fig.(3:6) Variation of Fermi level with x for $Ga_xIn_{(1-x)}As$ alloys 115

Fig.(3:7) Values of E_0 corresponding to $\alpha = 50cm^{-1}$ along with the fitted parabolic curve for $Ga_xIn_{(1-x)}As$ alloys 120

Fig.(3:8a) Absorption curves for $GaAs_xSb_{(1-x)}$ alloys 124

Fig.(3:8b) Absorption curves for $GaAs_xSb_{(1-x)}$ alloy 125

Fig.(3:9) Values of energy gap for $GaAs_xSb_{(1-x)}$ alloys along with the fitted parabolic curve 127

Fig.(4:1) Electro-optical system for infrared reflectivity measurement 150

Fig.(4:2) Specimen holder for reflectivity measurement 151

Fig.(4:3) Hall probe 151

Fig.(4:4) Electrical circuit for Hall effect measurement 157

Fig.(4:5) Typical plasma reflection curves for $Ga_xIn_{(1-x)}Sb$ alloys 171

Fig.(4:6) Typical graphs of ε vs λ^2 for $Ga_xIn_{(1-x)}Sb$ alloys 172

Fig.(4:7) Variation m_0^*/m with composition for $Ga_xIn_{(1-x)}Sb$ alloys 175

Fig.(4:8) Variation of ε_∞ with composition for $Ga_xIn_{(1-x)}Sb$ alloys 176

Fig.(4:9) Typical plasma reflection curves for $Ga_xIn_{(1-x)}As$ alloys 179

Fig.(4:10) Typical graphs of ε vs λ^2 for $Ga_xIn_{(1-x)}$ alloys 180

Fig.(4:11) Variation of ε_∞ with x for $Ga_xIn_{(1-x)}As$ alloys 181

Fig.(4:12) Variation of longitudinal and transverse optical phonon frequencies for $Ga_xIn_{(1-x)}As$ alloys 184

Fig.(4:13) Graphical solution to obtain m_0^*/m and E_F for two typical samples of $Ga_xIn_{(1-x)}As$ alloys 185

Fig.(4:14) Variation of m_0^*/m with composition for $Ga_xIn_{(1-x)}As$ alloys 186

Fig.(4:15) Typical plasma reflection curves for $InAs_xSb_{(1-x)}$ alloys 191

Fig.(4:16) Typical graphs of ε vs λ^2 for $InAs_xSb_{(1-x)}$alloys 192

Fig.(4:17) Variation of ε_∞ with composition for $InAs_xSb_{(1-x)}$alloys 193

Fig.(4:18) Variation of m_0^*/m with composition for $InAs_xSb_{(1-x)}$alloys 196

LIST OF TABLES

Table(1,1) Some band parameters of III - V compounds 16

Table(1,2) Some properties of III - V compounds 23

Table(3,1) Absorption data for $Ga_xIn_{(1-x)}As$ alloys 112

Table(3,2) Thermoelectric power data for $Ga_xIn_{(1-x)}As$ alloys 114

Table(3,3) Energy gap values using different criteria for $Ga_xIn_{(1-x)}As$ alloys 117

Table(3,4) Values of A, B and C for $Ga_xIn_{(1-x)}As$ alloys 119

Table(3,5) Absorption data for $GaAs_xSb_{(1-x)}$alloy 126

Table(3,6) Values of A, B and C for $GaAs_xSb_{(1-x)}$ alloys 122

Table(4,1) Typical Hall data 170

Table(4,2) Experimental data for $Ga_xIn_{(1-x)}Sb$ alloys 173

Table(4,3) Computed values for $Ga_xIn_{(1-x)}Sb$ alloys 174

Table(4,4) Computed values from plasma minimum for $Ga_xIn_{(1-x)}Sb$ alloys 177

Table(4,5) Experimental data for $Ga_xIn_{(1-x)}As$ alloys 182

Table(4,6) Computed values for $Ga_xIn_{(1-x)}As$ alloys 183

Table(4,7) Computed values from plasma minimum for $Ga_xIn_{(1-x)}As$ alloys 187

Table(4,8) Experimental data for $InAs_xSb_{(1-x)}$ alloys 195

Table(4,9) Computed values for $InAs_xSb_{(1-x)}$ alloys 196

Table(4:10) Computed values from plasma minimum for $InAs_xSb_{(1-x)}$alloys 197

CHAPTER 1

REVIEW OF THE BAND THEORY

1.1 Historical note on semiconductors

Semiconductors are materials which have become increasingly important because of their technological applications. The semiconducting property was first discovered by Faraday in I833 (F1) by noticing the negative temperature coefficient of resistivity of silver sulphide. This was followed by the discovery of the phenomenon of rectification in solids by F. Braun in 1872 (B1) and photoconductivity by W. Smith in 1874 (S1). Later in 1879 (H1) the discovery of Hall effect led to a better understanding of the conduction process in semiconductors and thus to the classification of Selenium, Tellurium and Germanium as semiconductors. The discovery of transistor action in 1949 (B2) and its possible application in electronics industry resulted in an intensive study of the properties of elemental semiconductors Germanium and Silicon of the group IV.

Even though the existence of other compound semiconductors was predicted as early as 1907, it was in 1952 that Welker in his classic paper (52W1) demonstrated that many of III-V compounds have semiconducting properties similar to Germanium and Silicon. Soon many other compounds in the group II and VI, and I and VII, were also shown to be semiconductors with similar properties. Since pure semiconductors of the compounds were technologically more difficult to prepare, investigatio of their properties was hindered. The study of the properties of III-V compounds and their alloys has become increasingly important after the demonstration of the possible application of these materials for detectors, light generators and Gunn oscillators.

1.2. Energy band theory of solids

A satisfactory explanation for some of the properties of solids was first given by the classical free electron theory proposed by Drude and Lorentz. According to this theory, any solid is composed of positively charged ions and their valence electrons are dissociated from their parent atoms forming a free electron gas inside the boundary of the solid. Even though many of the metallic properties were explained by Drude - Lorentz theory, it yielded incorrect magnitudes for the specific heat and paramagnetic suceptibility. Sommerfeld in 1928 (28S1) applied quantum mechanics to the free electrons. He predicted a quasi-continous energy spectrum and a parabolic dependence of energy on the electron wave vector. He used Fermi-Dirac Statistics instead of Maxwell - Boltzmann Statistics for the electrons, required by quantum theory. This was a move in the right direction, but, still did not give any insight into the electrical properties of the category of solids Viz conductors, insulators and semiconductors.

Bloch (28B1) stated that the electron moves in a periodic potential, which has the periodicity of the atoms in a crystal lattice. The electronic wave functions are then obtained from the solution of the Schröedinger equation,

$$\nabla^2 \Psi + \frac{2m}{\hbar^2} [E - V(\vec{\gamma})] \Psi = 0$$

where $V(\vec{\gamma}) = V(\vec{\gamma} + \vec{d})$ and d = lattice constant along $\vec{\gamma}$

The solutions are called Bloch functions given by

$$\Psi(\vec{\gamma}) = U_k(\vec{\gamma})\ exp(i\vec{k}\cdot\vec{\gamma})$$

with $U_k(\vec{\gamma} + \vec{d}) \equiv U_k(\vec{\gamma})$

These are plane waves describing the motion of electrons in the crystal. The eigenvalues corresponding to the Bloch functions are the allowed energy values. The main problem arising here is to find a realistic potential $V(\vec{\gamma})$. The one dimensional problem was treated by Kronig and Penny (31K1) and Kramers (35K1) using different potentials. But they all lead to the same general result that the free electron parabolic energy splits up into bands of allowed and forbidden energy. The discontinuities in the parabola occur when k has the values

$$k = \frac{n\pi}{a} \qquad \text{where } n = \pm 1,\ \pm 2,\ \pm 3\ ---$$

Here "a" refers to the lattice constant in the one dimensional case. The treatment was carried out to three dimensions by Wigner and Seitz (33W1), again leading to the existence of forbidden energy gaps, the only difference being that it is possible to have the forbidden band in one k direction overlapping with the allowed band in another k direction.

Since k is inversly proportional to the lattice spacing, in three dimensions one can define a k-space, which is the reciprocal of the real space formed by the lattice points. Taking a certain origin in k-space one could find a surface which is the locus of all the first discontinuities of energy. The volume enclosed by this surface is called the first Brillouin zone. Corresponding to the second, third discontinuities etc. one could define second, third Brillouin zones etc.

It is easy to show that each zone contains all the non-equivalent values of $\vec{k}$. Hence any quantity in the crystal lattice could be represented as a function of $\vec{k}$ in the first Brillouin zone. The shape of the Brillouin zone depends on the crystal structure. The first Brillouin zone for a body centered cubic lattice is a rhombododecahedron and that for a face centered cubic lattice is a truncated octahedron.

The foregoing discussion was based on the "one electron" approximation, where it was assumed that the complete wave function for a system of n electrons can be described by the product of the individual electron wave functions. The mutual Coulomb interactions between electrons can be replaced by an average potential. The energy eigenvalues are then the sum of the energies of n noninteracting electrons. The "exchange" and Coulomb interactions can be treated exactly by solving the Hartree-Fock self consistent equations using an antisymmetric linear combination of the wave functions, known as the "slater determinant". A calculation taking into account all these factors is extremely complicated and one is satisfied with the "one electron approximation " for the purpose of comparing with experimental results.

1.3. Band structure representations

We have seen that the energy E of the electron in the crystal is a function of the electron wavevector $\vec{k}$, and this dependence results in a band structure for the solid. Both these quantities can not be represented simultanously in a three dimensional space. So the usual practice is to construct constant energy surfaces in k-space, or to draw E as a function of $\vec{k}$ in different directions. The position of the bands and the forbidden energy gap will be different in different directions of $\vec{k}$. In a semiconductor there is a finite energy gap between the highest filled band (valence band) and the lowest empty band (conduction band). These are band extrema which occur at $k(000)$, or along the directions of high symmetry in the crystal. The first method of representation of band structure is useful to study fermi surface in metals and the shape of energy surfaces near band extrema in semiconductors. When the bands are not degenerate we can write $k \approx o$

$$E = E_0 + Ak_x^2 + Bk_y^2 + Ck_z^2$$

For a crystal with cubic symmetry $A = B = C$ and the energy surfaces are spherical. The energy surfaces near extrema at other points in the Brillouin zone are ellipsoids or more complicated surfaces. This will be seen later when more specific cases are considered.

The second method of representation is used when general band theory is considered. Since characteristic features of the band structure of a solid always occur along the directions of high symmetry, it is customary to draw E-*k* curves from *k*(000) along these directions and ignore the other directions. For a crystal with cubic symmetry these are the <100>, <111>, and <110> directions.

There are three different schemes to represent E Vs *k* in the Brillouin zone. In the extended zone scheme the E -*k* curves are drawn in the first, second, third zones etc. showing the discontinuity at each zone boundary. Since all the Brillouin zones are equivalent it is possible to map the E -*k* curves occuring in other zones into the first zone by translating them with one or a multiple of a reciprocal lattice vector. This is called the reduced zone scheme and is frequently used in this thesis. In the periodic zone scheme the reduced zone is periodically repeated through all of *k*-space. More detailed discussions are given in well known text books by Callaway (64C1) and Jones (60J1).

1.4. Band structure of Ge and Si of the Group IV

Both Ge and Si belong to the group IV of the periodic table. They crystallize in the diamond structure, which consists of two interpenetrating f.c.c. lattices with the one sublattice displaced from the other by a vector $\vec{a}(\frac{1}{4},\frac{1}{4},\frac{1}{4})$, where "a" is the length of the sides of the elementary cube. The band structures of the two elements are similar in nature. The Brillouin zone for a diamond lattice is shown in Fig. (1:1). The various directions and symmetry points shown are according to group theoretical notation and is used in all the band structure diagrams drawn in this thesis. The band structure of Ge is shown in Fig. (1:2). The conduction band has four equivalent minima along <111> directions at the zone boundary. The constant energy surfaces are ellipsoids of revolution about this axis. For Si the conduction band has six equivalent minima occuring along the <100> direction at $0.8k_z$, where k_z corresponds to the value at the zone boundary in these directions from the centre of the zone.

The valence band maxima of both Ge and Si occur at k (000). The existance of two valence bands corresponding to "heavy holes" and "light holes" was first observed by R.K. Willardson etal (54W1). The third valence band due to spin orbit splitting is much lower at k(000). An excellent review on the band structure of Ge and Si is given by F. Herman (55H1)

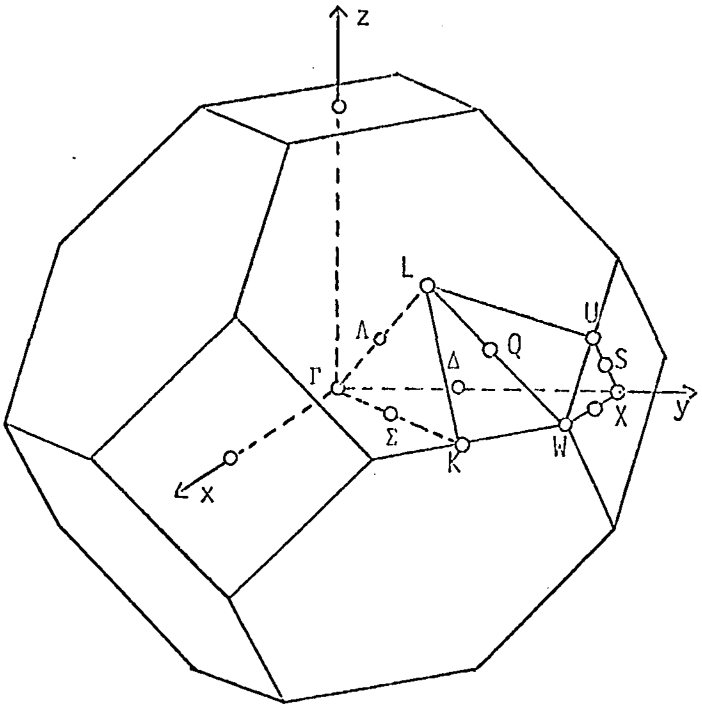

Fig.(1:1) Brillouin Zone for a diamond lattice

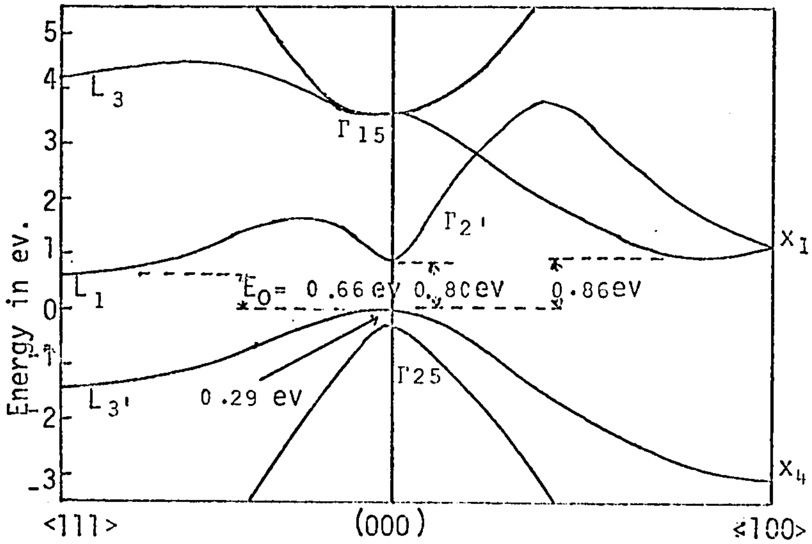

Fig.(1:2) Band structure of Germanium (66C3)

1.5. Band structure of III - V compounds

a) Method of Band calculation

The principal III-V compound semiconductors are InSb, InAs, InP, GaSb, GaAs, GaP, AlSb, AlAs and AlP. All these crystallize in the zinc-blende structure, which is similar to diamond structure, except for the fact that the two nearest neighbours are one of group III and the other group V atom. Hence the inversion symmetry present in a diamond lattice is absent in the zinc-blende lattice. As it was already mentioned, once the crystal potential is roughly known, the first step is to solve the Schrödinger equation and obtain some qualitative information about the band structure. Knowledge of the crystal structure provides information about the symmetry properties of wave functions at characteristic symmetry points and directions in the Brillouin zone. The next procedure is to calculate the energy bands at the symmetry points and then to extend to the surrounding regions by perturbation theory. Two of the earlier methods of band calculation are the OPW method introduced by Herring (40H1) and the tight-binding approach. The former is best suited for high energy electronic states and the latter for low energy electronic states. Herman (52H1) first applied the OPW method to covalent semiconductors and Slater and Koster (54S1) used the tight binding approach as an interpolation procedure. Recently the OPW method has been carried out to many III-V compounds (63B2). Dresselhaus (55D1) was the first to take into account the effect of spin orbit interaction on the electronic states by the so called $\vec{k}\cdot\vec{p}$ perturbation method. Kane (57K1) calculated the band structure for InSb by treating the interaction of the valence and conduction bands exactly via $\vec{k}.\vec{p}$ interaction. Since Kane's theory is generally applicable to all III - V compounds with suitable approximation, and is the basis of the analysis of most of the experimental work in this thesis, it will be considered in detail. Taking into account the interaction of higher bands Cardona (63C1) carried out detailed calculation of the band parameters of group IV, III -V and II - VI compounds, near the Γ point. This model involves the knowledge of many parameters, and is more difficult to be used in practice. The pseudopotential method developed by Phillips (58P1) and the $\vec{k}.\vec{p}$. method by Cardona and Pollak (66C1, 66C2) have been useful in calculating the band structure inside the full zone. More detailed developments are given in many recent books (64C1, 66W1).

b) Kane's band calculation

Kane's theory considered in this section is the one taking the two fold degenerate conduction band wave functions having Γ_1 symmetry and the six fold valence band wave function having Γ_4 symmetry and treating the interaction exactly via $\vec{k}.\vec{p}$ terms. Only the principal steps and the results are given here and the reader is referred to the original paper by Kane (57K1) for further details.

The Schrödinger equation for an electron in the periodic potential $V(\vec{r})$ including the spin orbit interaction can be written as

$$\left[\frac{p^2}{2m} + V(\vec{r}) + \frac{\hbar}{4m^2c^2}\left(\vec{\nabla}V \times \vec{p}\right).\vec{\sigma}\right]\Psi_k(\vec{r}) = E_k\,\Psi_k(\vec{r}) \qquad [1:1]$$

where p is the momentum operator and σ the Pauli spin operator. The wave functions used are the Bloch functions

$$\Psi_k(\vec{\gamma}) = U_k(\vec{\gamma}) \; exp(i\vec{k} \cdot \vec{\gamma})$$

Now equation [1:1] becomes

$$(H_0 + H_1 + H_2 + H_3) U_k = E_k' U_k$$

where

$$H_0 = \frac{p^2}{2m} + V(\vec{\gamma})$$

$$H_1 = \frac{\hbar}{m} \vec{k} \cdot \vec{p}$$

$$H_2 = \frac{\hbar}{4m^2c^2} (\vec{\nabla} V \times \vec{p}) \cdot \vec{\sigma} .$$

$$H_3 = \frac{\hbar^2}{4m^2c^2} (\vec{\nabla} V \times \vec{k}) \cdot \vec{\sigma}$$

$$E_k' = E_k - a k^2 \quad \text{where } a = \frac{\hbar^2}{2m}$$

Here m is the free electron mass and H_1, H_2, H_3, are the perturbation terms.

The zero order basis functions taken are the two S-state functions S_+ and S_- representing the conduction band and the six p-state wave functions $X_\pm$, $Y_\pm$, $Z_\pm$, representing the valence bands. The + and - signs correspond to spin up and down.

Now the 8 X 8 interaction matrix can be written and a first order perturbation calculation can be carried out. When the symmetry properties of the wave functions are used most of the matrix elements vanish except the following

$$P = -\frac{i\hbar}{m} \quad < S|\ p_z|\ Z >$$

and
$$\Delta_0 = \frac{3\hbar i}{4m^2c^2} \quad < X|(\ \vec{\nabla}V \times \vec{p})_z|\ Y >$$

The solutions of energy values are obtained by the condition that the secular determinant should vanish. This results in the equation (writing E' instead of E_k')

$$E'[\ E'\ (E' - E_0)\ (E' + \Delta_0) - k^2P^2\ (E' + \frac{2}{3}\Delta_0)] = \ 0 \ldots [1:2]$$

where P^2 is the square of the momentum matrix element, Δ_0 the spin orbit splitting of the valence band at the Γ point and E_0 the energy gap.

The solutions of equation [1:2] at $k = 0$ are

$$E_1' = E_0$$
$$E_2' = E_3' = 0$$
$$E_4' = -\Delta_0$$

The first solution corresponds to the conduction band, the second and third correspond to the valence bands degenerate at $k = 0$, and the fourth corresponds to the third valence band split off by the spin orbit coupling. Solving equation [1:2] under the approximation $\Delta >> kP,\ E_0$ Kane showed the following picture of the band structure of InSb. All the bands are parabolic at $k = 0$. The conduction band is highly non-parabolic away from $k = 0$. The first two valence bands are degenerate at $k = 0$, but separated by a finite energy in all directions. The upper one (heavy hole band) is parabolic while the lower one (light hole band) is non-parabolic like the conduction band. The main features and some band parameters of InSb are shown in Fig. (1:3). When the spin degeneracy is taken into account the conduction band, the light hole band and the spin split off valence band are all doubly split in all directions except in the <100> and <111> directions. The heavy hole band is degenerate only in <100> direction. The maximum of the heavy hole valence band no longer lies at the centre of the zone, but it is located at a small distance along the <111> direction.

Since GaAs has a much larger energy gap than InSb, its band structure is also illustrated for comparison. Fig. (1:4) shows the band structure of GaAs derived by k. p method (66P2). The conduction band is less non-parabolic. The valence band extrema occur at the centre of the zone. The band structures for other compounds are very similar in nature. The <111> subsidiary band is the second lowest conduction band for most of the compounds while for GaAs, the <100> band is the second lowest.

A summary of some band parameters of some III - V compounds is given in Table (1,1).

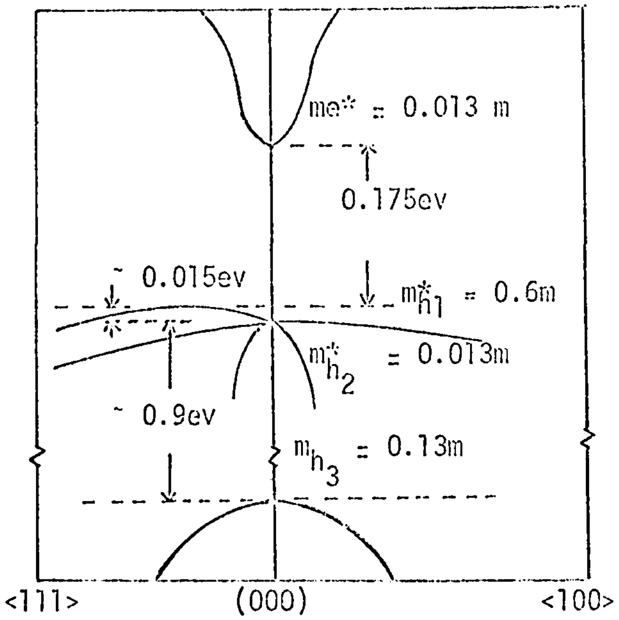

Fig.(1:3) Shematic diagram of the band structure of InSb near the Γ point, after E.O. Kane

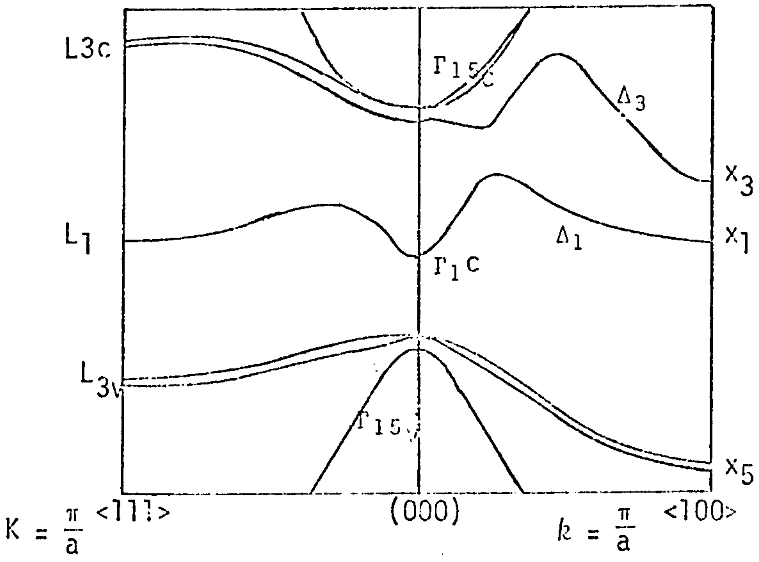

Fig.(1:4) Band structure of GaAs (66P2)

Compound	E_0 (ev)	Δ_0 (ev)	lowest conduction band	second lowest conduction band
InSb	0.18	0.9	(000)	<111>
InAs	0.35	0.43	(000)	<111>
GaSb	0.74	0.8	(000)	<111>
GaAs	1.43	0.34	(000)	<100>
In P	1.27	0.24	(000)	<100>
Ga P	2.25	0.13	(100)	(000)

Table (1,1) Some band parameters of III - V compounds (300^0K)

1.6 Concept of effective mass

The effective mass is an important parameter describing the band structure of the regions surrounding the extrema. There are different definitions used in the literature and should be distinguished from each other. Since the dynamics of electrons and holes can be treated in a similar way all the concepts defined in this section for electrons can be applied to holes also.

a) Band curvature effective mass

If an electron in a crystal is subjected to an external electric field F, the acceleration of the electron can be shown to be

$$\vec{a} = \frac{1}{\hbar^2} \nabla_k \nabla_k E \cdot \vec{F}$$

If this equation is compared with the Newtonian equation for force a quantity having the dimensions of mass can be defined.

$$\frac{1}{m^*} = \frac{1}{\hbar^2} \nabla_k \nabla_k E$$

where m^* is called the effective mass and is a tensor quantity. It has nine components in general. However, for cubic symmetry, by choosing a proper axis of reference they can be reduced to three components along the diagonal.

$$\frac{1}{m^*} = \begin{pmatrix} \frac{1}{m_{11}} & 0 & 0 \\ 0 & \frac{1}{m_{22}} & 0 \\ 0 & 0 & \frac{1}{m_{33}} \end{pmatrix} = \hbar^{-2} \begin{pmatrix} \frac{\partial^2 E}{\partial k_x^2} & 0 & 0 \\ 0 & \frac{\partial^2 E}{\partial k_y^2} & 0 \\ 0 & 0 & \frac{\partial^2 E}{\partial k_z^2} \end{pmatrix}$$

When the energy surfaces are ellipsoids of revolution $m_{11} = m_L$, the longitudinal effective mass and $m_{22} = m_{33} = m_T$, the transverse effective mass. If the energy surfaces are spherical $m_{11} = m_{22} = m_{33}$. For spherical energy surfaces the effective mass is isotropic and it may be written

$$\frac{1}{m^*} = \frac{1}{\hbar^2} \frac{d^2 E}{d k^2}$$

This defenition of the effective mass is called the band curvature effective mass, since it is directly proportional to the curvature of the energy band in k-space. This is the effective mass usually quoted in theoretical calculations.

b) Cyclotron effective mass

An electron in a crystal under the influence of a magnetic field moves in "orbit" with the characteristic cyclotron frequency

$$\omega = \frac{eH}{m^*C}$$

where m^* is defined as the cyclotron effective mass. It can be shown that this mass is related to the area enclosed by the orbit in the plane normal to H (60Z1).

$$m^* = \frac{\hbar^2}{2\pi} \frac{\partial A}{\partial E}$$

For spherical energy surfaces $A = \pi k^2$ and

$$\frac{1}{m^*} = \frac{1}{\hbar^2 k} \frac{dE}{dk}$$

Cyclotron effective mass is usually obtained from experiments like cyclotron resonance (55D 2) and Faraday rotation (58S1), where the effects of electrons in a magnetic field are studied. If the energy surfaces are ellipsoids of revolution the measured effective mass can be shown to be

$$\frac{1}{m^*} = \frac{1}{m_T} \left[\frac{m_L + 2 m_T}{3 m_L} \right]^{\frac{1}{2}}$$

c) Density of States effective mass

This is the effective mass defined in most of the electrical transport properties and is an effective mass averaged over all the occupied states (59S1). The carrier concentration may be defined in terms of the density of states (59S1) by

$$n = 4\pi \left(2m^*_{ds} KT/\hbar^2\right)^{3/2} F_{\frac{1}{2}}\left(\frac{E_F}{KT}\right)$$

where m^*_{ds} is the density of states effective mass and $F_{\frac{1}{2}}\left(\frac{E_F}{KT}\right)$ is the standard Fermi integral. When the energy surfaces are ellipsoids

$$m^*_{ds} = \left(m_L m_T^2\right)^{1/3} .$$

d) Conductivity effective mass

Another definition of the effective mass appearing in transport properties and some times referred to as the conductivity effective mass is given by

$$E = \frac{\hbar^2 k^2}{2 m^*}$$

Here m^* is the proportionality factor in the energy momentum relation of the electrons in the crystal. If energy surfaces are ellipsoidal

$$\frac{1}{m^*} = \frac{1}{3} \left(\frac{1}{m_L} + \frac{2}{m_T} \right)$$

The effective mass anisotropy $k = \frac{m_L}{m_T}$, has usually been determined from angular magneto-resistance measurements in single crystals (56P2, 56F2). Values of m_L , m_T and k for the lowest conduction band for GaSb in the <111> direction have been determined from Faraday rotation measurements (64P1). Recently combined measurements of Faraday rotation, infrared reflectivity, Hall effect, and magneto resistance have successfully yielded accurate values of m_L and m_T for GaSb <111>minima (68L1, 69V1).

An extensive discussion of the functional form of the different effective masses for a non-parabolic band is given in a number of recent papers (60K1, 61K1, 62K2, 62K1). Since the effective mass is definedin different ways, and is a function of energy, one should be careful in comparing the values obtained by different experimental methods. For a parabolic band all these effective masses are identical.If the band is non-parabolic different values are obtained. The effective mass increases with impurity content(doping). Ifthe specimens used are sufficiently degenerate ($E_F >> KT$), the experimental effect observed would be mostly due to electrons near the fermi level and the values obtained are the effective mass values at the fermi level. However in a nondegenerate material all the electrons in the band take part in the specific process and it may be difficult to define an effective mass at a certain position of the band. The only effective mass which is a characteristic of the material and is independent of the definition used is the effective mass at the bottom of the specific band considered. The usual practice is to obtain this value when comparisons are made between values obtained by different experimental techniques. One way of doing this would be to determine the effective mass as a function of doping and extrapolate to zero carrier concentration. However, this method may not be suitable in case of alloy work, where it is difficult to prepare samples of the same composition, but differring in carrier concentration. Another method would be to consider a certain model representing the band and analyse the experimental data on the basis of the specific process involved and this is a complicated procedure. This procedure will be further amplified in the case of plasma reflection described in a later chapter of this thesis. The bottom of the band effective mass values and some physical properties for the common III - V compounds are recorded in Table (1,2). $\frac{m_o^*}{m}$ is the ratio of effective mass to free electron mass and is a dimensionless quantity. This ratio is commonly referredto as effective mass and is understood in all future contexts.

Compound	Melting point (°C)	Lattice constant A°	High frequency dielectric constant (300°K)	μ(000) (300°K) electron	$\left(\frac{m_0^*}{m}\right)$ (000)band
InSb	530	6.479	16.8	80,000	.013
InAs	942	6.058	11.7	33,000	.025
GaSb	706	6.095	14.0	5,000	.045
GaAs	1238	5.653	11.1	7,500	.070
InP	1058	5.869	10.9	4,500	.073
GaP	1467	5.45	8.8	100	0.135

Table (1,2) Some properties of III - V compounds

1.7 Temperature dependence of the effective mass

The change in effective mass of the electrons is contributed by two factors. There is a positive temperature dependence of the effective mass due to the non-parabolicity of the conduction band and a negative dependence of the bottom of the band mass due to lattice dilation. The net change is small and accurate measurements have to be made to determine the change. Cardona (61C1, 60C1)measured the change of effective mass in GaAs, In P, and InAs between 80 to 297^{O}K from infrared reflectivity and Faraday rotation measurements, and found it to be less than 2%. He calculated the effect of lattice dilation from the known temperature coefficient of the energy gap, the compressibility and its thermal expansion coefficient. He also estimated the increase in effective mass due to non-parabolicity and the net change observed was in good agreement with the experimental result.

Ehrenreich (57E1) has shown that the temperature variation of the bottom of the band mass can be estimated from the relation

$$\frac{m_0^*\ (T)}{m} = \frac{m_0^*\ (0)}{m}\ \frac{E_0^*\ (T)}{E_0\ (0)}$$

where (0) refers to temperature 0^{O}K, (T) a finite temperature and E^*_0 is an "effective mass band gap", which is defined in section 1.8 b.

1.8 Kane Band Model

a) Kane equation for the conduction band

It was shown in section (1.5b) that Kane's determinant solution is a fourth degree equation and one of the solutions represents the conduction band. Neglecting the solution $E' = 0$, equation [1:2] becomes

$$E' \, (E' - E_0) \, (E' + \Delta_0) - k^2 \, P^2 \, (E' + \frac{2}{3} \Delta_0) = 0 \text{ --[1:3]}$$

where E' is measured from the top of the valence band. If energy E is measured from the bottom of the conduction band equation [1:3] should be transformed with the substitution

$$E' = E + E_0 - ak^2$$

Now equation [1:3] becomes

$$(E - ak^2) \, (E + E_0 - ak^2) \, (E + E_0 + \Delta_0 - ak^2) - a \, k^2 P^2 \, (E + E_0 + \frac{2}{3} \Delta_0 - ak^2) = 0 \text{ -- [1:4]}$$

In order to solve this cubic equation and obtain E in terms of k in a convenient mathematical form various approximations have been made. Here the approximation made by Cardona (61C1) is considered, since it is a good approximation for all the III - V compounds for low energies.

ie $\quad E < E_0 + \frac{2}{3} \Delta_0$

Under the above approximation equation [1:4] becomes

$$(E - ak^2)(E + E_0 - ak^2)(E_0 + \Delta_0) - ak^2P^2(E_0 + \frac{2}{3}\Delta_0) = 0$$

Solving this equation and taking the +ve root corresponding to the conduction band

$$E - ak^2 = -\frac{E_0}{2} + \frac{1}{2}\left[E_0^2 + ak^2 \gamma p^2\right]^{\frac{1}{2}}$$

$$\text{where } \gamma = \frac{4\left(E_0 + \frac{2}{3}\Delta_0\right)}{(E_0 + \Delta_0)} \qquad \text{--- [1:5]}$$

$$\text{or } E = ak^2 + \frac{E_0}{2}\left[\left(1 + \frac{ak^2 \gamma p^2}{E_0^2}\right)^{\frac{1}{2}} - 1\right] \qquad \text{--- [1:6]}$$

The cyclotron effective mass at the bottom of the conduction band is given by

$$\frac{1}{m_c^*} = \frac{1}{\hbar^2 k} \frac{dE}{dk} \quad \text{evaluated at } k = 0$$

This leads to an expression for P^2 in terms of the effective mass.

$$P^2 = \frac{4\,E_0}{\gamma}\left(\frac{m}{m_0^*} - 1\right) \quad \text{--- [1:7]}$$

substituting for P^2 in [1:6] we get

$$E = ak^2 + \frac{E_0}{2}\left\{\left[1+\frac{4a}{E_0}\left(\frac{m}{m_0^*} - 1\right)k^2\right]^{\frac{1}{2}} - 1\right\} \quad \text{--- [1:8]}$$

This form of the Kane equation can be widely used for all III - V compounds without much restriction.

b) Effective mass band gap

Ehrenreich (57E1) has pointed out that at finite temperatures the energy gap to be used in equation [1:8] is not the band gap at that temperature, but an 'effective mass band gap' E_0^* which determines the curvature near the bottom of the band. The change in band gap with temperature is produced by the lattice dilation and the interaction with the phonon field. The interaction with the phonon field both in polar and non-polar materials causes a shift in the band gap without a change in curvature. But the lattice dilation produces an appreciable change in curvature along with the shift in band gap. Hence the energy gap determined by lattice dilation, E_0^* is the band gap which determines the effective mass.

The E_0^* can be theoretically related to the pressure induced increase in band gap. The gap at pressure p will be

$$E_0^* (T,p) = E_0^* (T,0) + \Delta E_g$$

where ΔE_g is the change in band gap produced by pressure p. The quantity $\left(\frac{\partial E_0^*}{\partial T} \right)_p$ which determines the effective mass band gap can be thermodynamically related to $\left(\frac{\partial E_0}{\partial p} \right)_T$ (56B2) by the equation

$$\left(\frac{\partial E_0^*}{\partial T} \right)_p = - \frac{3\ell}{c} \left(\frac{\partial E_0}{\partial p} \right)_T$$

where ℓ and c are respectively the coefficient of linear expansion and the compressibility. From measurement of the Hall coefficient as a function of pressure, $\left(\frac{\partial E_0}{\partial p} \right)_T$ can be determined. Since experimental values of ℓ and c are readily available $\left(\frac{\partial E_0}{\partial T} \right)_p$ can be easily calculated. Hence at a finite temperature E_0^* can be determined from the equation

$$E_0^* (T) = E_0(0) - \left(\frac{\partial E_0^*}{\partial T} \right)_p T$$

Ehrenreich finds that the shift in band edge due to dilation is about 1/3 of the total shift in InSb.

CHAPTER II

PREPARATION AND PROPERTIES OF III-V SEMICONDUCTOR ALLOYS

2.1. Introduction

An alloy semiconductor is formed by alloying two element or compound semiconductors. If x atoms of the type A are randomly substituted at B lattice sites a binary alloy (substitutional alloy) of molecular composition $A_xB_{(1-x)}$ will be formed. The simple examples of element semiconductor alloys are Ge-Si and Se-Te alloys. The alloy systems considered in this thesis are pseudo-binary alloys of III-V compounds with one element in common. Single phase solid solutions of these alloys can be formed over a wide range of composition without creating localised donor or acceptor states. However, the preparation of the alloys poses many problems as will be seen later. Random distribution of the atoms ensures that disordered alloy will have the same crystal structure as the constituents. Most of the physical properties of mixed crystals vary from one constituent to another in a smooth fashion. This behaviour has certain advantages. One advantage is that band structure parameters of one component can be studied in detail by investigating these parameters across the alloy system.

Another importance is the possibility of making new semiconductors having optimum properties for particular device applications.

One of the earlier reviews on the theory of alloy semiconductors and its comparison with experimentwere given by Parmenter (60P1). Since then, more theoretical and experimental work have been done in this field. Here a brief summary with references whenever possible will be given. The most thoroughly investigated alloys are the Ge-Si system. Stohr and Klemm (39S1) first showed that these alloys can be formed over the complete composition range and the lattice constant varies linearly with composition. The electrical and optical properties have been investigated by various workers.

2.2. Virtual crystal model

Since it is difficult to obtain a realistic picture of the crystal potential in an alloy, band structure calculations are extremely difficult, although some progress has been made recently with the advent of high speed computers. The pioneer work on three dimensional alloys was carried out by Nordheim (31N1) and Muto (38M1). They introduced the concept of virtual crystal, stating that the aggregate atoms are arranged at random on the sites of some periodic lattice, whose form depends only upon the alloy composition. The potential acting on an electron moving through the disordered alloy can be decomposed into a periodic part and a non-periodic part as follows.

$$V_{\text{alloy}}(\gamma) = V_{\text{per}}(\gamma) + V_{\text{non-per}}(\gamma)$$

where $V_{\text{per}}(\gamma)$ is the average of the alloy potential over all the random configuration of the atoms for a given molecular composition and $V_{\text{non-per}}(\gamma)$ is the deviation of the potential of the real crystal from $V_{\text{per}}(\gamma)$. The virtual crystal is defined by the periodic component, and the effect of disorder is represented by the non-periodic component. The energy levels for the virtual crystal can be calculated knowing $V_{\text{per}}(\gamma)$. Now the energy levels for the alloy can be obtained by perturbation theory, taking $V_{\text{per}}(\gamma)$ as the unperturbed potential and $V_{\text{non-per}}(\gamma)$ as the perturbing potential. Muto (38M1) showed that the first order perturbation theory does not produce any shift from the energy levels of the virtual crystal.

Parmenter (55P1, 56P1) in a one dimensional analysis extended this work to higher orders of perturbation theory and showed that there is a shift in energy levels and the band edges are smeared out into the forbidden bands. But, always there is a finite energy gap and it is possible to associate a band structure. If there is a very substantial disorder, the perturbing potential may be so large that a perturbation treatment breaks down. But such a case is impossible in practice, since the solid solution is impossible to form.

According to virtual crystal approximation the lattice constant varies linearly with composition. This is known as Vegard's law. It is a useful guide for determining the molecular composition when a new alloy system is produced. Slight deviations from Vegard's law have been observed in alloys (58W1). Eventhough many of the parameters used in theoretical calculations (69V3) can be assumed to be linear with composition according to virtual crystal concept, the resulting band structure parameters like various energy seperations, effective masses etc. need not vary linearly. Usually there is a concave deviation and it is due to the virtual crystal and the aperiodicity. These effects causing a non-linear variation of the fundamental energy gap will be discussed in section 3.3.

Band structures for the alloys are similar to those for the compounds. Herman (54H1, 54H2) first showed that the band structures of Ge-Si alloys are intermediate between that of Ge and Si. Bassani and Brust (63B1) made an accurate calculation of the band structure using pseudo-potential method and obtained quantitative agreement with experiment.

2.3 Review of III-V semiconductor alloys

There are many review papers (61E1, 66C3, 69V3) and recently some review books (64M1, 66W1) on III-V compounds and their alloys. Since these books are readily available no attempt has been made to give an exaustive list of references. Special emphasis has been given to energy gap measurements and optical properties. Al compounds are not considered here.

Folberth (55F1) first demonstrated the existance of solid solutions of $InAs_xP_{(1-x)}$ and $GaAs_{(1-x)}P_x$ over the entire composition range. He investigated the energy gap variation for $GaAs_{(1-x)}P_x$ alloys by optical absorption measurements and found that the band structure changes from that of GaAs to GaP at a certain composition. Allen and Hobdy (63A1) reported that this crossover is at $x = 0.53$ Preleminary investigations have been made by Welker and Weiss (56W2) also. Spitzer and Mead (64S1) made a study of the variation of energy gap with composition using measurements of the photovoltaic response of metal-semiconductor surface barriers. Room temperature energy gap values have been systematically investigated by electroreflectance measurements (66T1) also. Since this system has the energy gap in the visible region and, hence the potential application as light emitters, its optical properties have been extensively investigated. Injection laser action was first observed by Holonyak and Bevacqua (62H1, 63H1). Both spontanous and stimulated emission have been observed in such diodes (63K1, 65P1). Optical energy gap variation for the $InAs_xP_{(1-x)}$ system was measured by Oswald (59O1).

He reported a linear variation. The $0^{o}K$ energy gap values extrapolated from electrical measurements (56W1) between 90 to $470^{o}K$ also show a linear variation.

First crystals of $Ga_xIn_{(1-x)}Sb$ system were produced by Goryunova and Federova (55G1). High quality single phase and homogeneous alloy of the system was prepared by Woolley and Smith (56W3). Optical properties (59I1, 59W2, 61W1) have been investigated by many workers. The anomaly in the electrical energy gap above $x = 0.6$ observed by Woolley and Gillet (60W2) has been investigated by Coderre and Woolley (69C3) taking into account many secondary effects. They have shown that the electrical gap values agree with the optical gap values extrapolated to $0^{o}K$.

$Ga_xIn_{(1-x)}As$ system has been prepared (57W1, 58W2, 59A1) and electrical energy gap values have been determined by Coderre (69C2). Room temperature optical energy gap variation has been investigated by several workers (61W2, 59A1,66H1). Homogeneous samples of $InAs_xSb_{(1-x)}$ in the composition ranges $0 <x< 0.45$ and $0.8 <x< 1.0$ have been produced by Woolley and Warner (64W3). They studied the variation of optical energy gap as a function of composition and temperature by optical absorption measurements. The samples in the middle region were annealed compressed powders and were not homogeneous. However room temperature measurements indicate that there is a minimum gap of 0.10 ev at about $x = 0.3$, which is lower than the values of either of the compounds.

The temperature coefficient of the energy gap determined from measurements in the range 96 to 360°K, shows linear variation with composition between the compounds. Sirota and Bolvanovich (67S3) from high temperature Hall effect and conductivity measurements reported that the extrapolated 0°K gap shows a minimum of 0.13 ev at $x = 0.4$. Kudman and Ekstrom (68K1) have reported the minimum to be at $x \approx 0.1$ from a similar type of analysis. In neither of the above analysis the effect of non-parabolicity was taken into account. The absolute zero gap values obtained taking this effect into account (68C1) show that the minimum is at $x = 0.4$ with a value of 0.17 ev. Good homogeneous bulk samples of GaAs - GaSb system have not been prepared. The author had been working on the system and the results available will be discussed in the thesis.

Very little has been done on the determination of the effective masses of these alloys. Oswald determined the electron effective mass values of $InAs_xP_{(1-x)}$ (5901) from free carrier absorption measurements and found a smooth variation with composition.

No mention is made about reflectance measurements above the fundamental energy gap or electroluminescence measurements. The reflectance results are discussed by Thompson (66T2) and Vishnubhatla (69V5).

2.4. Present work

The investigation into the preparation and properties of III-V semiconducting alloys is a work started by Dr. J.C. Woolley at the University of Nottingham. This work has been continued by the semiconductor group at the University of Ottawa. Since the group was working as a team where each member was involved in the preparation and measurement of certain properties, there is overlap in some parts of the work, but the work of one member has always been of a complementary nature for another. When there has been collaboration in the author's work, it will be mentioned.

When the present work was started in September 1965 room temperature optical energy gap values in $Ga_xIn_{(1-x)}As$ alloys had been reported by several workers (60A1, 61W2, 66H1). There was considerable descrepancy in the results. At this time Thompson and Woolley (67T1) reported that the energy gap variations of all the III-V alloys are parabolic and the deviation from linearity can be predicted by an empirical relation.The empirical relation was found to hold good for III-V alloy systems on which data were available at that time. For GaAs - InAs system none of the data available seemed to fit the empirical relation. Hence more accurate measurements were carried out by the author on good homogeneous alloys of InAs - GaAs (68W3) to determine the value of energy gap and check the validity of the empirical relation. Another alloy system on which very little data are available and extremely difficult to prepare is GaAs - GaSb. Considerable effort has been put into the preparation of these alloys and was met with some success. Energy gap measurements have been made in the composition range produced.

Since the effective mass values of electrons in most of these alloy systems had not been investigated, it was felt that some good work in this area is necessary. van Tongerloo in the group started Faraday rotation measurements and Aubin pursued magneto-thermoelectric power measurements. The first aim of the author was to obtain effective mass values at the bottom of the band of some of these alloy systems by magnetoabsorption measurements. However, this project had to be abandoned, since the magnetic field available with the D.C. magnet (3.2 W/m^2) was not high enough and the optical system was not sensitive enough to detect very small signals and yield reasonably accurate values of the effective mass. Since all the III-V alloys have high electron mobility, if the samples are sufficiently doped, one could observe a sharp plasma reflection minimum in the infrared region at room temperature. This method has been used by several workers to obtain accurate values of effective mass in many semiconductor compounds. Alloy systems of InSb-GaSb, InAs-GaAs and InSb-InAs with sufficient electron concentration have been prepared and using the above technique effective mass values at the bottom of the band have been determined by the author.

2.5 Method of Preparation of III-V alloys.

The first step in the preparation of alloys is to establish the range of solid solution, the T - x phase diagram and the variation of lattice parameter with composition. In order to determine the range of solid solution, the mixture of a certain molecular composition of the two compounds is compressed and placed inside an evacuated capsule. It is annealed at a fixed temperature for a long time successively increasing the temperature until equilibrium conditions are reached. From x-ray powder photograph the lattice constant corresponding to the composition can be determined. This is a long and tedious process. Once lattice parameter variation is established, the next step is to determine the T - x phase diagram. The liquidus curve is determined by the cooling curve method (52H2). There are two ways of determining the solidus curve. The method used by Woolley and co-workers (58W2, 59W3) is to hold the mixture in equilibrium at a certain temperature below the liquidus and suddenly quench it. This is satisfactory only for materials with very low diffusion rates in solid phase. The composition is obtained from lattice parameter determined by x-ray method. A discussion of the various methods used for the different III-V alloys is given by Woolley (62W1). Once the phase diagram is established enough information is available to proceed for the preparation of single phase homogeneous solid specimen. The method of annealing below the solidus curve is not practical, since it requires annealing times of few months.

Growing from molten state is faster. Several methods have been tried in this laboratory and polycrystalline and homogeneous alloys have been grown. A detailed discussion of the different techniques is given by Coderre(69C2). The methods used by the author will be described here, with brief indication of the other possible methods. Only polycrystalline materials are produced by the following methods. Single crystals of some of these alloys have been produced in other laboratories, using different methods.

There are three principal methods of growth used in this laboratory. Samples of full composition range of the alloys $Ga_xIn_{(1-x)}Sb$, $Ga_xIn_{(1-x)}As$, $InAs_xSb_{(1-x)}$ and a limited composition range of $GaAs_xSb_{(1-x)}$ have been produced.

a) Gradient Freeze method

This has been the method used by Woolley and coworkers for growing III - V alloys in the past (60W2, 60W1, 61W2, 64W1). The composition of the initial charge necessary to produce a given range of the alloy is determined from the T - x phase diagram. Then the two constituent compounds are accurately weighed and the mixture is enclosed in an evacuated quartz capsule. It is then melted in a furnace at a temperature higher than the melting points of the two constituents and is mixed thoroughly by agitation. It is quenched in air and a solidified inhomogeneous ingot is formed inside the capsule. The ingot is then placed inside a Gradient Freeze Furnace.

A typical G.F.F. consists of approximately a two feet length

of refractory "mullite" tubing with an inner diameter of 1½ inches. Kanthal resistance wire is wound on the tube in a coil fashion in order to produce the desired temperature gradient. The wire is coated with 'Kyanex' refractory cement to ensure good heat conduction.
The tube is mounted centrally along the axis of a rectangular box made of aluminum walls and of approximately 10" x 10" x 24" dimensions. The space inside is filled with insulating material. A Pt - Pt Rh(13%) thermocouple is cemented to the furnace tube near the centre. The temperature is controlled within one degree centigrade by an "Ether Transitrol" proportional controller which employs a saturable reactor. The temperature can be lowered 5- 10°C a day by changing the set point on the controller with a motor "Meccano" gear assembly. The temperature profile has a gradient of approximately 5°C/cm The temperature of the cold end of the G.F.F. is usually adjusted to be few degrees above the melting point of the high melting point compound before the capsule is placed inside. The temperature is then slowly lowered by the "Meccano" gear system. The high melting point composition of the alloy freezes first and an ingot of varying composition along the length is produced. Usually it takes two to three months to grow an ingot 15 to 20 cms long.

The only advantage this method has is the fact that the ingot is not mechanically disturbed throughout the period of growth, but there are many drawbacks. The difficult problem is constitutional supercooling which results in in-homogeneous solidification at the freezing interface. At the liquid solid interface there is a depletion of the high melting point compound causing a localized drop in liquidus temperature. Ideally equilibrium is established by diffusion from the molten part of the ingot. Since diffusion cannot begin until acomposition gradient is established, there is always a localized depletion region and a region of supercooled materiel is formed immediately in advance of the freezing interface. Another disadvantage which makes it impractical for growing ingots with high melting point compounds like GaAs is that, it is not possible to make a temperature gradient steep enough, without exceeding the softening point of quartz ~ 1300°C. At this high temperature compounds containing Arsenic builds very high pressure and the capsule may explode.

b) <u>Step Freeze Method</u>

The step Freeze method is essentially the same as horizontal Bridgman method. The furnace for this method is constructed on the same lines as G.F.F. The main feature is that there are two furnaces, each with a flat temperature profile and a steep temperature gradient between the two. While one furnace is hotter than the melting point of either compound, the other furnace is cooler than either melting point. The tubular furnaces are separated by

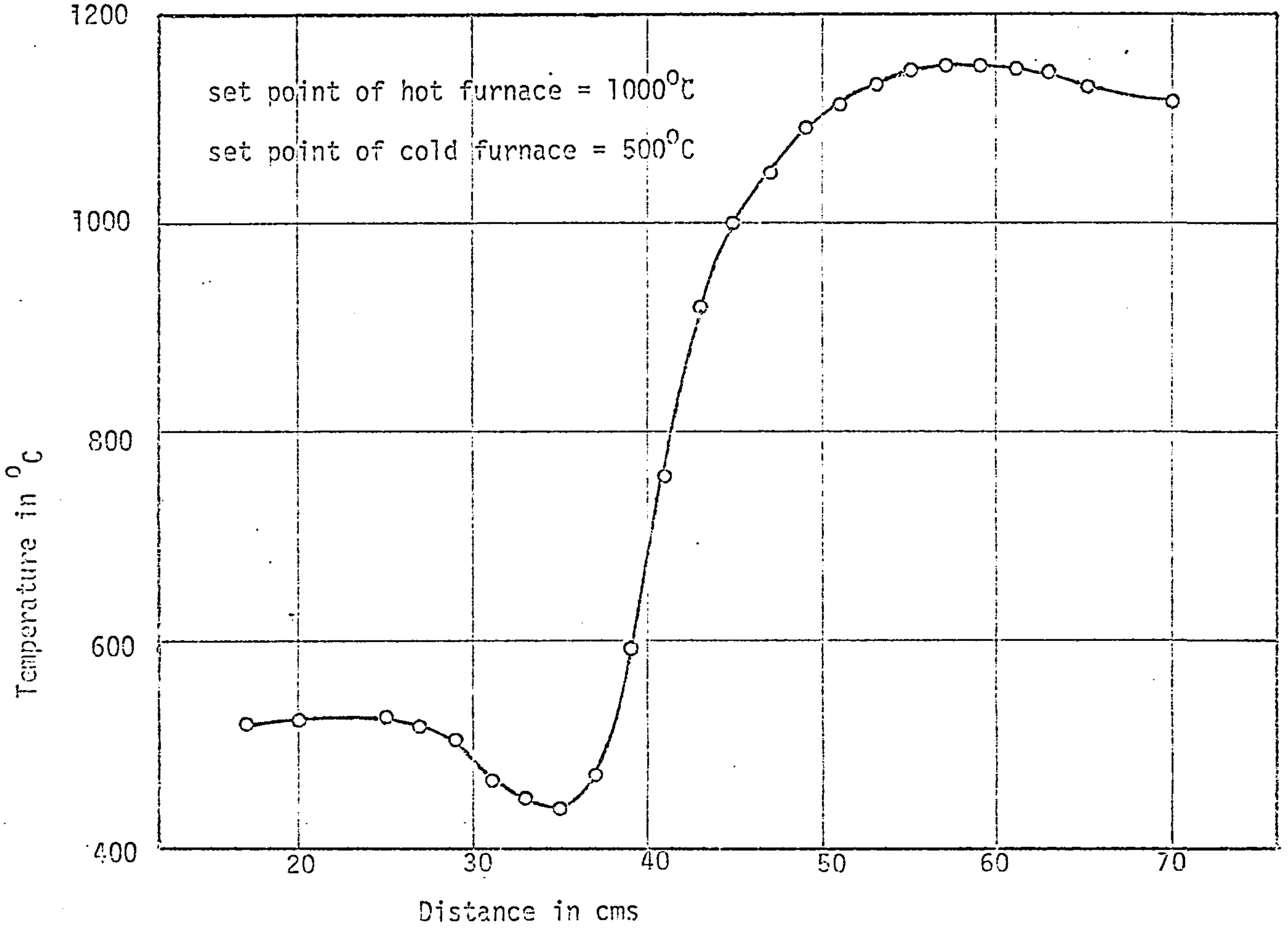

Fig.(2:1) Temperature profile of the step freeze furnace a one inch air gap. Water cooled copper baffles are placed on either side of the gap. Thus the two temperature zones are insulated from each other and a steep temperature gradient is ensured. The furnaces are enclosed in an aluminum sheet metal box of approximately 10" x 10" x 30" size. Pt - Pt Rh(13%) thermocouples are cemented on each of the furnaces. The high temperature zone is controlled by an "Ether Transitrol" proportional controller which employs a saturable reactor. Since no high stability is required, the cold temperature zone is controlled with a Philips on-off type controller which maintains a stability of 3°C with in the set point. A typical temperature profile of the furnace is shown in Fig.(2:1).

The capsule containing the ingot was placed in a quartz or "Mullite" carrying tube of approximately 1" diameter. The tube was mounted on small wheeled dollies on tracks at either end of the furnace. A "Meccano" worm and gear assembly slowed the rate of a Barber Colman motor from 0.3 r.p.m. to a rate which moved the capsule through the step of the furnace from 0.5 to 2 cm/day depending on the material being grown. Ingots of 15 to 20cms long could be grown ina period varying from two weeks to three months depending on the alloy system being grown.

There are many advantages for this method over the G.F. method. The solid liquid interface is fixed by the position of the thermal step and hence the rate of solidification is controlled by the motion of the ingot rather than the composition of the molten phase. The steep temperature gradient ensures no constitutional supercooling. The high temperature zone need not be at excessively high temperature above the melting point of high melting point constituent and the temperature of the two zones need not require high stability. If the composition range of the alloy very near high melting point compound is not required, the temperature of the high temperature zone can be kept even lower than the melting point of the high melting point compound. The low temperature zone can be kept at room temperature if the constituents do not contain highly volatile substances.

c) Travelling Zone Method

This is a method originally developed by Pfann and coworkers (53P1) for the purification of Germanium and later used for pulling single crystals from a polycrystalline charge. In this laboratory a furnace was constructed by Coderre for the preparation of $InAs_xSb_{(1-x)}$ alloys. This system has a large separation between the liquidus solidus curves and hence homogeneous material in the middle composition range was difficult to produce by the methods described previously.

In the Travelling Zone method a small zone of the furnace at the centre is raised to a temperature above the melting point of the alloy keeping either side of the hot zone at a flat temperature profile below the melting point of either constituent. The molten zone in the solid ingot thus created is then caused to traverse the length of the ingot either by moving the ingot through the zone or by moving the zone over the ingot. If a narrow width of the zone is used "zone levelling" takes place and the ingot grown will have one single composition along the length, with a steep gradient at either end. However, by using a larger zone width (ie. one third of the ingot length), zone equilibrium will not be quickly established and it is possible to grow an ingot slowly varying in composition along the length.

The T.Z. furnace was made by two flat profiled furnaces similar to those in a S.F. furnace, but separated by a 5cm wide hot zone. Water cooled copper baffles were placed on either side of the zone to keep the zone width narrow. The zone was heated by two silicon-carbide "Norton" globars which were mounted horizontally, at right angles to the furnace axis, one above and one below the ingot. The walls of the hot chamber were made by "transite" boards coated with liquid porcelain. Power to the glowbars was supplied through a step down transformer at 40 amperes and 5 volts. The hot zone temperature was monitored by Pt - Pt Rh(13%) thermocouple and was controlled with a "Ether Transitrol" controller in conjunction with a saturable reactor. A steady temperature within 5°C at 1000°C was obtained. The flat profile furnaces were controlled by a

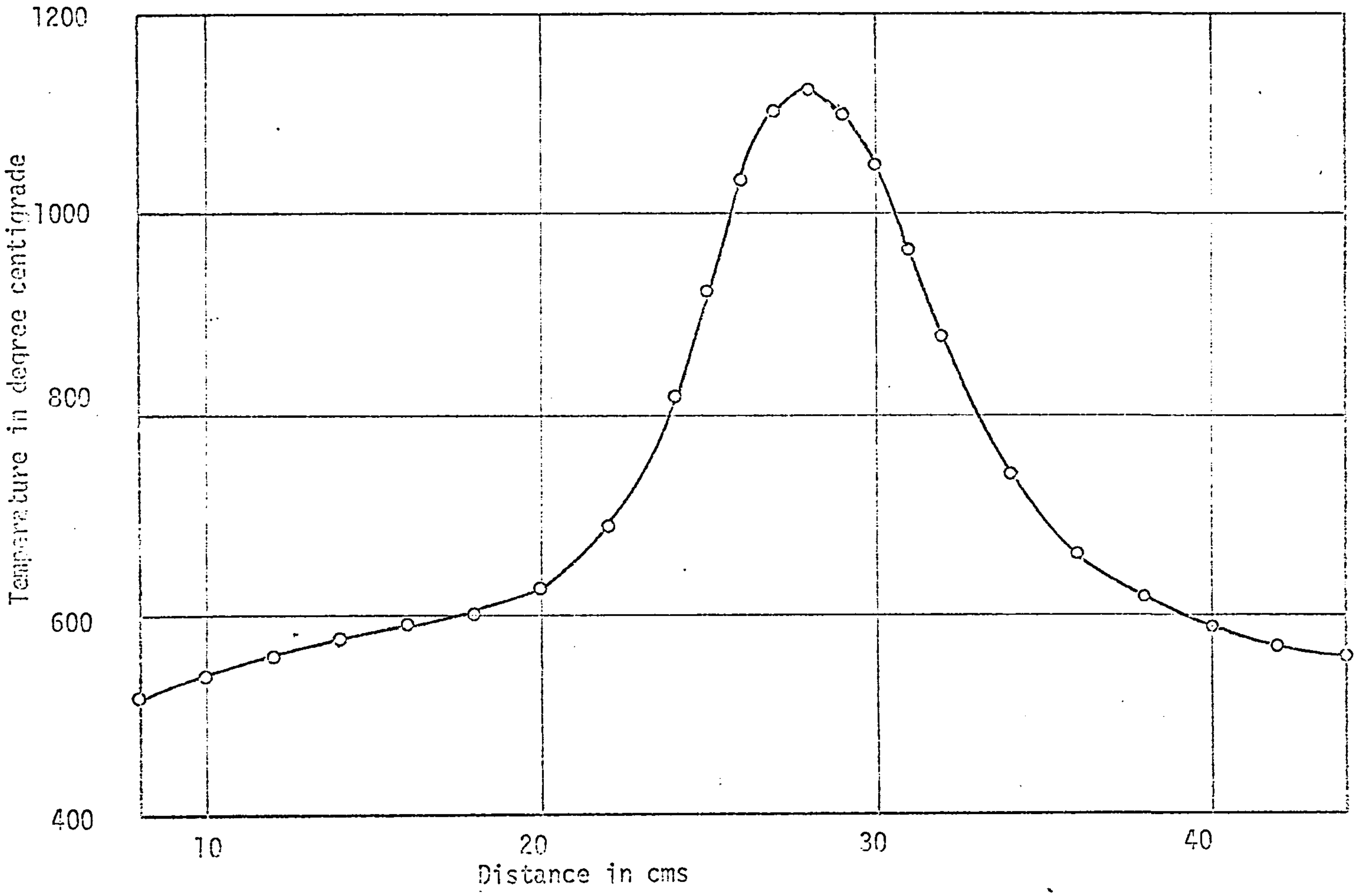

Fig.(2:2) Temperature profile of the Travelling zone furnace

Phillips on-off controller within 2 to 3°C of the set point. A typical temperature profile of the furnace is shown in Fig. (2:2)

The entire furnace assembly was mounted on a cart driven on tracks using a 0.3 r.p.m. motor geared down by a "Meccano" worm and gear assembly to move the furnace at a rate of 0.5cm/day. About 3 months were taken for growing an ingot approximately 15cms long. The furnace and the ingot were moved on a slightly inclined track to prevent build up of crystal at the end to freeze last.

The biggest difficulty is in producing and keeping the width narrow, since the melting point of the material undergoes drastic variation. Hence great success has not been achieved by this method.

d) Other possible methods

There are some techniques used successfully by other workers, but not in this laboratory. One of them is the step levelling method developed by Dismukes (65D1) and applied by Kudman et al to GaSb - InSb (67K1), InAs - GaAs (66H1) and InSb -InAs (68K1) alloys. The method of solutebuild up has been reported by Stambaugh et al and Sirota et al (63S1). Growing alloys by Czochralski pulling method is also recently used (62T1).

2.6 Alloys Prepared

a) $Ga_x In_{(1-x)} Sb$ alloys

Most of the ingots of this alloy were prepared by van Tongerloo and Coderre. The compound InSb in polycrystalline ingot form was obtained from Cominco and had electron concentration of $10^{22} m^{-3}$. The GaSb was made in this laboratory from high purity elements of Ga obtained from Merck and Sb pellets from Cominco. These elements were weighed accurately according to the proportion of atomic weights and placed inside an evacuated quartz capsule. It was mixed thoroughly and placed inside a furnace whose temperature was above the melting point of GaSb (706°C). Finally it was quenched in air. The GaSb was found to be always p-type with approximately $10^{23} m^{-3}$ acceptors. The acceptors are due to nonstoichiometry in the compound, which produces Antimony vacancies.

The liquidus solidus phase diagram for this alloy system has been well established and the variation of lattice parameter (58W1) with composition is found to obey Vegard's law. Many polycrystalline ingots of this alloy system have been produced over the complete composition range by the gradient freeze technique from an initial charge varying from $x = 0.7$ to $x = 0.3$. Nearly 50 days were required to produce an ingot of 15cms length. The alloys obtained by this method were of relatively poor homogeneity, but, were sufficient for most experimental purposes. Undoped ingots had carrier concentrations varying from $10^{23}m^{-3}$ donors at the InSb end to $10^{23}m^{-3}$ acceptors at the GaSb end; the middle range had much lower carrier densities due to compensation. Since it was necessary to have doped materials for the experimental measurements, a small quantity of Tellurium was added in the melt in order to obtain a doping in the range of 10^{24} electrons/m^3.

To avoid inhomogeneity by constitutional supercooling and obtain faster growth rate, later step freeze method was tried and an ingot 15cms in length covering the whole composition range was produced in about 20 days. The hot zone temperature was maintained at about 750°C and the cold zone was kept at room temperature, since there was no easily volatile component like Arsenic present in the two compounds. The composition as a function of ingot length for three ingots used by the author for the experimental measurements is shown in Fig. (2:3).

The step frozen ingots had higher homogeneity across the cross-section and the variation of composition with length was more gradual than those grown by the gradient freeze technique. Ingots grown by step freeze method were also doped with Tellurium to obtain carrier concentrations in the range of 10^{24} electrons m^{-3}. Cross-sectional slices of approximately 1mm thick were cut and homogeneity was determined by x-ray powder photograph method. The carrier concentrations were determined from Hall effect measurements.

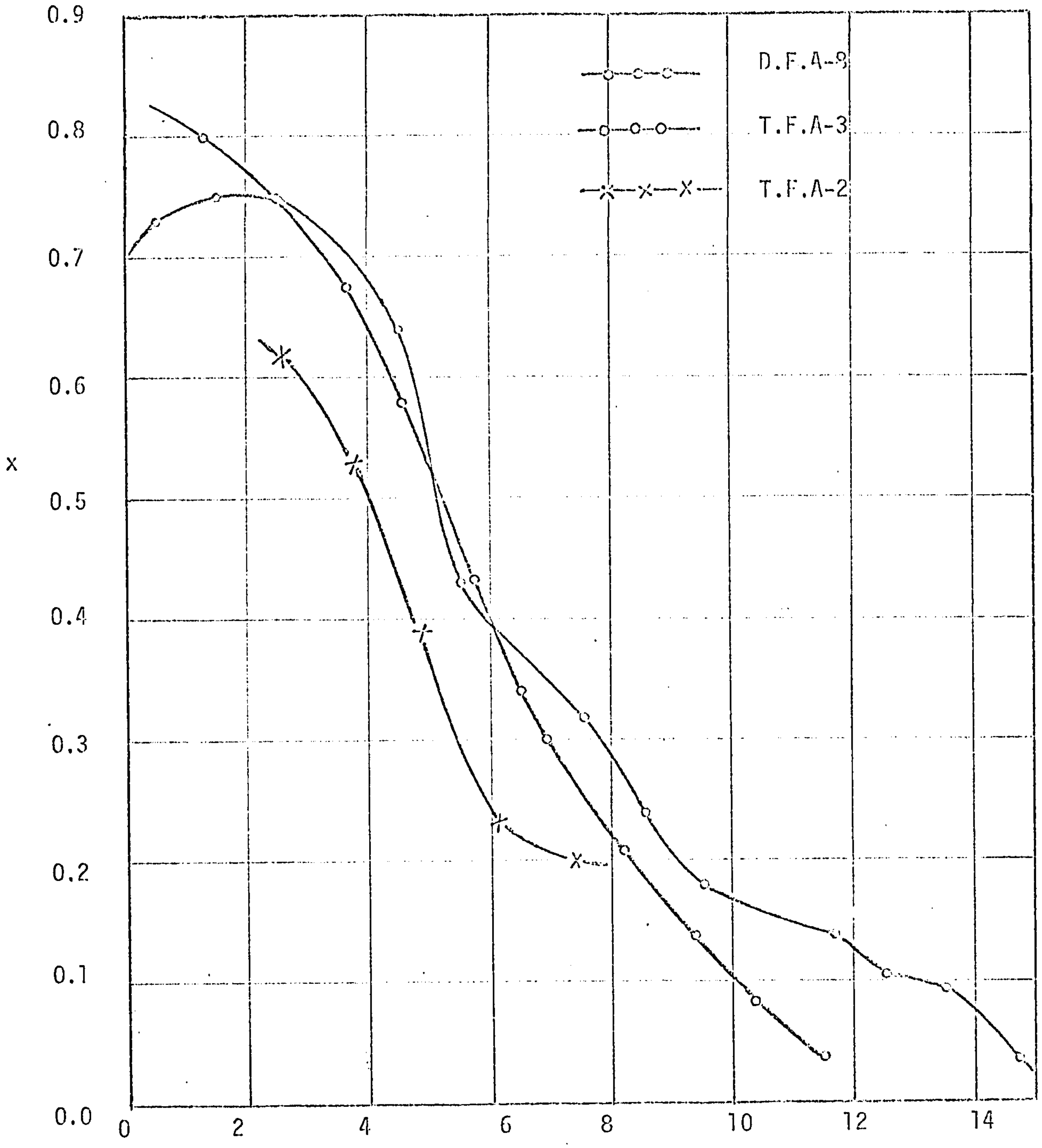

Fig.(2:3) Variation of composition along the length of the ingot for $Ga_xIn_{(1-x)}Sb$ alloys

b) $Ga_xIn_{(1-x)}As$ alloys

This alloy system was prepared from the pure compounds. InAs obtained from Cominco had electron concentration in the range of $4 \times 10^{22} m^{-3}$ and GaAs obtained from consolidated Electrodynamics Inc. had electron concentration in the range of $8 \times 10^{21} m^{-3}$. Both the materials were polycrystalline.

Woolley and Smith (58W1) have shown that the phase diagram of the system is pseudo-binary and the variation of the lattice parameter with composition obeys Vegard's law. In this laboratory two ingots were first produced by Thompson (67T1) using the gradient freeze method. An initial charge of $x = 0.3$ was sufficient for an ingot with x varying from 0 to 0.8. With a temperature gradient of 10°C/cm the hot end of a 15cm ingot had to be raised to 1230°C and at this temperature quartz capsule started to soften. The ingots were of poor homogeneity and multiphase over a large length due to constitutional supercooling. Thompson later used step freeze method with an initial charge of $x = 0.3$. The hot zone was maintained at a temperature of about 1120°C and the cold zone was kept at about 650°C in order to maintain a reasonable As pressure over the length of the ingot. For the 50gm ingot 0.2gm of excess As was added in the capsule in order to compensate for the As lost from the ingot during growth. The ingot was moved at the rate of 1.2cm/day. The resulting ingot was n-type and had carrier concentrations ranging from $1.3 \times 10^{24} m^{-3}$ at $x = 0.82$ to $1 \times 10^{25} m^{-3}$ at the InAs end. The homogeneity along the thickness was good within $x = 0.01$ for 1mm thick slices cut from the ingot. A second ingot grown by the same method starting with $x = 0.55$ yielded a very homogeneous ingot in the range $0.45 < x < 0.92$ with lower electron concentrations in the range $10^{23} m^{-3}$. Later Coderre has grown many homogeneous ingots with lower carrier concentration in the range of composition $0 < x < 0.9$. Ingots with x greater than 0.9 are difficult to grow, since the hot end of the furnace should be maintained at temperatures higher than the melting point of GaAs (1235°C), and at this temperature the As vapour builds excessively high pressure inside the capsule and may explode. It is also necessary to start with an initial charge of high GaAs content.

Since doped samples were necessary for plasma reflection measurements and sufficiently doped samples of $x > 0.5$ were not available, a 50gm ingot was grown by the author from an initial charge of $x = 0.5$. Approximately 50mg of Tellurium was added in the capsule along with the mixture of the compounds. The set point of the hot furnace was 1100°C. The cold zone temperature was set at 600°C. The ingot was moved at the rate 0.5cm/day and an 8cm long

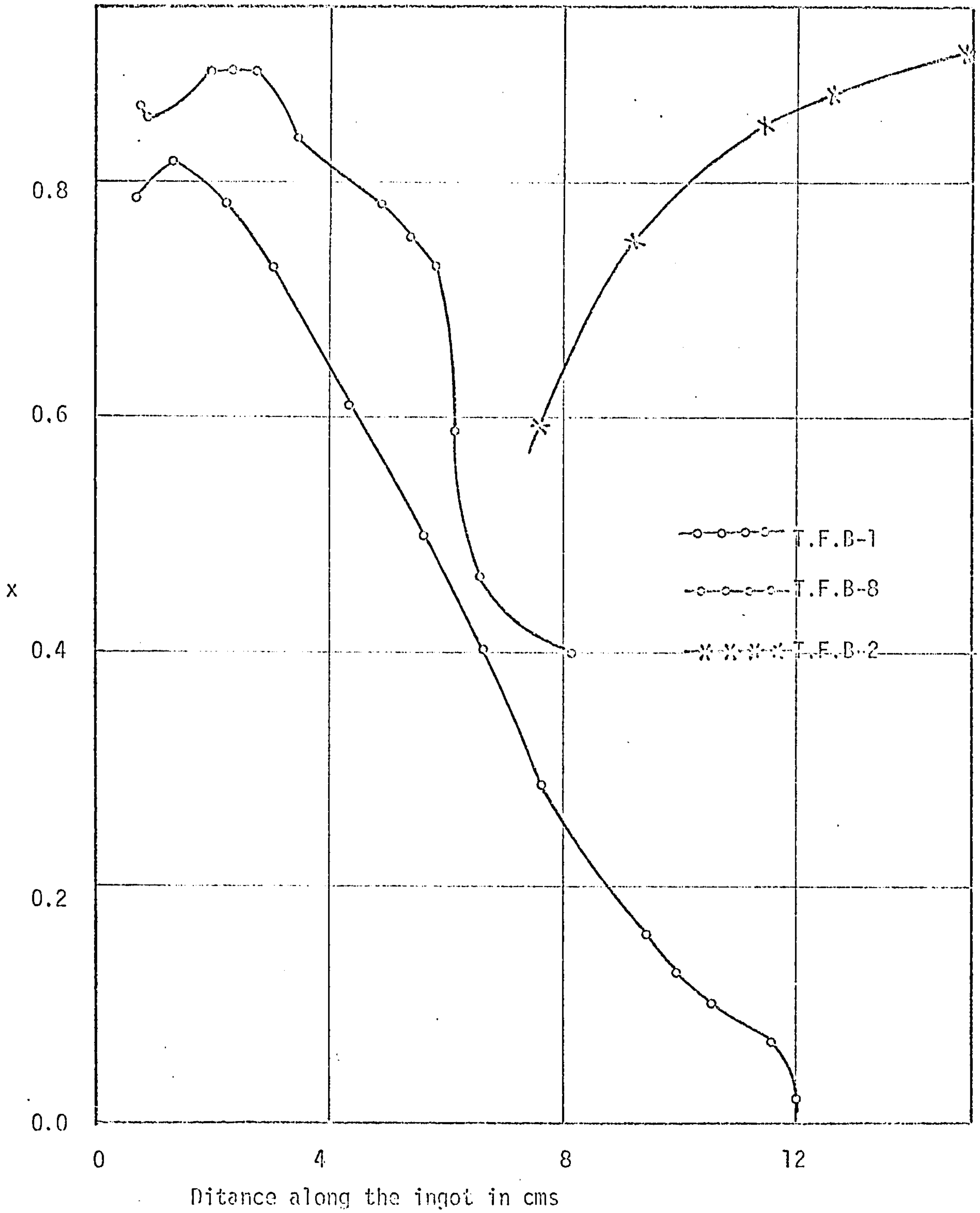

Fig.(2:4) Variation of composition along the length of the ingot for $Ga_xIn_{(1-x)}As$ alloys ingot was produced in about 40 days. Homogeneous samples in the range $0.3 < x < 0.9$ with electron concentration changing from approximately $6 \times 10^{24} m^{-3}$ to $1 \times 10^{24} m^{-3}$ were obtained. The concentration was decreasing towards the GaAs rich part of the alloy. All the alloys were structurally good with no void or crack. Fig. (2:4) shows the variation of composition with length of the ingots used by the author for the experimental measurements.

c) $InAs_xSb_{(1-x)}$ alloys

This alloy system has proven very difficult to prepare over the complete composition range. The liquidus curve of the phase diagram was determined by Shih and Peretti (53S1) and the solidus curve was determined by Woolley and Smith (58W1). The large separation between the liquidus solidus curves accounts for the difficulty of preparing this alloy system. The variation of lattice parameter with composition was determined by Woolley and Smith (58W1) and shows considerable deviation from Vegard's law.

The alloy system was prepared from ingots of polycrystalline compounds obtained from Cominco. The materials were n-type and had carrier concentration in the range $10^{22} m^{-3}$. Since this alloy system has been proven difficult to grow (64W3), the gradient freeze method was not worth trying. Travelling zone technique was the only method which offered some hope of producing alloys towards the middle region. Hence a T.Z. furnace was constructed by Coderre. The constituents were enclosed in an evacuated quartz capsule and melted in a furnace at 1000°C. The contents in the capsule were mixed thoroughly and then quenched in air, resulting in a multiphase polycrystalline ingot. The capsule containing the ingot was then placed in the T.Z. furnace so that the end of the ingot was just in the hot zone. The hot zone was set at 1000°C and the background furnaces were kept at 500°C. Relatively homogeneous materials in the ranges $0.0 < x < 0.4$ and $0.7 < x < 1.0$ have been produced. Even with repeated attempts it has not been possible to produce samples in the middle region. Since the step freeze method was successful in producing other alloys, it was tried for this system also. After several attempts one or two ingots produced had continuous variation of composition along the length. But there was rapid change of composition in the middle region. The samples cut from this region were homogeneous only within 3 mol % along the thickness of 1mm, while samples of the end region had homogeneity better than 1 mol%.

The author prepared few ingots by step freeze method from an initial charge of $x = 0.2$. A 30gm mixture with 7mg of Tellurium moved through the step at the rate of 0.45cms/day resulted in a 6cm ingot of composition ranges $0.0 < x < 0.4$ and $0.7 < x < 1.0$ and electron concentration ranging from 3 to $8 \times 10^{24} m^{-3}$. Further attempts to produce alloys in the

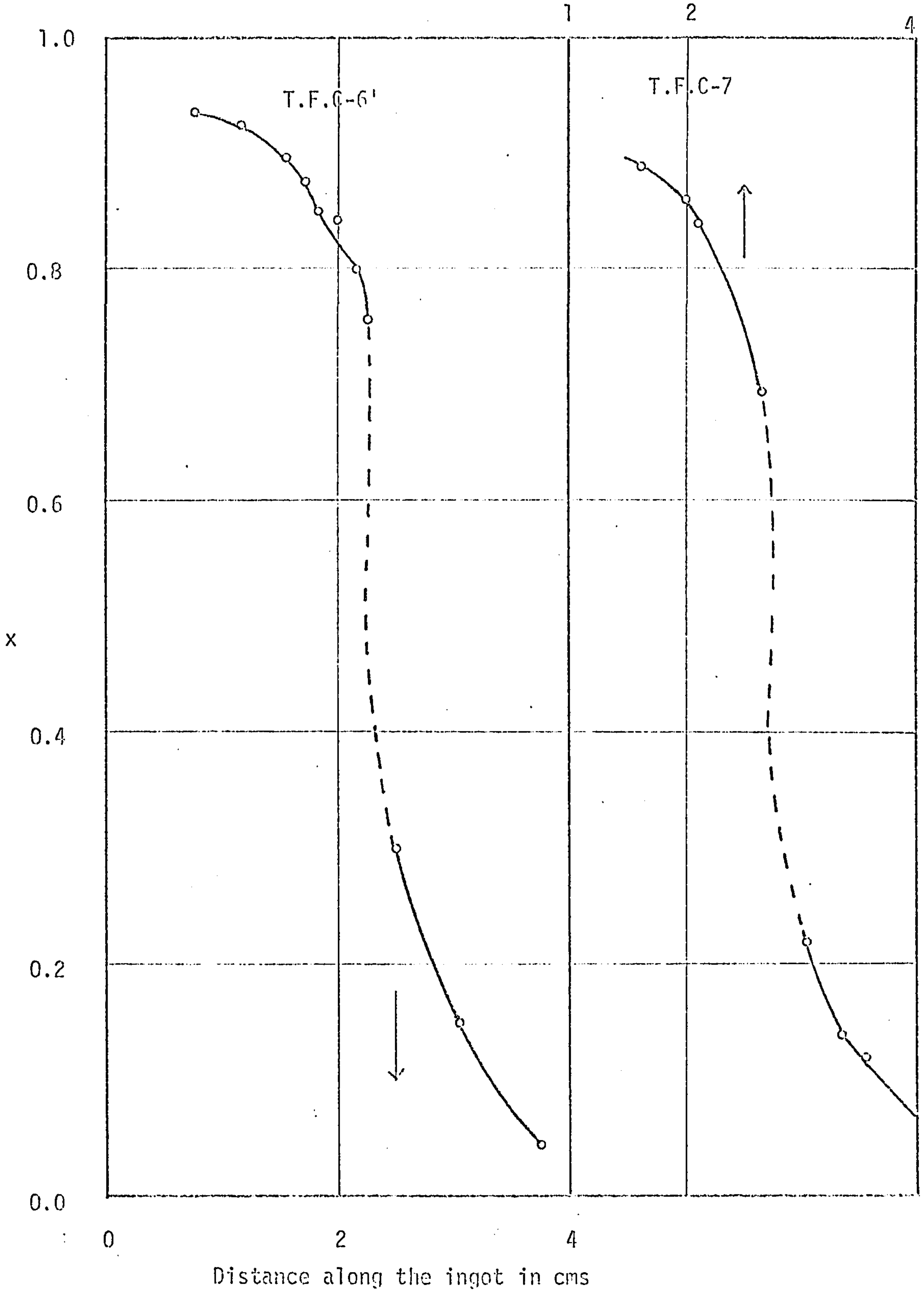

Fig.(2:5) Variation of composition along the length of the ingot for $InAs_xSb_{(1-x)}$ alloys region $0.3 < x < 0.7$ were not successful. It appears that either a very narrow zone method or some other new method should be tried to produce homogeneous alloy materials in the middle region. Fig. (2:5) shows the variation of composition with length of two ingots doped with Tellurium.

d) $GaAs_xSb_{(1-x)}$ alloys

Very little work has been done on this alloy system. Homogeneous bulk samples over the entire range of composition have not yet been produced. Complete solid solution exists and the solidus curve determined by Woolley (62W1) is shown in Fig. (2:6). A guess of the liquidus curve is also shown by the dashed curve. The extreme separation between the liquidus solidus curves and the steepness of the solidus curve make it very difficult to produce this alloy system.

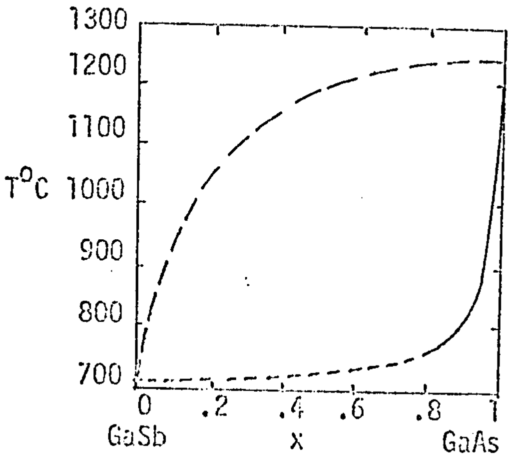

Fig. (2:6) T-x Phase diagram for $GaAs_xSb_{(1-x)}$ alloys

According to Muller and Richards (64M2) a miscibility gap will exist in a III-V alloy system when the atomic radius difference between the atoms undergoing substitution exceeds a critical value of 17%. Arsenic and Antimony atoms have a radius mismatch of 17% and is just at the limit. This mismatch accounts for the extreme difficulty for forming these alloys. The difficulties in this system are enhanced above the InAs - InSb system by the fact that the constituents have high melting points and high vapour pressure.

The variation of composition with lattice parameter has never been accurately determined. Preparation of epitaxial layers of the alloys of full composition range was first reported by Potter and Stierwalt (64P3). They assumed Vegard's law to determine the composition from lattice parameter. Straumanis and Kim (65S1) have produced alloys of this system annealing powders for very long time. They have reported from lattice parameter measurements that Vegard's law is obeyed in the range $0 < x < 0.45$ and above this range homogeneousmaterial is not obtained. Sahm ad Press (67S1) had partial success in producing GaSb rich end of the alloy by the method of pressure sintering of powders. There was composition spread of 5 mol % in the samples and the samples near the middle region showed two phase behaviour.

The project of growing this alloy system was taken up by the author. GaSb was made in the laboratory from the elements as described in section 2.6a and GaAs was obtained from Monsanto Chemical Company. As a first trial compressed powders of the mixture at few compositions were annealed at the appropriate temperature below the estimated solidus curve for nearly three months. X-ray powder photographs on the samples showed that the lines corresponding to the two compounds were coming closer. The samples were annealed for longer times and the x-rays after that still showed the existence of two phase. However the equilibrium condition was not reached. The success of step freeze technique in producing InAs - InSb alloys,prompted to apply the method for these alloys also. The hot zone of the furnace was set at 1100°C and the ingot was moved at the rate of 0.8cms/day, towards the cold zone kept at a temperature of 600°C. From a initial composition of $x = 0.3$, a 20grm ingot produced by this method showed a slow variation of composition along the length from $x = 0$ to 0.08 and $x = 0.90$ to 0.1 with a break in between as shown in Fig. (2.7). The compositions were determined from cross-sectional slices by x-ray powder photographs assuming Vegard's law. The x-ray back reflection lines were very well defined showing good homogeneity of the specimens. One more trial of the same method did not show any improvement in the composition range obtained. It was thought, that travelling zone method should prove more feasible, since the melting points of the

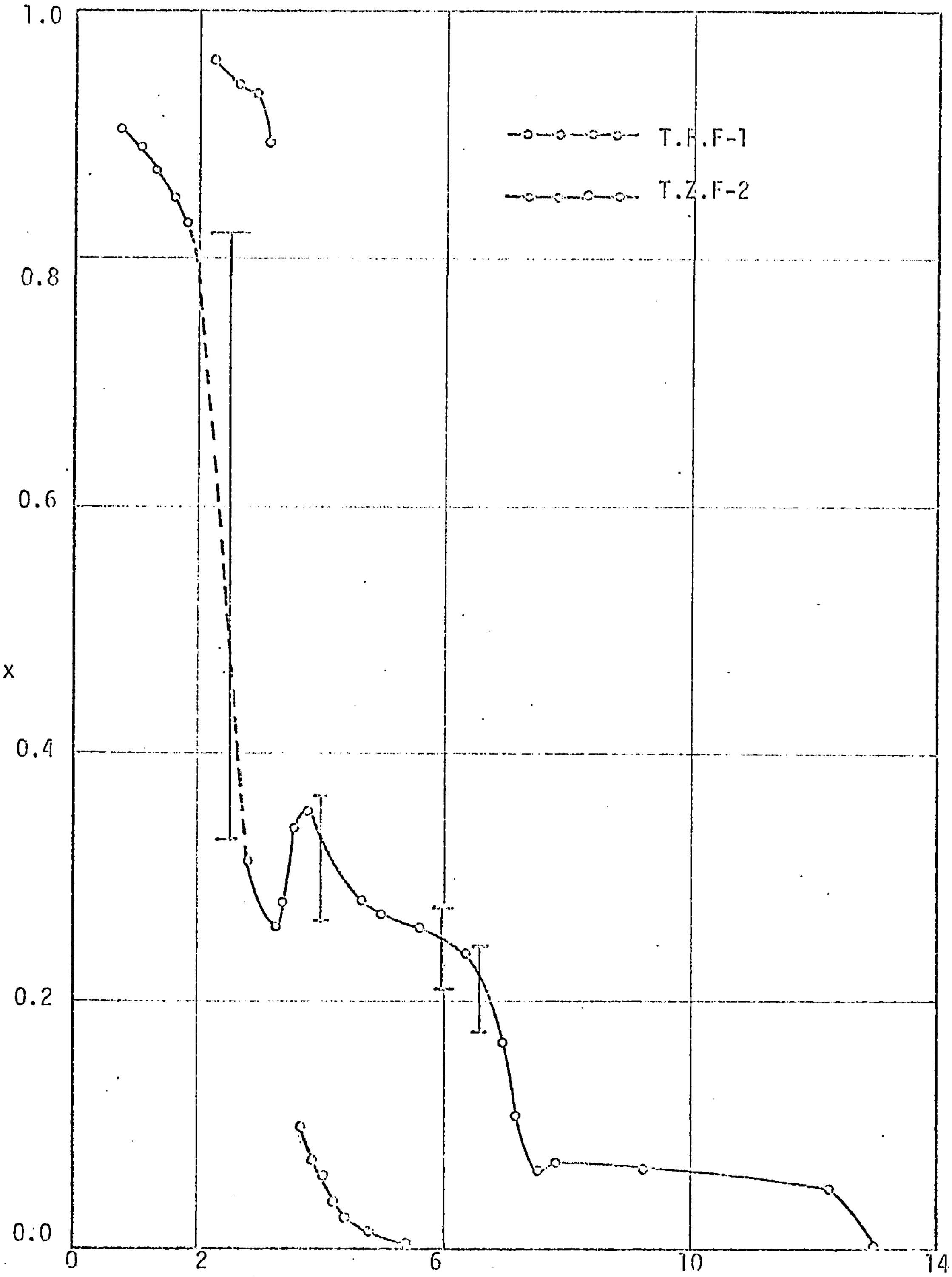

Fig.(2:7) Variation of composition along the length of the ingot for $GaAs_xSb_{(1-x)}$ alloys components are high and the zone width at this temperature is narrow. This technique was tried with a 4" zone at a temperature of 1100^{o}C (This temperature was the safe high temperature limit for the furnace) and background temperatures of 600^{o}C on either side. A 50gm ingot with an initial charge of $x = 0.3$ was placed inside the zone furnace and the furnace was moved at the rate 0.5cm/day. A 12" ingot was produced in about 50 days, which showed a nonuniform variation of composition along the length with several multiphase regions in between as shown in Fig. (2:7). The bars (I) indicate the extent of two phase and its spread along the length. The nonuniform variation of composition indicates that zone levelling was indeed taking place, but it was soon upset by the difficulty to maintain equilibrium condition. In many samples the x-ray back reflection lines were slightly blurred showing inhomogeneity. However samples with relatively good homogeneity for optical measurements were obtained in the regions $0 < x < 0.34$ and $0.85 < x < 1.0$. The samples near the GaAs end were n-type, while the samples near GaSb end were p-type. The next attempt by the same method did not produce any better results. Hence the step freeze method was tried few times setting the hot and cold zone at relatively higher temperatures than in the previous attempts and making a steeper temperature gradient in between the zones. In most cases the result was Ga separating from the ingot with little or no alloy being produced. The author has tried to grow nearly ten ingots of this system. The only hope for further success is to either use a very narrow hot zone in a T.Z. furnace or to try some other methods such as the step levelling or the solute build up method mentioned in section 2.5d. Recently growth of single crystals from vapour phase has been reported (69C1).

CHAPTER III

OPTICAL ABSORPTION AND THERMOELECTRIC POWER

3.1 Optical Absorption in Semiconductors

The determination of the optical constants of a semiconductor over a wide range of wavelength can provide a wealth of information about the band structure. Optical constants are determined from reflection and absorption measurements. Thin samples are necessary for absorption measurements. There are three major processes of absorption to be considered. At short wavelengths the photons can excite electrons from the valence to the conduction band and this process is called interband absorption. The process starts at a wavelength corresponding to the energy gap of the semiconductor. The absorption coefficient is very high in this region of wavelength and falls off sharply past the energy gap towards the longer wavelength side. This rapid decrease in absorption coefficient occurs over a very small energy range and the absorption curve in this region is called the absorption edge. Careful study of the position and internal structure of the absorption edge can provide very useful information about the structure of the conduction and valence bands, especially the regions very close to the extrema. The most extensive study of these edges has been carried out in Germanium (57M1) and Silicon (58M1). After the development of high resolving power infrared spectromters and the discovery of magneto absorption, the study of the absorption edge has become a very powerful technique for the investigation of the band structure of the semiconductors near the fundamental gap.

At longer wavelengths the semiconductor is nearly transparent. However, in an impure sample the long wavelength photons can interact with the free electrons and holes and the resulting transitions take place either within the valence or the conduction band. This process is called free carrier absorption and it can give information about the effective mass and mobility of the carriers in the appropriate band.

At wavelengths longer than about 10μ there can be also interaction between the photons and the lattice. There is a strong absorption of electromagnetic radiation corresponding to the transverse optical phonon frequency of the lattice and this is responsible for the reststrahlen absorption band. The coupling of the photons with the optical phonon modes is very strong in polar semiconductors, for example in III - V compounds.

Another minor process is the absorption due to impurity levels in the forbidden gap, and this can produce small bumps on the absorption edge. There is also another process to be considered. Bound electron-hole resonant states called excitons are formed below the threshold energy and transitions into these levels give rise to a hydrogen like absorption spectrum. Because of the large dielectric constant in semiconductors the electrons and holes are strongly screened and the exciton effects are weak, while in insulators these effects are very strong. Since the author was not studying the fine structure of the absorption edge, these effects were not considered and it will not be discussed here. Good references (66P1) on this subject are available.

a) Classical theory of free carrier absorption

An electromagnetic wave propogating through a refractive medium can be written as

$$E\,(x,t) = E_0 \; exp\,[\,i\,\omega\,(\,t - \frac{n^* x}{c}\,)\,]$$

where η^* is the complex refractive index defined by $\eta^* = \eta - i\kappa$. η is the real part of the refractive index and κ is the absorption index.

$$\text{or} \quad E = E_0 \; exp \; [i\,(\,\omega\,t - \frac{\omega\eta x}{c}\,)\,] \;.\; exp\,(\,-\frac{\omega\kappa x}{c}\,)$$

The absorption coefficient α which measures the attenuation of the wave is defined by

$$\alpha = \frac{2\omega\kappa}{c} = \frac{4\pi\kappa}{\lambda} \qquad \ldots\ldots \; [3:1]$$

The equation of motion of electrons in a solid under the influence of an electric field $E = E_0 \, exp\,(i\omega t)$ can be expressed as

$$m^* \ddot{x} + \frac{m^*}{\tau} \dot{x} = e \, E_0 \, exp \, (i\omega t) \quad \ldots \; [3:2]$$

where m^* is the characteristic effective mass of the electrons, x is the displacement, and τ is the relaxation time. This equation can be solved for x and the free carrier susceptibility can be calculated. The total susceptibility of the crystal can be obtained by adding the bound carrier and lattice contributions. This quantity is generally complex. It is a usual practice to separate the real and imaginary parts and hence obtain the real and imaginary parts of the dielectric constant, ε_1 and ε_2 (59M1). Since τ and m^* are functions of energy these quantities should be averaged over all energies. If there are more than one type of carriers involved ε_1 and ε_2 may be expressed as (M.K.S. Units are used)

$$\varepsilon_1 = \eta^2 - \kappa^2 = \varepsilon_\infty - \sum_j \frac{n_j e^2}{\varepsilon_0} \left\langle \frac{\tau_j^2}{m_j^*(1 + \omega^2\tau_j^2)} \right\rangle \quad \ldots \; [3:3]$$

$$\varepsilon_2 = 2 \, \eta \, \kappa = \sum_j \frac{n_j e^2}{\varepsilon_0 \, \omega} \left\langle \frac{\tau_j}{m_j^* \, (1+\omega^2\tau_j^2)} \right\rangle \quad \ldots \; [3:4]$$

where the averages are defined by

$$\langle A \rangle = \frac{\displaystyle\int_0^\infty \frac{\partial f_0}{\partial E} A k^3 \, dE}{\displaystyle\int_0^\infty \frac{\partial f_0}{\partial E} k^3 \, dE}$$

In the above equations ε_0 is the dielectric constant of free space, ε_∞ is the lattice contribution to the dielectric constant and is a constant at high frequencies (optical dielectric constant), j refers to each type of carriers and n_j is the concentration of carriers of the type j. The absorption coefficient can be calculated from equations [3:1] and [3:4].

$$\alpha = \sum_j \frac{n_j e^2}{n \varepsilon_0 c} \left\langle \frac{\tau_j}{m_j^* (1 + \omega^2 \tau_j^2)} \right\rangle \quad \ldots [3:5]$$

In order to interpret the energy band structure in terms of the absorption coefficient, equation [3:5] should be rigorously evaluated using quantum mechanical treatment for the particular scattering mechanisms involved. However, for one type of carriers, under the assumptions of energy independent relaxation time and $\omega\tau >> 1$, it can be easily shown that equation [3:5] reduces to the simple expression having a quadratic dependence on the wavelength.

$$\alpha = \frac{n e^3 \lambda^2}{4\pi^2 \varepsilon_0 m^{*2} c^3 \eta\mu}$$

where μ is the mobility. The λ^2 dependence of α is also obtained for acoustic phonon scattering from the general equation [3:5]. Moss (59M1) has observed the quadratic dependence for n-type InSb with carrier density $3.5 \times 10^{23} m^{-3}$. Visvanathan (60V1) has calculated a wavelength dependence $\lambda^{2.5}$ for polar scattering. For ionized impurity scattering the power factor can be as high as 3.5.

b) Interband absorption

There are two types of transitions possible from the valence to the conduction band. If both band extrema lie at the same point in the Brillouin zone, and if states are available, transition between the upper edge of the valence band to the lower edge of the conduction band is possible. This process is called direct transition, where k values do not change. When the band extrema lie at different k values only phonon assisted transitions are possible between the two bands. This type of transitions are referredto as indirect transitions, where k

values of the electron before and after the transition are different.

The problem of interband absorption has to be treated from quantum mechanical considerations. The absorption coefficient associated with this process depends on the probability per unit time that an electron will make a transition from the valence to the conduction band. If we consider radiation as a beam of photons falling normally on a semiconductor, the absorption coefficient α is given by the number of quanta absorbed per unit time per unit volume divided by the flux density. Thus for a simple parabolic band the absorption coefficient due to direct transitions can be shown to be (67W1)

$$\alpha_a = \frac{c}{\eta \pi \nu} \left(\frac{2m_r}{\hbar^2} \right)^{3/2} \cdot \left| H_{cv}(0) \right|^2 (h\nu - E_0)^{\frac{1}{2}}$$

$$\equiv A \ (h\nu - E_0)^{\frac{1}{2}} \qquad \ldots\ldots [3:6]$$

If direct transitions are forbidden the absorption coefficient is given by

$$\alpha_f = \frac{c}{\eta \pi \nu} \left(\frac{2m_r}{\hbar^2} \right)^{3/2} \left| \frac{\partial H_{cv}(k)}{\partial k} \right|^2_{k=0} (h\nu - E_0)^{3/2}$$

$$\equiv B \ (h\nu - E_0)^{3/2}$$

where η is the index of refraction, m_r is the reduced mass of the electron hole pair, H_{cv} is the optical matrix element between the conduction and valence band states and ν is the threshold frequency. Thus for a simple parabolic band the absorption coefficient is proportional to $(h\nu - E_0)^{\frac{1}{2}}$. If the implications of Kane model are considered equation [3:6] is not strictly true. Instead of using the density of states for parabolic band, the density of states obtained from Kane's equation should be used in deriving the absorption coefficient. Also the optical matrix element will be given by (57K1)

$$\left| H_{c,v}\,(0) \right|^2 = \frac{2m^2 p^2}{3\hbar^2}$$

However, from detailed calculations of the absorption coefficient using Kane model and comparing with experimental results, it has been shown that the relation $\alpha \propto (h\nu - E_0)^{\frac{1}{2}}$ still holds good for InSb (67W1) and InAs (60S1) over a wide range of photon energy.

The theory of indirect transitions involving acoustical or optical phonons is more complicated. It may be shown that for a simple band the absorption coefficient has the form (67W1)

$$\alpha = C\,(h\nu - E_0 \pm k\,\theta)^2$$

where $k\,\theta$ is the phonon energy. If transitions are forbidden to the intermediate state at $k = 0$, then a cubic dependence is obtained.

c) Burstein effect

In a degenerate sample the position of absorption edge is shifted towards energies higher than that for the pure sample. This was correctly explained by Burstein (54B3) as due to the population of energy bands with carriers. In such a case transitions are not possible at $k = 0$ and take place at a slightly different value of k where states are available. Fan (56F1) has shown that the absorption corresponding to a given value of k is given by

$$\begin{aligned} \alpha\,(k) &= \alpha_0\,(k)\,\left(f_V - f_C\right) \\ &= \alpha_0(k)\left[1 - \frac{1}{1 + exp\left(\frac{E_C(k) - E_F}{KT}\right)}\right] \qquad \ldots[3:7] \end{aligned}$$

where $\alpha_0(k)$ is the absorption coefficient if it were possible to have transitions at $k = 0$. The photon energy corresponding to a given transition is given by

$$h\nu\,(k) = E_0 + E_C\,(k) + E_V\,(k)$$

substituting for $E_C(k)$ from equation [3:7]

$$h\nu\,(k) = E_0 + \left[E_F + KT\,\ell n\,\left(\frac{\alpha/\alpha_0}{1-\alpha/\alpha_0}\right)\right]\left[1 + \frac{E_V(k)}{E_C(k)}\right] \qquad \ldots\,[3:8]$$

At a finite temperature, since the tail of the Fermi function extends approximately 4 KT below the Fermi energy, transition starts at this energy.

For parabolic bands $\frac{E_v(k)}{E_c(k)} = \frac{m_c}{m_p} << 1$

This is true for Kane bands also. Hence the term $\frac{E_v(k)}{E_c(k)}$ in equation [3:8] is negligible.

The term $KT\, \ell n \left(\frac{\alpha/\alpha_0}{1-\alpha/\alpha_0}\right)$ is also very small and can be neglected as a first approximation. Thus equation [3:8] may be written, when $E_F > 4KT$

$$h\nu\,(k) = E_0 + E_F - 4KT \qquad \ldots [3:9]$$

3.2 Theory of thermoelectric power

When a thermal gradient ΔT is set up along the length of a semiconductor sample, a small voltage ΔV is developed between the ends and the thermoelectric power of the material is defined by

$$\theta = \frac{\Delta V}{\Delta T}$$

It is independent of the shape of the sample and is usually in the microvolt range. The thermoelectric power of a semiconductor depends on carrier concentration and the energy band structure of the populated bands. Information such as the position of the Fermi level, structure of the band and scattering mechanisms can be obtained from thermoelectric power measurements.

It may be shown that in general, for spherical energy surfaces the thermoelectric power is given by (6221)

$$\theta = -\frac{K}{e}\left[\frac{\displaystyle\int_0^\infty \left(-\frac{\partial f_0}{\partial k}\right) \mu\, \xi\, k^3 \; dE}{\displaystyle\int_0^\infty \left(-\frac{\partial f_0}{\partial k}\right) \mu\, k^3 \; dE} - \zeta\right] \quad \ldots [3:10]$$

where $\xi = \frac{E}{KT}$ is the reduced energy, $\zeta = \frac{E_F}{KT}$ is the reduced Fermi energy, μ is the mobility of the carriers, K is

Boltzmann constant,

and $f_0 = \dfrac{1}{1+exp(\xi-\zeta\ )}$ is the Fermi distribution function.

Remembering $\mu = \dfrac{e\tau}{m^*}$ and using the definition for the effective mass

$$\frac{1}{m^*} = \frac{1}{\hbar^2 k} \frac{dE}{dk}$$

equation [3:10] may be written as

$$\theta = -\frac{K}{e} \left[\frac{\displaystyle\int_0^\infty k^2 \left(-\frac{\partial f_0}{\partial k}\right) \left(\frac{dE}{dk}\right) \tau\, \xi\, dE}{\displaystyle\int_0^\infty k^2 \left(-\frac{\partial f_0}{\partial k}\right) \left(\frac{dE}{dk}\right) \tau\, dE} - \zeta \right] \quad \ldots [3:11]$$

Equation [3:11] is a general expression for any dispersion law E vs k and the integrals have to be evaluated for the particular E - k relation.

a) Scattering mechanisms

In order to evaluate the above integrals one has to define a relaxation time for the particular scattering process involved. Hence a knowledge of the scattering process is necessary in order to interpret the results of thermoelectric power measurements. However,the thermoelectric power in a high magnetic field (Longitudinal Nernst - Ettingshausen effect), is independent of the scattering mechanism and combining the two measurements is a convenient method of investigating the scattering process in a semiconductor (68A1).

For a parabolic band the relaxation time τ is related to k or E by a power factor, usually defined as the scattering parameter. One can write for instance

$$\tau = \tau_0 E^s \qquad \text{........ [3:12]}$$

where s takes different values for each scattering mechanism.

$s = -\frac{1}{2}$ for acoustic phonon scattering

$s = +\frac{1}{2}$ for optical phonon scattering
or piezoelectric scattering

$s = +\frac{3}{2}$ for ionised impurity scattering

For a nonparabolic band the simple equation [3:12] is no longer true and more complicated expressions have to be used.

<u>Acoustic phonon or deformation potential scattering</u>

Due to the thermal energy of the lattice, lattice vibrations are produced causing the lattice spacing to vary periodically resulting in small periodic perturbation of the crystal potential. This deformation potential is responsible for the acoustic mode of scattering and a quantum mechanical treatment using perturbation theory has to be carried out to obtain the relaxation time. It has been shown that the relaxation time for a nonparabolic band is given by (59E1)

$$\tau = \frac{\pi \hbar d u_l^2}{E_1^2 \ KT} \quad \frac{1}{k^2} \quad \frac{dE}{dk} \qquad \ldots [3:13]$$

where the substitution $\rho(k) = \frac{k^2}{\pi^2} \frac{1}{(\frac{dE}{dk})}$ for the density of states of a nonparabolic band (67W1) has been used. U_l is the velocity of longitudinal sound waves, d is the density, and E_1 is the deformation potential constant.

Optical phonon scattering

For optical mode of vibration the adjacent atoms have a vibrational phase difference of 180°. This causes a polarisation of the crystal and an interaction with the carriers may result. The interaction is very strong in compound semiconductors where the adjacent atoms are of opposite ionic charge. The energy associated with the optical modes is greater than that associated with the acoustic modes and is approximately $h \omega_l = K T_l$, where T_l is the longitudinal optical phonon temperature and is a few hundred °K for semiconductors.

For low temperatures ie $T < T_1$ it is not possible to define a relaxation time because the energy change on scattering is not small compared to the total energy of the scattered carriers (59E1, 61E1). At high temperatures $T > T_1$ a relaxation time can be defined and it may be shown (53H1, 57E1)

$$\tau = \frac{M\, v\, \hbar\, \nu_0^{\,2}}{4\,(e\, e^*)^2 KT} \; \frac{dE}{dk} \qquad \ldots [3:14]$$

where M is the reduced ionic mass, v is the volume of the unit cell of the lattice, e^* is the effective ionic charge and ν_c is the frequency of optical phonons.

Ionised impurity scattering

The coulomb filed of an ionised impurity atom causes scattering of the carriers. First theoretical calculation of the relaxation time was carried out by Conwell and Weisskopf (50C1). Brooks and Herring (55B2) later carried out a more accurate calculation taking into account the screening of the coulomb field by the free carriers. There have been many further refinements tothese equations (59T1). An expression for relaxation time based on Brooks - Herring equation, applicable for nonparabolic bands has been obtained by Barrie (56B1)

$$\tau = \frac{\hbar\,\varepsilon^2}{2\pi\, e^4\, N}\; k^2\; \frac{dE}{dk} \left[\ln\left(1+\frac{4k^2}{q^2}\right) - \frac{4k^2/q^2}{1+4k^2/q^2} \right]^{-1} \qquad \ldots\ [3:15]$$

where N is the concentration of scattering centres, ε is the dielectric constant, and q is the screening constant of the scattering centres. It can be shown that the term inside the bracket is a slowly varying function of k, and it can be treated as a constant for all practical purposes.

There are various other scattering mechanisms which may be of importance under special conditions. Some of them are, electron-electron scattering (54D1), electron-hole scattering (57E1), alloy scattering (31N1, 55B2), neutral impurity scattering (50E1, 56S1), intervalley scattering (55H2, 57B1, 55B1) and dislocation scattering (52D1). Since III - V compounds are cubic crystals lacking inversion symmetry, there can be electric polarisation associated with the acoustic mode of the lattice vibrations and this can cause scattering. This is called piezoelectric scattering (56H1) and may be an important mechanism in III - V compounds at low temperatures (64K1). An excellent discussion of the various scattering mechanisms with particular emphasis on galvenomagnetic experiments is given by Beer (63B3).

Equation [3:13] , [3:14] and [3:15] can be generalised for all the three scattering mechanisms and for an arbitrary band shape.

$$\tau = \Lambda k^{2s-1} \frac{dE}{dk} \quad \ldots [3:16]$$

where Λ is a constant. When more than one scattering mechanisms are involved, the total relaxation time can be taken to add up reciprocally. For a parabolic band equation [3:16] reduces to the familiar equation [3:12]. In most of the III - V compounds the effect of nonparabolicity is extremely important as reported by Zawadzki (62Z1) and should be taken into account.

b) Expressions for thermoelectric power

Parabolic band

For a parabolic band the dispersion law is

$$E = a k^2$$

Using this dispersion law and equation [3:12] it may be easily shown from equation [3:11]that

$$\theta = -\frac{K}{e}\left[\frac{(s+\frac{5}{2}) \quad F_{s+3/2}(\zeta)}{(s+3/2) \quad F_s(\zeta)} - \zeta\right] \quad \ldots [3:17]$$

where F_s is the standardFermi integral defined by

$$F_s = \int_0^\infty \frac{\xi^s}{1 + exp(\xi - \zeta)} \quad d\xi$$

Equation [3:17] is applicable for general degeneracy. However, for a non-degenerate case ζ is negative and the Fermi integrals can be expanded in terms of gamma functions

$$\text{ie} \qquad F_s = \exp(\zeta)\ \Gamma(s + 3/2)$$

Using this expansion we get

$$\theta = -\frac{k}{e}\left[(s + 5/2) - \zeta\right]$$

The Kane band

The Kane equation [1:8] for the conduction band, for $\frac{m}{m_0^*} << 1$ gives

$$k = A\left[\frac{E}{E_0^*}\left(1 + \frac{E}{E_0^*}\right)\right]^{\frac{1}{2}} \qquad \ldots [3:18]$$

where A is a constant. Using equation [3:18] in equation [3:11] and neglecting terms in β^2 and higher order it may be shown (61G1)

$$\theta = -\frac{K}{e}\left[\frac{(s + 5/2)\ \beta F_{s+5/2}(\zeta) + (s + 5/2)\ F_{s+3/2}(\zeta)}{(s + 5/2)\ \beta F_{s+3/2}(\zeta) + (s + 3/2)\ F_s(\zeta)} - \zeta\right] \ldots [3:19]$$

where $\beta = \frac{KT}{E_0^*}$

Multiband transport

If more than one type of carriers are involved in the conduction process, the combined effect will be the weighted sum of the different bands involved.

ie $$\theta = \gamma_1 \theta_1 + \gamma_2 \theta_2 + \gamma_3 \theta_3$$

where $\gamma_i = \frac{\sigma_i}{\sigma}$, σ being the conductivity. If the thermoelectric power is expressed in terms of the conductivities and mobilities

$$\theta = -\frac{K}{\sigma} \sum_i \left[\frac{< \mu_i \xi >}{< \mu_i >} - \zeta_i \right] \mu_i n_i$$

where ζ_i is measured from the extrema of the band involved, n_i is the carrier concentration and

$$< A > = \int_0^\infty \left(-\frac{\partial f_0}{\partial k} \right) A \; k^3 \, dE$$

Similarly for a Kane band

$$\theta = -\frac{K}{\sigma} \sum_i \left[\frac{(s + 5/2) \beta F_{(s+5/2)}(\zeta_i) + (s + 5/2) F_{(s+3/2)}(\zeta_i)}{(s + 5/2) \beta F_{(s+3/2)}(\zeta_i) + (s + 3/2) F_s(\zeta_i)} - \zeta_i \right] \mu_i n_i$$

In the case of contribution of electrons and holes the thermoelectric power for parabolic bands becomes

$$\theta = -\frac{K}{\sigma}\left\{\left[\frac{(s + 5/2)\ F_{s\ +\ 3/2}\,(\zeta_n)}{(s + 3/2)\ F_s\ (\zeta_n)} - \zeta_n\right]\mu_n\ n\right.$$

$$\left. - \left[\frac{(s + 5/2)\ F_{(s\ +\ 3/2)}\,(\zeta_p)}{(s + 3/2)\ F_s\ (\zeta_p)} - \zeta_p\right]\mu_p\ P\right\}$$

where $\zeta_n \quad = \quad \dfrac{E_F - E_c}{KT}$

and $\zeta_p \quad = \quad \dfrac{E_v - E_F}{KT} \quad = \; - \left(\zeta_n + \dfrac{E_0}{KT}\right)$

For a nondegenerate case this equation becomes

$$\theta \;=\; -\frac{K}{\sigma}\left\{[(s+5/2) - \zeta_n]\ \mu_n\, n \;-\; [(s + 5/2) - \zeta_p]\ \mu_p\ P\right\}$$

Similar equations can be written for Kane bands also.

3.3 Energy gap variation in III - V alloys

It was widely believed (38M1, 60P1) that the virtual crystal model would give rise to a linear variation of energy gap with composition. However, recently it has been pointed out by Van Vechten and Bergstresser (69V3) that even for a virtual crystal approximation, one does not expect the variation of the energy gap to be linear because the energy gap is not a linear function of the assumed potential for any of the commonly used methods of band structure calculation. They have used the dielectric method of band calculation (69P1, 69V2), taking the parameters of the theory to vary linearly with composition in the spirit of virtual crystal approximation, in order to calculate the variation of energy gap in the alloys. The resulting deviation of the energy gap from linearity has been shown to be concave and parabolic.

There exists no rigorous theory for the effect of the disorder in the crystal potential. However, during the early development of the theory of alloys Mott and Jones (36M1) have shown that this effect also produces a concave deviation of the energy gap, if a second order perturbation calculation is carried out. This may be seen from some simple arguments.

Consider an alloy of x mole fraction of material A and (1-x) mole fraction of material B. Then the average potential of each atom is

$$V = x V_A + (1-x) V_B$$

The deviation from this potential for atom A is

$$V - V_A = (1-x)(V_B - V_A)$$

and $V - V_B = x (V_A - V_B)$ for atom B

Hence the probabilities that an electron will be scattered or involved in any other similar process due to these deviations in potential are proportional to $(1-x)^2$ and x^2 respectively. Since there are x atoms of A and (1-x) atoms of B, the total probability is proportional to

$$x(1-x)^2 + (1-x) x^2 \equiv x(1-x)$$

This suggests that the deviation of E_0 from linearity due to disorder potential could be parabolic. From a consideration of the expectation value of the deviation of the actual potential Van Vechten and Bergstresser have calculated this deviation and shown to be parabolic. Thus total deviation of E_0 of an alloy from the straight line joining the values of the compounds is the sum of two effects. One is an intrinsic effect (virtual crystal effect) and the other is an extrinsic effect (effect of disorder potential). Hence the variation E_0 with the mole fraction x for a III - V alloy system is parabolic and may be written

$$E_0 = A + B\ x + C\ x^2 \quad \ldots[3:20]$$

where $A = E_0$ for compound #1

$A + B + C = E_0$ for compound #2

and $C = C_i + C_e \quad \ldots [3:21]$

C_i and C_e represent the intrinsic and extrinsic deviations. C is also equal to four times the deviation from linearity at $x = 0.5$. An equation of the form [3:20] has been successfully applied by Cardona (63C2) to the energy gap variation of the alloys of Silver and Cuprous hallides, and by Thompson and Woolley (67T1) to the energy gap variation of III - V alloys. From a consideration of data for four III - V alloy systems, C appeared to satisfy an empiricalrelation

$$C = \alpha\ E_{om}^{-\frac{1}{2}} \quad \ldots [3:22]$$

where α is a constant of value approximately 0.3 $ev^{3/2}$ and E_{om} is the mean value of E_0 for the two compounds concerned. Hence Thompson and Woolley suggested that the above relation should hold good for all III - V alloys and it is possible to predict the energy gap variation in other III - V alloys on which experimental results are not available. According to Van Vechten and Bergstresser C_i can be obtained from the energy gap variation calculated assuming virtual crystal model and C_e from the disorder potential. They have also shown that

$$C_e = C^2_{A,B} / L \qquad \text{... [3:23]}$$

where L is a constant and $C_{A,B}$ is the electronegativity difference (68P1) of the elements A and B being substituted in the alloy. Hence theoretically it is possible to calculate C and compare with experimental results. This would enable to check the validity of the empirical relation.

3.4 Review on energy gap measurements

The forbidden gap for all the III - V compounds has been studied extensively for its dependence on temperature, pressure, impurity concentration, magnetic field, electric field and similar parameters. The fine structure of the absorption edge has also been investigated. For all III - V compounds the energy gap has a negative temperature coefficient. Study of the pressure dependence of the absorption edge can provide considerable information about the relative positions of the bands in the Brillouin zone and their relative movement under pressure (61P1). The magnitude of the pressure coefficient for the various bands of a compound is very different. It could be different in sign also. For small amounts of impurity concentration the absorption edge is shifted to higher energies due to Burstein effect. Burstein shift was first observed in InSb by Tanenbaum and Briggs (53T1) and interpreted by Burstein (54B3). Later the same effect was observed in InAs (54H4, 54B2, 55K1, 54H3, 55S1), GaAs (63K2) and in GaSb (58R1, 61B1). However, in compensated samples strong doping can lead to a decrease in energy gap (59S3), because the impurity levels near the conduction and valence bands can broaden and merge with the bands. There is some evidence that high impurity concentration can alter the band structure also. Kwan and

Woolley (68K2) observed that for InAs, ΔE the energy separation between the (000) and <111> conduction band minima decrease with Tellurium content and it appeared that the (000)conduction band was moving away from the valence band. In GaSb (64W1, 69V1) again there is a decrease in energy separation between the <111> and (000) conduction bands with Tellurium content. In this case <111> minima is possibly coming down even lower than the (000) minimum. However, more theoretical and accurate experimental investigations are necessary before the above conclusions can be substantiated.

A brief review of energy gap measurements on the different alloy systems is given in section 2.3. Here the two alloy systems on which experimental data is presented, are considered.

a) $Ga_x In_{(1-x)}$ As alloys

The optical energy gap measurements on this system were first made by Abrahams et al (59A1), on very inhomogeneous samples. Their experimental points show considerable deviation from linearity. Since the samples used for measurements had composition spreads of 5 to 20 mol % the results are not reliable. Woolley et al (61W2) have reported from infrared transmission measurements that there is a linear variation of energy gap up to $x = 0.8$ and beyond this, there is a rapid increase towards the value for GaAs. Some of their samples were multiphase and the annealed solid specimens rich in GaAs had composition spreads of 5 to 10 mol %. Very homogeneous samples of composition up to $x = 0.7$ have been prepared by Hockings et al (66H1) and optical absorption measurements have been carried out. Their energy gap values show considerable deviation from linearity; at the same time there is no agreement with either of the previous measurements. Thompson - Woolley relation for the energy gap variation in III - V alloys (section 3.3) has been found to hold good for four alloy systems on which experimental data were available at that time. However, for this alloy system, there was uncertanity as to the experimental value of C. From the results of Woolley et al a value of $C = 0.28$ was obtained, although the data gave only poor fit to the quadratic equation, while the results of Hockings et al, with a better fit to the quadratic equation gave $C = 0.56$. Neither of the previous results could be expected to be accurate for the following reasons. (i) Neither took account of any Burstein shift which could raise the observed energy gap E_g above the intrinsic gap E_0, particularly in the InAs rich alloys. (ii) In the range $0.8 < x < 1.0$, Woolley et al used samples annealed in solid ingot form, which, as a result were not in a good homogeneous condition.

(iii) Hockings et al used the arbitrarily assumed criterion that the energy gap corresponds to the photon energy with half the maximum transmission. Points (i) and (ii) would account for the fact that the results of Woolley et al gave a poor fit to the quadratic equation while point (iii) could account for the low values of energy gap obtained by Hockings et al. Hence further work has been carried out to determine the energy gap variation from transmission measurements on homogeneous materials and clarify the validity of the empirical relations proposed by Thompson and Woolley.

b) $GaAs_xSb_{(1-x)}$ alloys

The present state of availability of this alloy system has been already discussed in section 2.6d. No good measurement has been made on this alloy system due to lack of material. Measurements of mobility, thermal conductivity and Seebeck coefficient have been made on samples of poor homogeneity by Sham and Pruss (67S1). Potter and Stierwalt (64P3) have made infrared reflection measurements near the reststrahlen region on epitaxial layers of the alloys. Recently electrical properties at 77°K and 300°K have been reported on vapour grown single crystals of the alloy (69C1).

No results of energy gap values are available, except the results reported in this thesis. The energy gap values in the region $o < x < 0.34$ and $0.85 < x < 1.0$ have been determined by the author from absorption measurements.

3.5 Equipment and Experimental Techniques

a) The optical system

The experimental set up for transmission measurements is standard and is similar to that used by previous workers (60W3). However, the design of the optical system for the present work had to be made a little complicated to fit the system into the pole gap of a 15" electromagnet and facilitate magneto-absorption measurements in the future. The Baird Associates double beam infrared spectrometer available in the department was modified to be used as a single beam monochromator. The radiation source used in the monochromator is a silicon carbide rod available under the trade name Globar. It is heated electrically by a regulated supply of 15 amps and 20 volts, to a temperature of 1100°C. The distribution of energy with respect to wavelength is approximately same as that of a black body at the same temperature, with a peak energy at about 2 microns. The infrared source is enclosed in a cylindrical, water cooled housing pierced by a rectangular aperture through which the source emits radiation. The beam from the source passes through the optical system in the monochromator and a monochromatic beam is produced at the exit slit. The monochromatic beam from the exit slit could come out of the enclosure through a 2½" x 2½" rectangular window on the side.

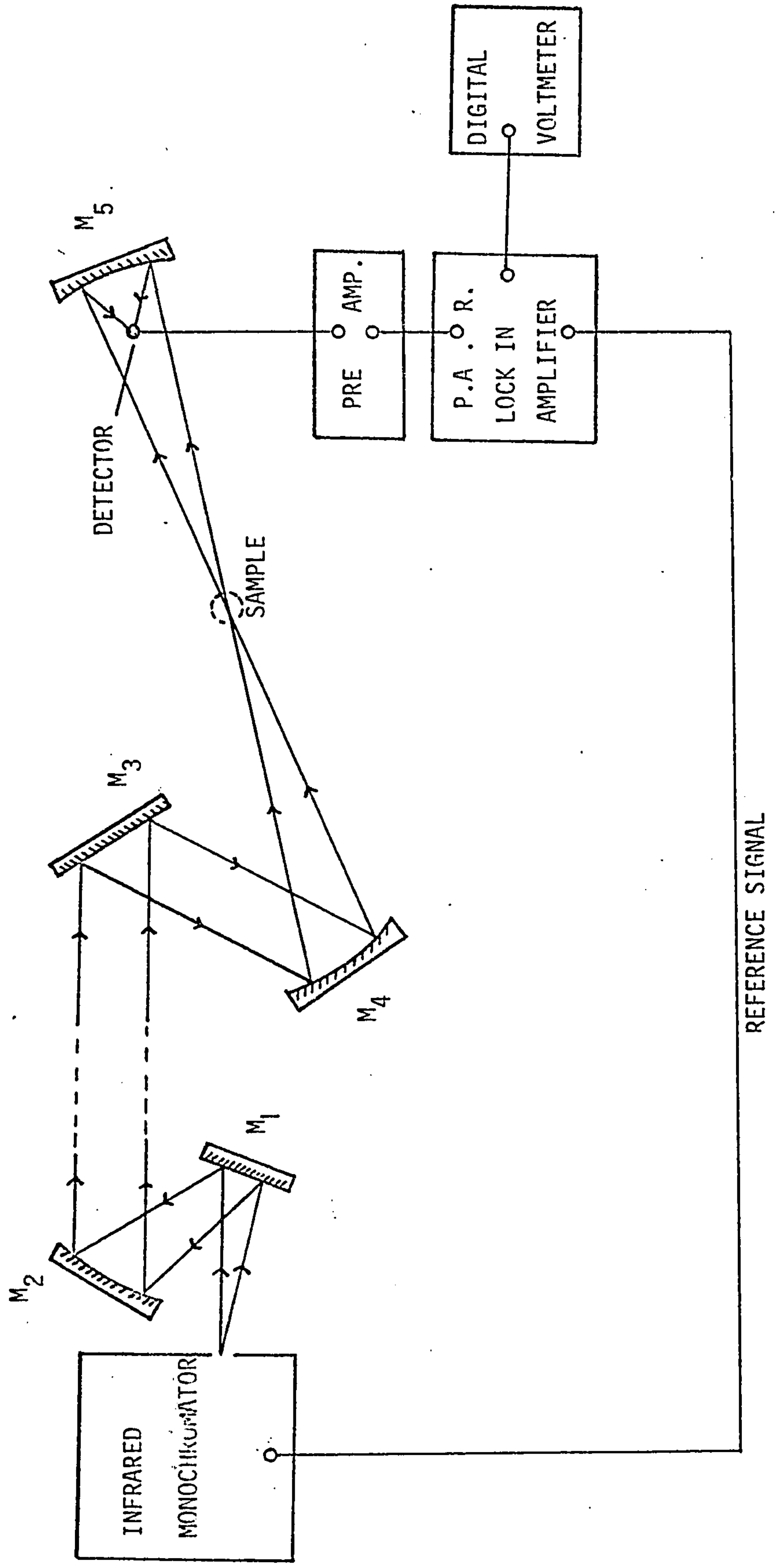

Fig.(3:1) Experimental layout used for absorption measurements

The exit optical system was designed by some mirrors previously used in the double beam spectrometer and some others made at N.R.C. according to specifications. A schematic diagram of the set up is shown in Fig. (3:1). The beam coming out of the monochromator exit slit is reflected by a 4" square plane mirror M_1 and falls on a concave mirror M_2 of focal length 70.5 cms, which is equal to the optical path of the beam from the exit slit. Hence M_2 renders a parallel beam in the horizontal direction. This beam falls on a rectangular plane mirror M_3 placed at 45° angle of incidence. The beam reflected from M_3 falls on a concave mirror M_4 of focal length 20.7 cms, which focuses the beam to an approximate size of 10 x 1 mm, where the sample is to be placed. The beam is then focussed by a concave mirror M_5 of focal length 5.8 cms on to the sensitive element of a bolometer detector which has a KBr window. The sensitive element in the bolometer is a small and extremely thin strip of platinum, with an approximately uniform response to all wavelengths of infrared radiation. The platinum is coated on its receiving side with a thin layer of gold black which serves as a highly efficient radiation absorber uniformly effective at all wavelengths. The bolometer element is mounted in an evacuated housing. The bolometer operates by virtue of the change in resistance of the platinum strip as a function of temperature. To render changes in its resistance measurable the strip is connected to one arm of a balanced Wheastone bridge excited by current from a 6v storage battery. The exciting current through the bolometer is such as to heat the strip to about 50°C above its sorroundings. A change in the temperature of the strip as little as 10^{-5}°C is measurable.

The specimen was mounted on a circular cup, which was held in position in a holder by a push fit arrangement. The mirrors M_1 and M_2 were mounted on a firm base fixed outside the enclosure of the monochromator. The mirrors M_3, M_4, M_5, the detector and the specimen holder were all mounted downwards from a rigid support, which can be moved up and down at an angle of 45°. The main feature of the system was that the distance between M_2 and M_3 could be varied according to convenience and the optics before and after these mirrors could be aligned separately. This kind of arrangement was necessary, since the monochromator associated with its electronics and the system of mirrors M_1 and M_2 were in one room while the rest of the optical system and the magnet were in another room. All the mirrors had three dimensional adjustments. The mirrors were aluminised and coated with silicon monoxide to prevent deterioration. The beam was chopped at the rate of 10cy/sec. Screened leads were taken from the output of the detector to a preamplifier and then to a sensitive amplifier tuned to 10 cycles. The output was rectified and the D.C. voltage was displayed on a digital voltmeter. The reading of the voltmeter was directly proportional to the intensity of the infrared beam incident on the detector. Later a P.A.R. Model 120 lock in amplifier at 10cy fixed frequency was used to obtain higher sensitivity and better signal to noise ratio. The lock in amplifier was operated in the selective external mode. The reference signal was obtained as follows. The output of a 1.5 volt battery in series with a ten thousand ohm resistance was connected to the alternating contacts of the chopper. (These contacts were used as synchronous rectifying contacts previously in the spectrometer). The spacing between the contacts was adjusted with the small screws provided for the purpose, so that a good square wave output of 1.5 volt amplitude was obtained. The output, being in phase with the chopped light beam, was used as the reference signal. The signal output from the preamplifier was fed into the lock in amplifier and then displayed on a digital voltmeter. The highest sensitivity scale available in the lock in amplifier was 100 microvolt giving a full scale deflection of 10 volts at the output. Output time constants of 1 millisecond to 30 seconds in 1, 3, 10 sequence were also available.

b) The wavelength range

For 2 to 16 μ range of wavelength a 60° NaCl prism was used in the monochromator. The spectral wavelength at the exit slit of the monochromator was varied through the use of a specially cut cam mounted on a bearing. A long lever, attached at one end to the rotational axis of a Littrow mirror and provided at the other end with a cam follower, varied the angular setting of the mirror in accordance with the position of the cam. The cam was driven through a train of gears coupled to a dial counter indicating the wavelength. One fast drive and two slow drives of 12 and 24 minutes in the forward direction, and a fast drive in the backward direction were available for scanning from 2 to 16 microns of the spectral range. In order to obtain uniform intensity over the whole spectral range there was a specially cut cam mounted on the same drive above the wavelength cam. The variation of the slit width and hence uniform intensity at the exit slit was accomplished by the cam associated with a system of levers.

If the slit width is made small higher resolution can be obtained, but the output intensity is reduced. However a compromise had to be effected between the two conflicting requirements and hence the over all resolution was limited by the signal to noise ratio. Calculations from the geometry of the system revealed that for a slit width of 0.1 mm, a resolution of 0.005 ev (0.015μ) at 2μ and 0.002 ev (0.096μ) at 7.4μ respectively could be obtained using NaCl prism. For 12 to 23μ region a similar KBr prism was used in the monochromator. A specially cut wavelength cam and slit cam were also used along with it.

The lower limit of wavelength obtainable using the NaCl cam was 2μ. Since it was necessary to obtain the wavelength region below 2μ, the cam was cut and calibrated to obtain the region as low as 1.4μ. The region from 1.5μ to 0.7μ was obtained by a different setting of the Littrow mirror and calibrating it against the counter reading. The calibration was done using mercury, neon and helium emission lines, the absorption lines of didymium glass and some organic liquids.

c) Apparatus for Thermoelectric power measurements

The apparatus is shown in Fig. (3:2). The sample could be held lengthways between two copper rods, one of the rods

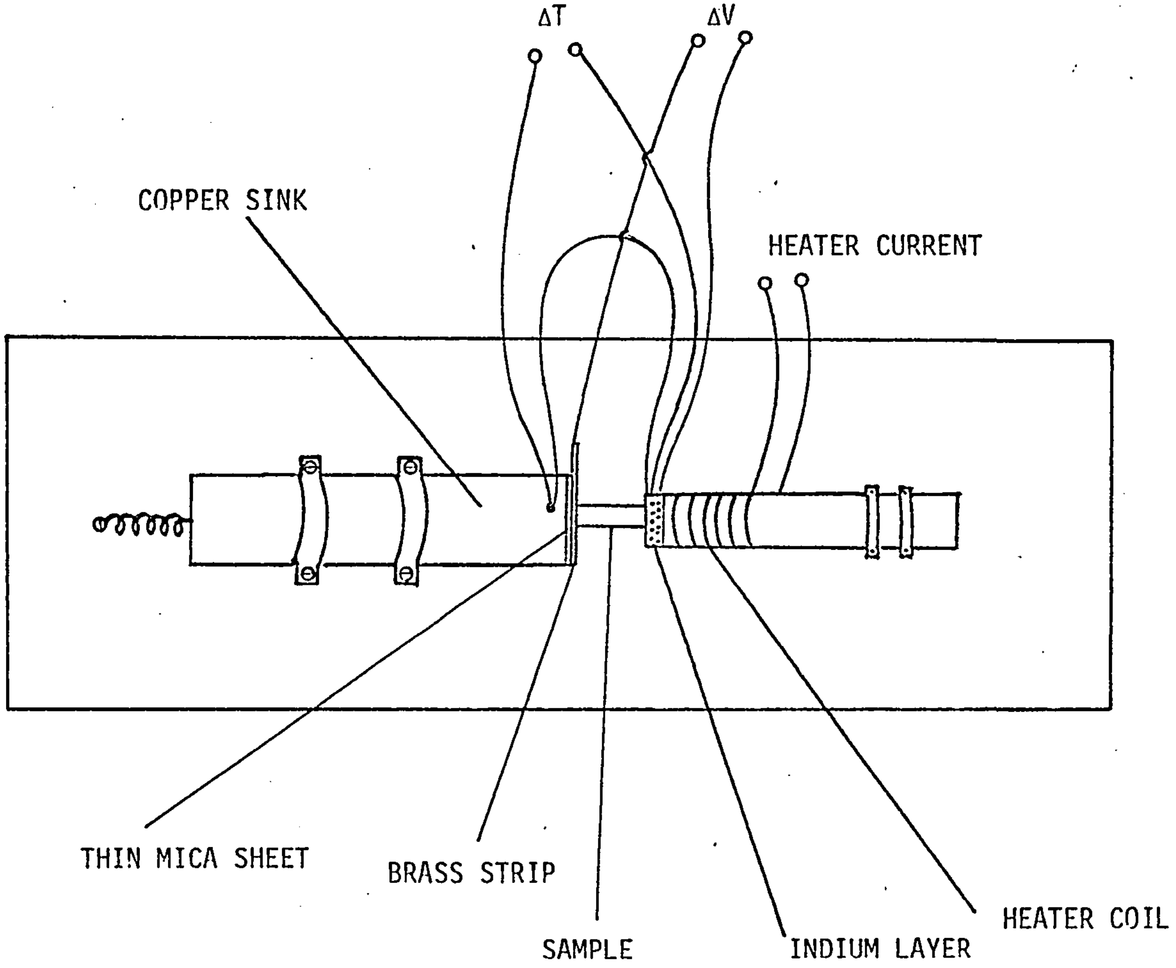

Fig.(3:2) Thermoelectric power apparatus being held under compression with a spring attached to it. One end of a copper rod was heated by a small helical furnace winding wound on it,so that a temperature of 3 or 4°C above room temperature could be obtained by passing current from a 1.5v battery. The rod at room temperature served as the heat sink. Thin layers of Indium were used to give good thermal contact at the hot end, while the sample was electrically insulated from the sink by a very thin layer of mica. A differential Chromel - alumel thermocouple with one junction in the Indium layer and the other in the copper sink was used to measure the temperature difference across the sample. Potential probes from either end of the sample were connected to a Hewlet Packard Model 419A D.C. Null voltmeter, which enabled the thermal emf to be measured to an accuracy of one microvolt. The thermocouple emf was also measured by the same voltmeter. Each voltage could be read on the voltmeter one after another by reversing a switch.

d) Sample preparation

Preparation of the alloys in the form of ingots varying in molecular composition along the ingot has already been discussed in section 2.6. For optical transmission measurements specimens of approximate dimensions 6 x 8 mm elliptical in cross-section and ½ mm thick were cut from the ingot using a 0.008" thick carborundum saw. The slice was mounted on a holder using glyptal and one side was ground mechanically using carborundum powder, and then polished to 0.5 micron grain size using alumina powder on cloth covered wheels. The sample was carefully removed from the holder dissolving the glyptal in acetone. Finally the other side was ground down until the specimen was nearly 100 microns thick and then polished to 0.05 micron grain size in a similar way.

Since the samples for optical measurement were ground very thin adjacent samples were taken from the same ingot for thermoelectric power measurements. These samples were cut to approximate dimensions 1 x 3 x 10 mm and the surfaces were lapped.

e) Absorption measurements

Before each set of absorption measurements the exit optical system was aligned using visible light. This was done using a Hg vapour lamp as the source inside the monochromator and obtaining the green line of the spectrum through the exit slit. A suitable hole was made on the specimen holder cup and the specimen was mounted to cover the hole ; special care was taken in handling the specimen. First a quick scan of wavelength was made to approximately locate the position of the absorption edge. The transmitted intensities I were measured by changing the wavelength towards shorter wavelength in suitable steps. Steps of 0.02μ were taken at the absorption edge, until transmission was almost reduced to zero. The specimen was removed and the incident intensities I_0 for the corresponding wavelengths were measured. The ratios I_0/I were calculated for these wavelengths. Later the specimen in - specimen out technique was tried to determine I_0/I for each wavelength, in order to eliminate errors produced by the fluctuations in the source temperature. The results showed that the first method was sufficiently accurate and hence the same procedure was adopted in all measurements.

After the transmission measurements the thickness of the specimen was measured with a micrometer capable of reading to an accuracy of one micron. The thickness was measured at five or six different places on the sample and the average value was taken. Finally the specimen was powdered and an x-ray powder photograph was taken to determine the correct composition.

f) Thermoelectric power measurements

The sample was placed between the copper rods and a difference of temperature of 2 to 3°C was maintained between the ends. The thermocouple emf and the thermo emf of the sample were measured after steady state was reached. For GaAs rich samples of the alloy it was necessary to electroplate either end of the sample with tin in order to ensure good electrical and thermal contact. For electroplating, the specimen was masked completely with nail polish except the end faces. The specimen held by tweezers was etched in a solution of 1 part HNO_3 and 7 parts HCl for a few seconds. It was rinsed in alcohol and water successively and finally dipped in the electroplating solution. The solution was prepared with 1 part anhydrous Stannic Chloride, 1 part H_2SO_4 and 20 parts H_2O. With the specimen as the cathode and a platinum wire as the anode, a current of 1 ma was passed for approximately 25 minutes. The sample taken out had the exposed ends coated with tin. The nail polish on the sample was dissolved in acetone and the tin contacts obtained this way were found to be good and ohmic.

The temperature and the thermo emf were measured a number of times and the average value of the thermoelectric power was taken. The thermo emf was also measured as a function of temperature difference increasing the temperature difference from 2 to 3°C and a graph was plotted between ΔV and ΔT. The graph was a good straight line and the slope yielded the thermoelectric power.

3.6 Data analysis and discussion

a) $Ga_xIn_{(1-x)}As$ alloys

All samples of this alloy system were taken from ingots T.F.B-1 and T.F.B-2. The samples were n-type with carrier concentration in the range 7×10^{22} to 10^{25} m^{-3}. The absorption curves for the various samples showing the variation of I_0/I with photon energy $h\nu$ are plotted in Figs. (3:3a and 3:3b).

The radiation falling on the sample is partially transmitted and partially reflected both of which can be expressed in terms of the reflection coefficient R and the transmission coefficient T. The two quantities for normal incidence are given by the well known expressions (67WI)

$$R = \frac{I_r}{I_0} = \frac{(n-1)^2 + \kappa^2}{(n+1)^2 + \kappa^2} \qquad \text{......[3:24]}$$

$$T = \frac{I_t}{I_0} = \frac{(1-R)^2 \; exp\,(-\,\alpha x)}{1 - R^2 \; exp\,(-2\,\alpha x)} \qquad \text{......[3:25]}$$

where I_0, I_r, I_t are the incident, reflected and transmitted intensities respectively. x is the thickness of the sample.

In all practical transmission measurements considered here the thickness of the sample is sufficiently large so that the effect of multiple reflections need not be considered. Generally R is a slowly varying function of photon energy and its maximum possible value is one. It is easily seen that $exp\ (-\ 2\alpha x) << R^2$. Hence the second term in the denominator of equation [3:25] can be neglected and it may be written (writing I instead of I_t)

$$\frac{I}{I_0} = C\ exp\ (-\ \alpha\ x)$$

$$\ell n\ \left(\frac{I_0}{I}\right) = \alpha\ x - \ell n(C)$$

where C is a constant. Denoting the background absorption by the subscript B and absorption at the energy gap by the subscript E_g , two similar equations can be written andby substracting, we get

$$\ell n_{10}\ \left(\frac{I_0}{I}\right)_{E_g} - \ell n_{10}\ \left(\frac{I_0}{I}\right)_B = \frac{(\alpha_{E_g} - \alpha_B)\ x}{2.303} \qquad ...[3:26]$$

The choice of $(\alpha_{E_g} - \alpha_B)$ is arbitrary, but the same value has to be chosen in determining the energy gap from each absorption curve. Different criteria have been used by previous workers. Woolley and Coworkers have previously chosen values of 300cm^{-1} and 150cm^{-1} for similar alloy systems. In the light of some new results, the analysis and the conclusion found in the paper already published (68W3) have been slightly modified in this thesis. In the present work, values of energy gap E_g for 300cm^{-1}, 150cm^{-1}, 100cm^{-1} and 50cm^{-1} have been determined for each absorption curve using equation [3:26]. The values of E_g for these values of absorption coefficient for a typical absorption curve are shown in Fig. (3:4a). Since, for all the alloys the absorption is due to direct transition, a plot of α^2 against $h\nu$ should give a straight line according to equation [3:6]. Determining $\alpha = \alpha_{E_g} - \alpha_B$ using equation [3:26], graphs of α^2 against $h\nu$ have been plotted for each sample and a typical result is shown in Fig. (3:4b). The straight line portion of the graph gives an intercept on the $h\nu$ axis, which again gives another value for E_g. Five values of E_g for each sample were obtained in this way. The results are summarised in Table (3,1). In Fig. (3:5) the values of E_g for the criteria $\alpha = 300\text{cm}^{-1}$, 50cm^{-1} and the straight line analysis, for each alloy sample are plotted as a function of composition.

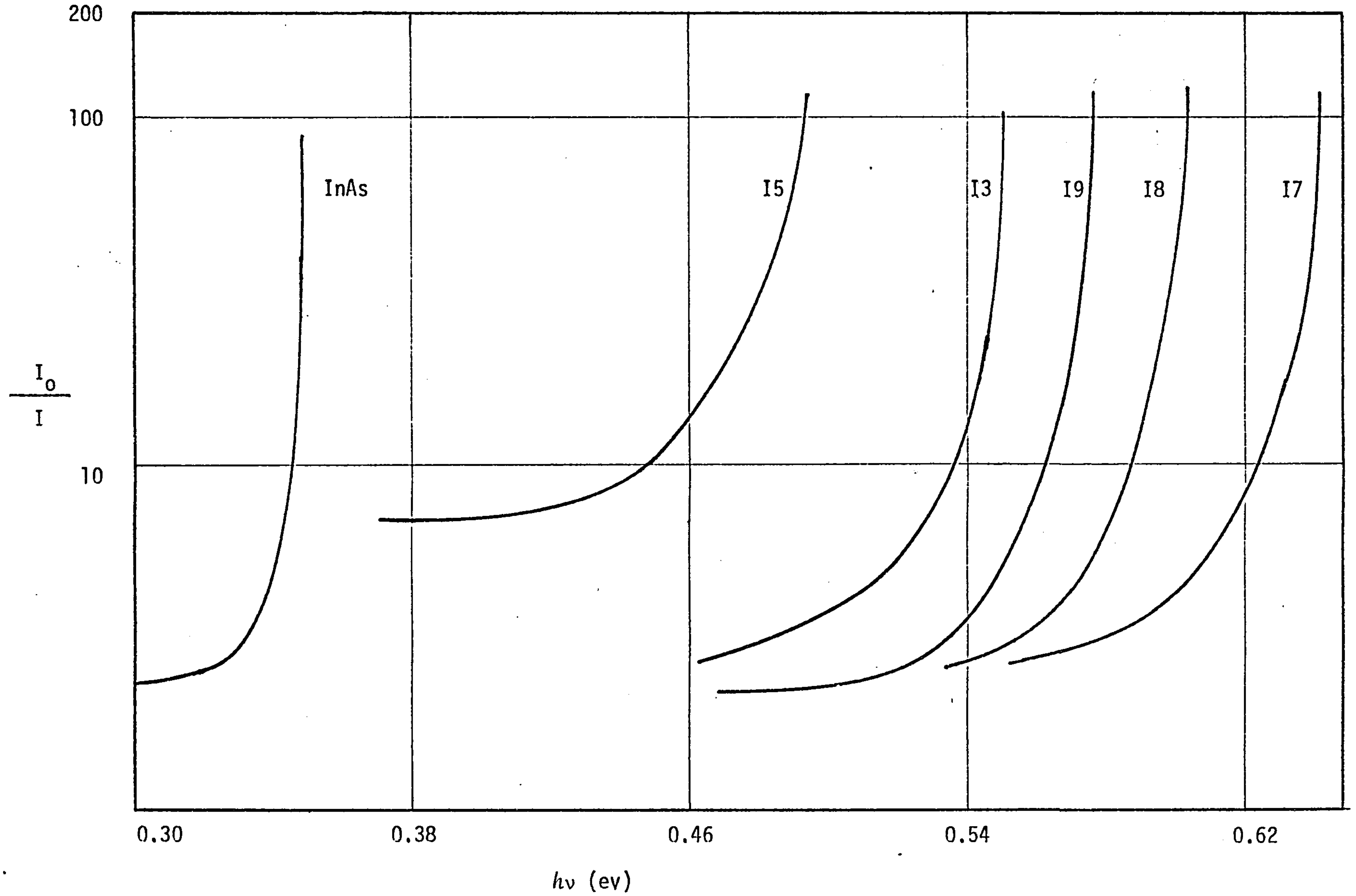

Fig.(3:3a) Variation of I_o/I with photon energy for $Ga_xIn_{(I-x)}As$ alloys

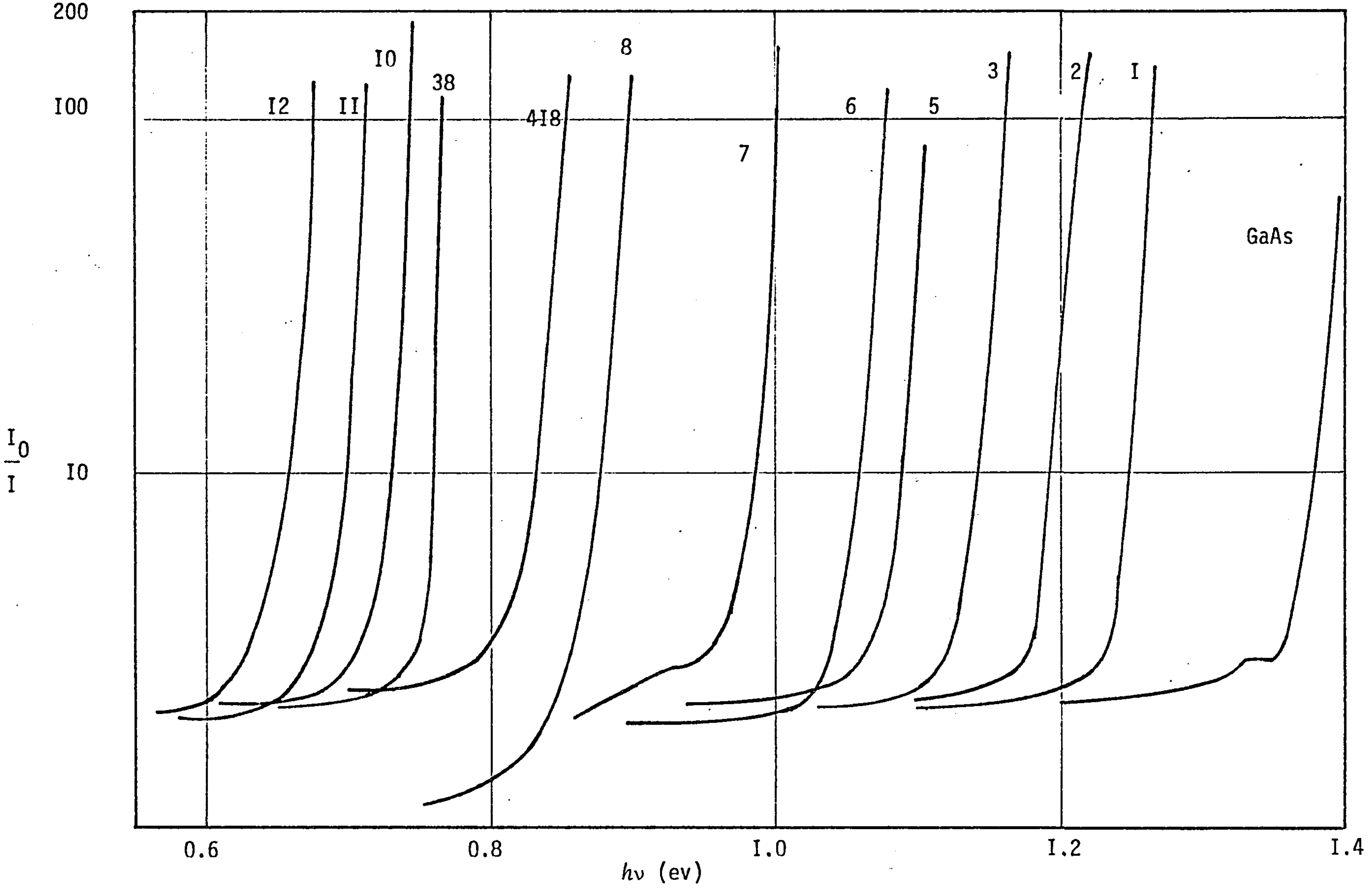

Fig.(3:3b) Variation of I_o/I with photon energy for $Ga_xIn_{(I-x)}As$ alloys

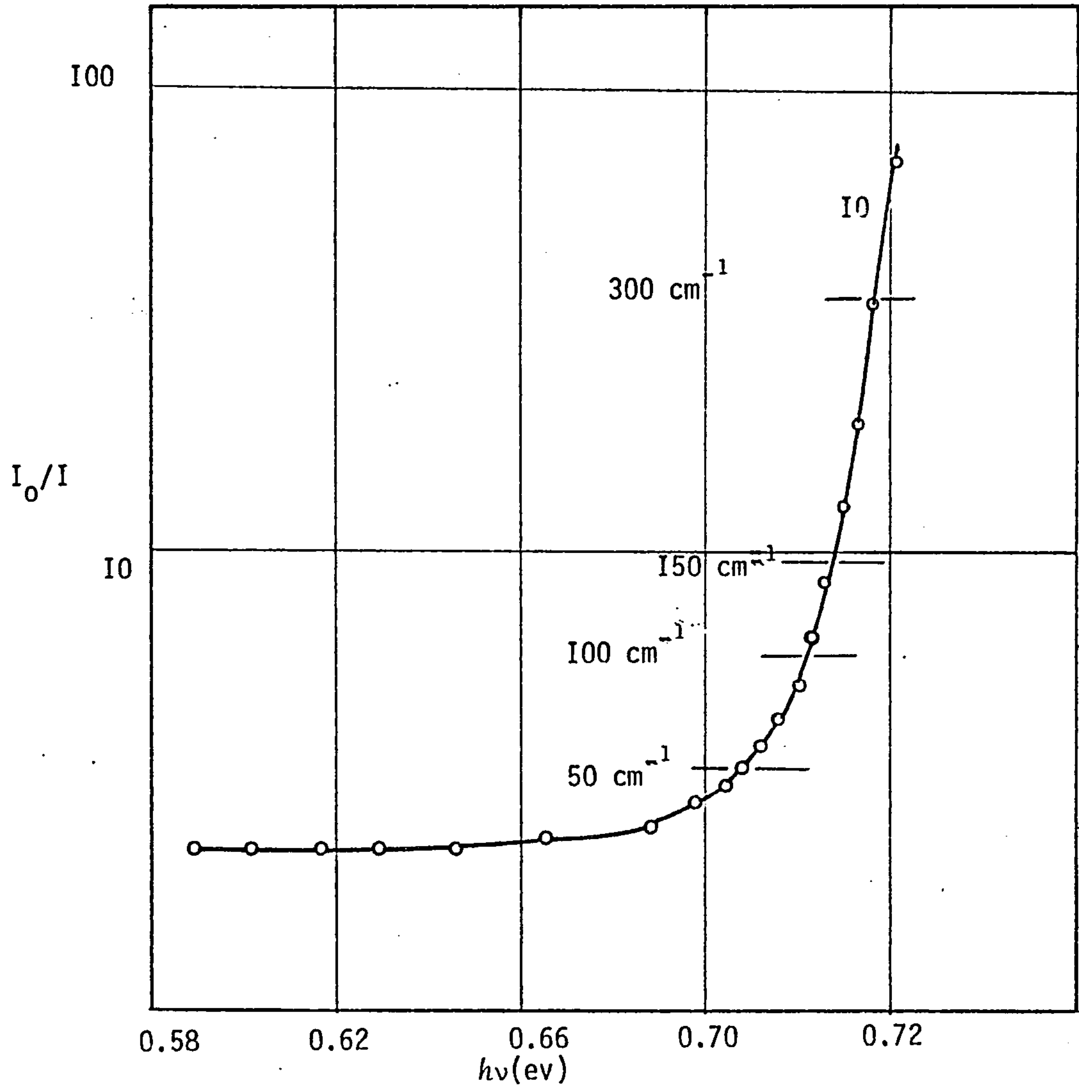

Fig.(3:4a) Variation of I_o/I with photon energy for a typical sample ($x = 0.435$) showing the values of E_g for different criteria

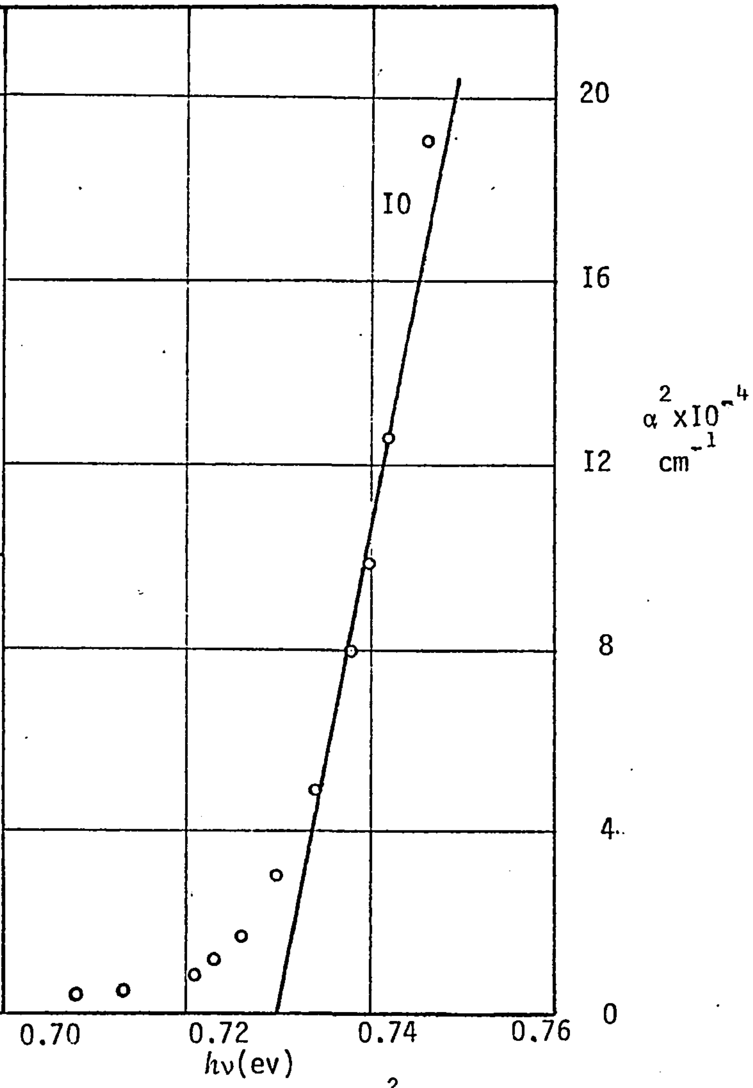

Fig.(3:4b) Variation of α^2 with $h\nu$ for a typical sample ($x = 0.435$)

Ingot	Specimen #	x	Thickness μ	$E_g(300)$ (ev)	$E_g(150)$ (ev)	$E_g(100)$ (ev)	$E_g(50)$ (ev)	$E_g(\alpha^2$ vs $h\nu)$ (ev)
-	InAs	0.000	82	0.348	0.343	0.341	0.337	0.344
T.F.B-1	15	0.040	70	0.49	0.476	0.462	0.448	0.481
T.F.B-1	13	0.150	80	0.548	0.542	0.522	0.502	0.544
T.F.B-1	19	0.195	58	0.577	0.562	0.553	0.545	0.561
T.F.B-1	18	0.260	90	0.601	0.591	0.579	0.566	0.593
T.F.B-1	17	0.300	56	0.635	0.624	0.606	0.594	0.632
T.F.B-1	12	0.350	80	0.675	0.661	0.650	0.634	0.666
T.F.B-1	11	0.390	94	0.707	0.695	0.687	0.657	0.700
T.F.B-1	10	0.435	96	0.739	0.723	0.722	0.712	0.730
T.F.B-1	38	0.480	136	0.766	0.761	0.765	0.750	0.762
T.F.B-1	418	0.550	92	0.847	0.832	0.824	0.808	0.84
T.F.B-2	8	0.585	85	0.885	0.868	0.858	0.847	0.889
T.F.B-2	7	0.690	100	0.998	0.988	0.981	0.970	0.980
T.F.B-2	6	0.755	40	1.050	1.041	1.035	1.025	1.048
T.F.B-2	5	0.785	90	1.100	1.085	1.081	1.072	1.083
T.F.B-2	4	0.810	110	1.12	1.11	1.105	1.095	1.104
T.F.B-2	3	0.840	110	1.157	1.143	1.135	1.125	1.134
T.F.B-2	2	0.870	110	1.204	1.192	1.188	1.180	1.188
T.F.B-2	1	0.910	135	1.265	1.251	1.245	1.238	1.244
-	GaAs	1.000	80	1.39	1.377	1.370	1.360	1.372

Table (3,1) Absorption data for $Ga_xIn_{(1-x)}As$ alloys. (300^0K)

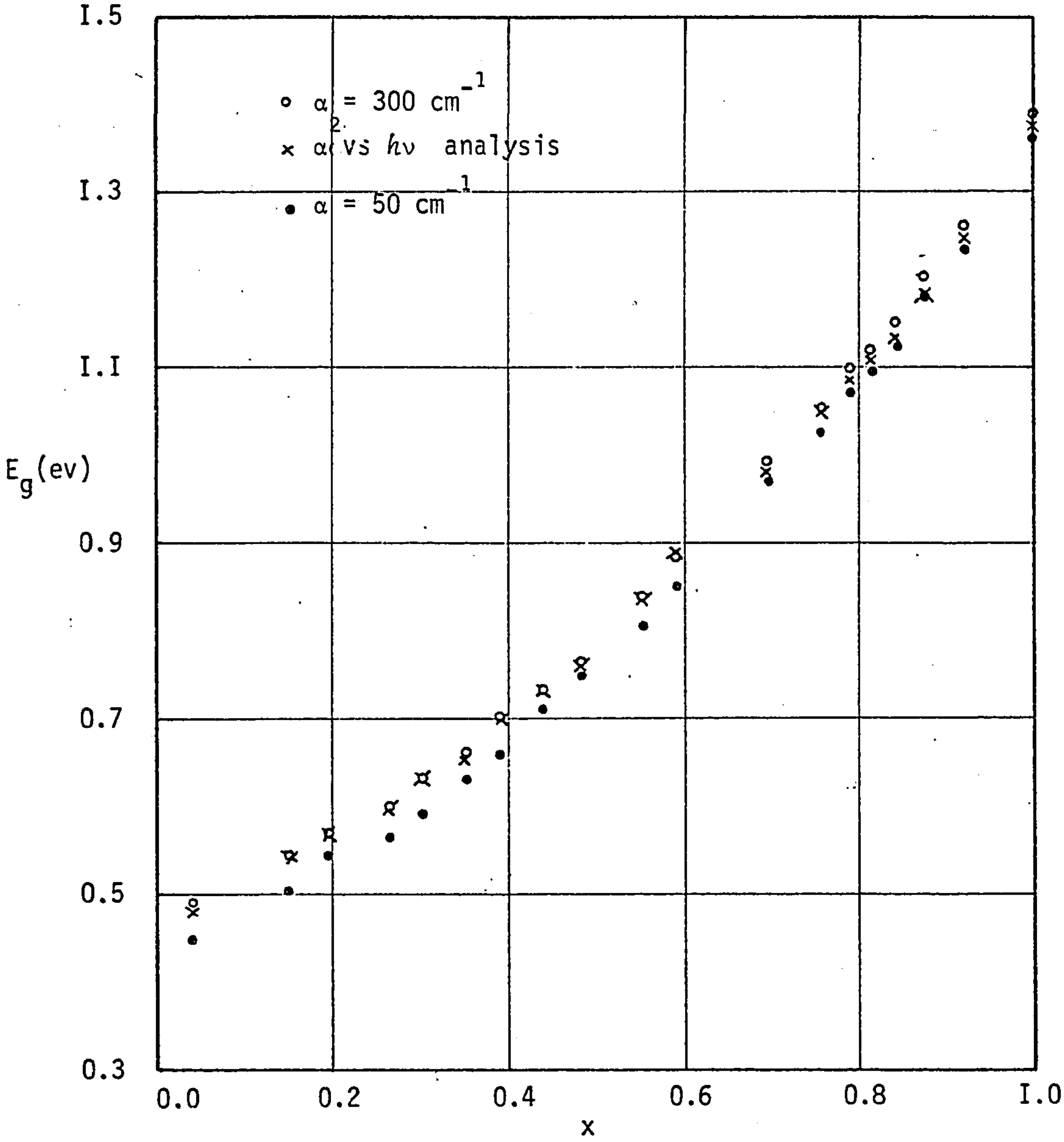

Fig.(3:5) Values of E_g for diffe rent criteria plotted as a function of x for $Ga_xIn_{(I-x)}As$ alloys

x	θ (μV /°C)	E_o (ev)	E_F (ev)
.035	- 44	0.351	0.208
.093	- 60	0.418	0.194
.15	- 74	0.459	0.180
.187	- 79	0.485	0.176
.23	- 82	0.509	0.174
.28	- 88	0.548	0.168
.30	- 96	0.568	0.16
.373	-120	0.626	0.136
.487	-128	0.731	0.13
.51	-136	0.772	0.122
.55	-143	0.813	0.116
.615	-152	0.879	0.108
.695	-170	0.972	0.095
.750	-178	1.045	0.089
.807	-181	1.100	0.087
.908	-289	1.245	0.027

Table (3,2) Thermoelectric power data for $Ga_xIn_{(1-x)}As$ alloys

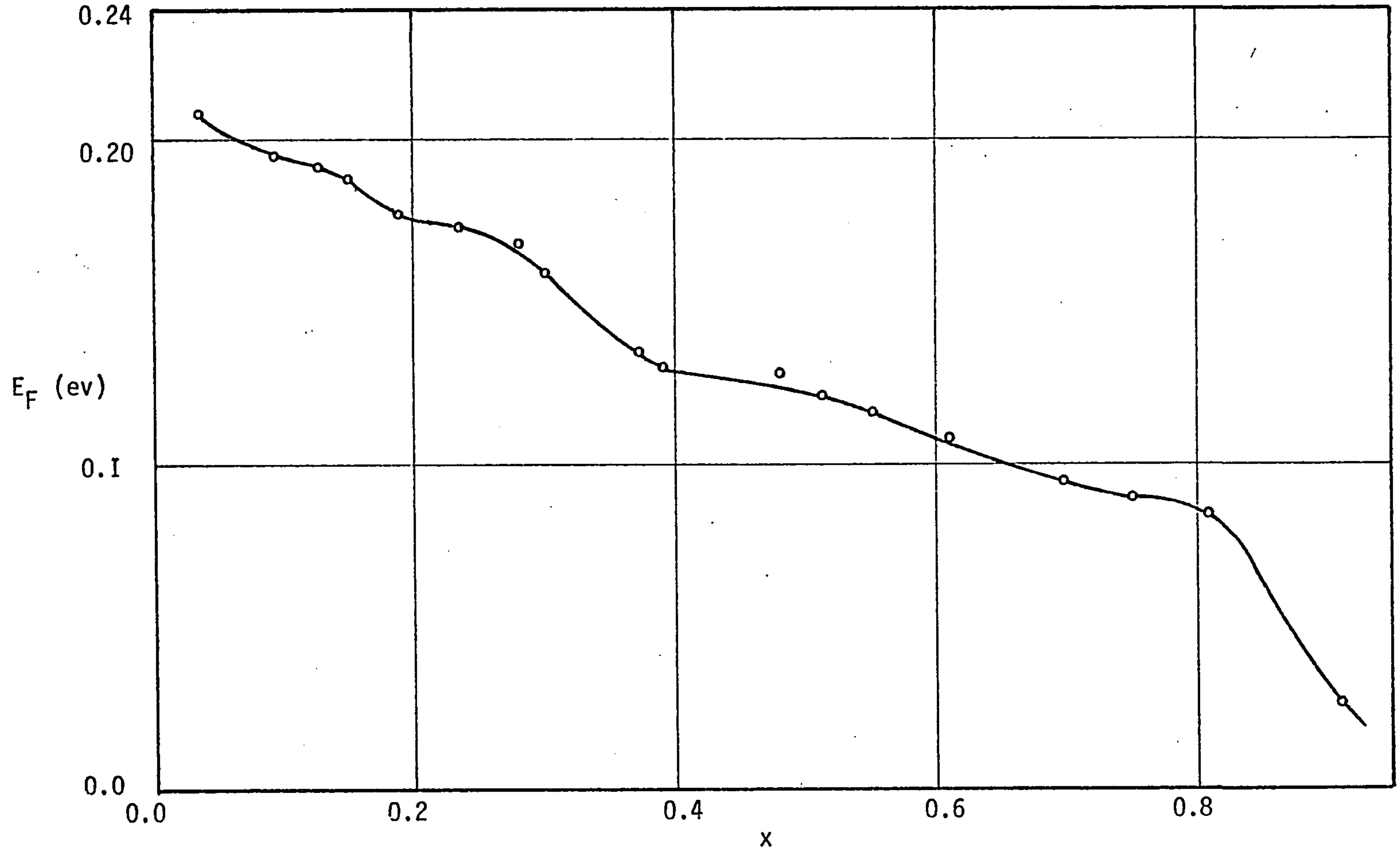

Fig.(3:6) Variation of Fermi level with x for $Ga_xIn_{(I-x)}As$ alloys

As it is seen from Fig. (3:5) the energy gap values of the alloys near the InAs end are shifted towards higher energies w.r.t. pure materials. In the composition range $0<x<0.6$ the samples were heavily doped in the range 2×10^{24} to 1×10^{25} m^{-3}, and hence the shift in energy is due to Burstein effect. The results of thermoelectric power measurements were used to determine the Fermi level and hence the Burstein shift. However, as it is seen from equation [3:19], one has to know the value of the scattering factor s in order to obtain an accurate value of the Fermi level. It was difficult to determine s without doing further experiments such as magneto-thermoelectric power measurements. For heavily doped samples considered here, it was assumed that impurity scattering predominated so that $s = 3/2$. Hence the Fermi energy for each specimen can be calculated from the thermoelectric power data using equation [3:19], if E_0^* is known. According to equation [3:9], when Burstein shift occurs, the intrinsic gap E_0 and the optical gap E_g are related by

$$\begin{aligned} E_0 &= E_g - E_F + 4KT \qquad \text{if } E_F > 4KT \\ \text{and} \quad E_0 &= E_g \qquad \text{if } E_F < 4KT \end{aligned} \qquad \ldots .[3:27]$$

Distance along the Ingot	Specimen #	x	$E_0(300)$ ev	$E_0(150)$ ev	$E_0(100)$ ev	$E_0(50)$ ev	$E_0(\alpha^2$ vs $h\nu)$ ev
-	InAs	0.000	0.348	0.343	0.341	0.337	0.344
11.85	15	0.040	0.398	0.368	0.357	0.340	0.373
9.5	13	0.150	0.460	0.454	0.434	0.414	0.456
8.75	19	0.195	0.502	0.487	0.478	0.470	0.486
7.9	18	0.260	0.532	0.522	0.510	0.497	0.524
7.45	17	0.300	0.576	0.565	0.547	0.535	0.573
7.0	12	0.350	0.633	0.619	0.608	0.592	0.624
6.6	11	0.390	0.677	0.665	0.657	0.627	0.670
6.25	10	0.435	0.715	0.699	0.698	0.688	0.706
-	38	0.480	0.744	0.739	0.734	0.728	0.740
5.1	418	0.550	0.832	0.817	0.809	0.793	0.825
7.7	8	0.585	0.875	0.858	0.848	0.837	0.879
8.6	7	0.690	0.998	0.998	0.981	0.970	0.980
9.25	6	0.755	1.050	1.041	0.035	1.025	1.048
9.65	5	0.785	1.100	1.085	1.081	1.072	1.083
10.15	4	0.810	1.120	1.11	1.105	1.095	1.104
11.15	3	0.840	1.157	1.143	1.135	1.125	1.134
12.4	2	0.870	1.204	1.192	1.188	1.180	1.188
14.8	1	0.910	1.265	1.251	1.245	1.238	1.244
-	GaAs	1.000	1.430	1.430	1.430	1.430	1.430

Table (3,3) Energy gap values using different Criteria, for $Ga_xIn_{(1-x)}As$ alloys

Thus, for each sample, a mean value of E_g was taken from Fig. (3:5) and used for E_0^* in equation [3:19]. Solving this equation a value of E_F was obtained. Then, using equation [3:27] a more correct value of E_0 was obtained. Thus a self-consistant iterative solution of equations [3:19] and [3:27] enabled an accurate value of E_F to be determined for each sample, from the thermoelectric power data. The thermoelectric power data and the results are summarised in Table (3,2). A graph of x vs E_F was plotted and is shown in Fig. (3:6). From this graph E_F for the specimens used for absorption measurements were determined. Again using equation [3:27] the corrected values of E_0 for each sample for any one of the above criteria can be obtained. Thus values of E_0 for all the samples corresponding to each one of the above criteria were obtained. The results obtained in this way are recorded in Table (3,3). It can be seen that the room temperature energy gap value obtained for GaAs in the present measurement is 1.37 ev which is much lower than recently reported value of 1.43 ev, obtained from very accurate measurements (62S1, 68W2). It is well established that GaAs has impurity levels just below the (000) conduction band and it is quite possible that in these measurements, electronic transitions were taking place to a level below the band edge and hence a lower value was obtained. Due to these uncertainities instead of the experimental value, 1.43 ev was taken as the value of E_0 for GaAs in all the above cases. The values of E_0 vs x given in each column of Table (3,3) have been fitted to the quadratic form of equation [3:20] by the method of least squares. The resultant values of A, B and C are given in Table (3,4). In the above curve fittings, energy gap values for compounds were given twice the weight of the alloys, since the values for compounds are acurately known. It is seen that the values of C are not very much different, but there is a systematic variation from 0.45 to 0.54, as the choice of α varies from 300cm^{-1} to 50cm^{-1}. It is more

Criterion	A	B	C	D=A+B+C
$E_0(300)$	0.359	0.599	0.449	1.407
$E_0(150)$	0.349	0.580	0.472	1.402
$E_0(100)$	0.342	0.564	0.494	1.401
$E_0(50)$	0.334	0.531	0.535	1.400
$E_0(\alpha^2$ vs $h\nu)$	0.351	0.600	0.445	1.396

Table (3,4) Values of A, B and C for $Ga_xIn_{(1-x)}As$ alloys

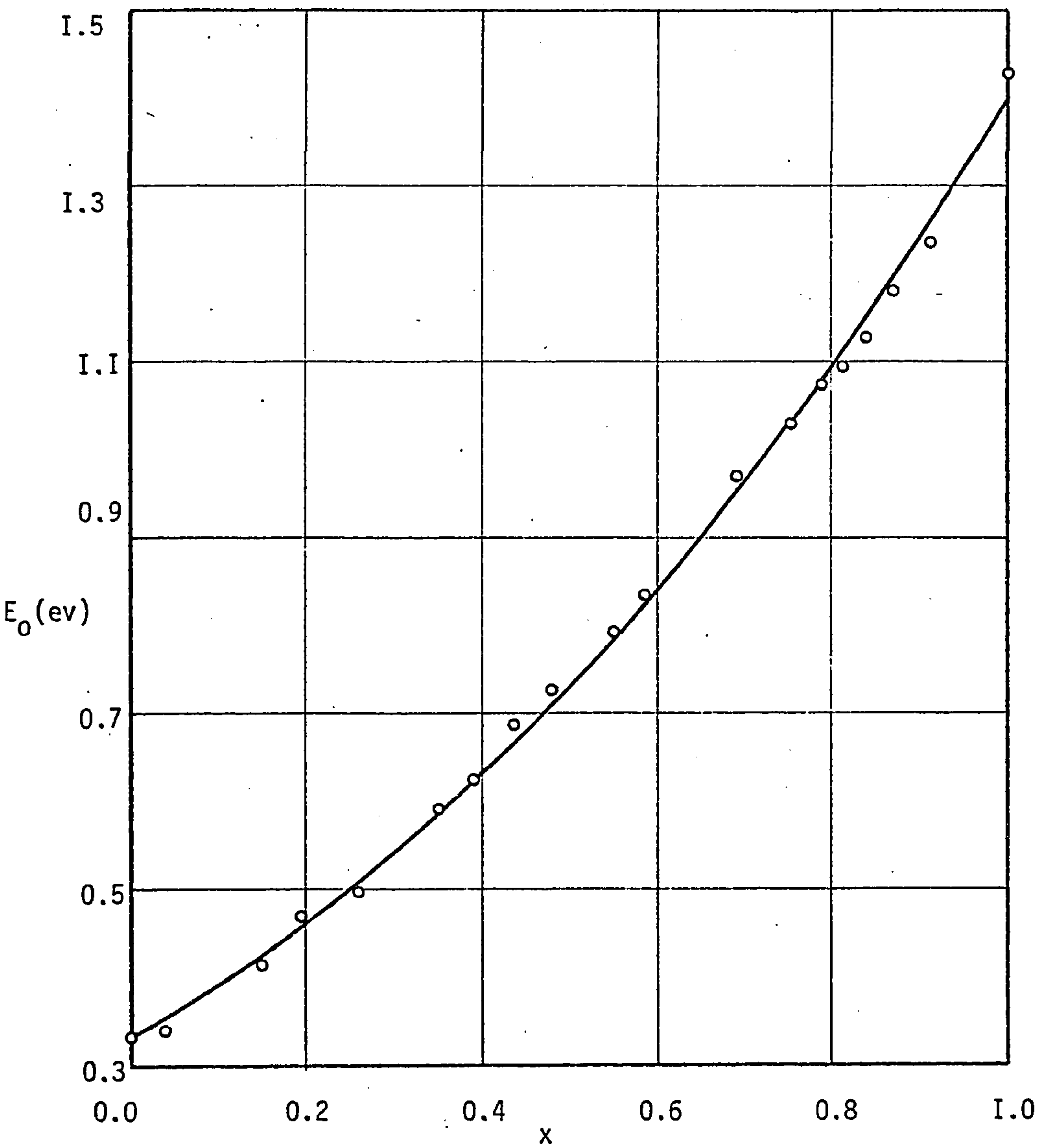

Fig.(3:7) Values of E_o corresponding to α= 50cm^{-1} along with the fitted parabolic curve for $Ga_xIn_{(I-x)}As$ alloys reasonable to take the value corresponding to a low value of α (50cm^{-1} in this case), since at higher values it is possible to miss a part of the bowing effect of energy gap produced by the disorder of the alloy. It may be concluded that the C = 0.28 obtained from Woolley et al (61W2) data is incorrect and the empirical relation does not hold good for these alloys.. From theoretical work, using the dielectric method of band calculation, Van Vechten and Bergstresser (69V3) have reported a value of C = 0.57. This value is in agreement with the present results with in experimental error. The values of C obtained from Hockings et al data (66H1) and William and Rehn (68W2) data are also in line with these results.

The experimental values of E_0 for the criterion $\alpha = 50\text{cm}^{-1}$ along with the least square fitted parabola are shown in Fig. (3:7). There could be some error introduced in the determination of E_F due to the assumption $s = 3/2$, since the contribution of optical phonon scattering will always make s slightly less than 3/2. This will not introduce any appreciable error in E_0, since even a 50% error in E_F can introduce only about 6% error in E_0. Hence the variation of energy gap as a function of composition shown in Fig. (3:7) should be accurate. However small errors in the value of E_0 could lead to comparatively greater errors in the value of C.

This could account for the small descrepancy between the present and the theoretical value of C.

b) Ga $As_xSb_{(1-x)}$ alloys

Only a limited range of alloys of this system has been produced. The samples were taken from ingots T.F.F-1 and T.Z.F-2. Samples rich in GaSb were p-type with carrier concentration lower than $10^{23}m^{-3}$, probably heavily compensated. GaAs rich samples were n-type in the range of 10^{22} carriers/m^3. Under these conditions no Burstein shift could be expected. The absorption curves for various samples are shown in Figs. (3:8a and 3:8b). Values of the energy gap for $\alpha = 300cm^{-1}$, $150cm^{-1}$ and plotting α^2 vs $h\nu$ as described in section 3.6a, were obtained. These values are recorded in Table (3,5). Each set of values was fitted to the quadratic form of

Criterion	A	B	C	D=A+B+C
$E_0(300)$	0.756	-0.500	1.166	1.422
$E_0(150)$	0.740	-0.559	1.235	1.416
$E_0(\alpha^2 vs\ h\nu)$	0.738	-0.485	1.157	1.411

Table (3,6) Values of A, B and C for $GaAs_xSb_{(1-x)}$ alloys equation [3:20] and the resultant values of C obtained are given in Table (3,6). Again for the reasons previously discussed E_0 for GaAs was taken to be 1.43 ev and twice the weight was given to E_0 values for the compounds. C is seen to be in the range 1.16 to 1.23 ev. This value compares very well with the theoretical value of 1 ev predicted by Van Vechten and Bergstresser (69V4). The value of C according to the Woolley - Thompson empirical relation is 0.28. Hence the validity of the empirical relation for III - V alloys may be ruled out and it was a strange coincidence for four alloy systems.

The fitted parabolic curve for the third set of E_0 values in Table (3,5) along with the experimental points is shown in Fig. (3:9). The curve fit is seen to be quite good. The curve serves to predict the values of energy gap of the alloys in the middle range of composition, where no samples were available. It is of interest to notice that similar to $InAs_xSb_{(1-x)}$ alloys the energy gap goes through a minimum at x= 0.2 and the value at the minimum is 0.685 ev which is lower than the values for both GaSb and GaAs.

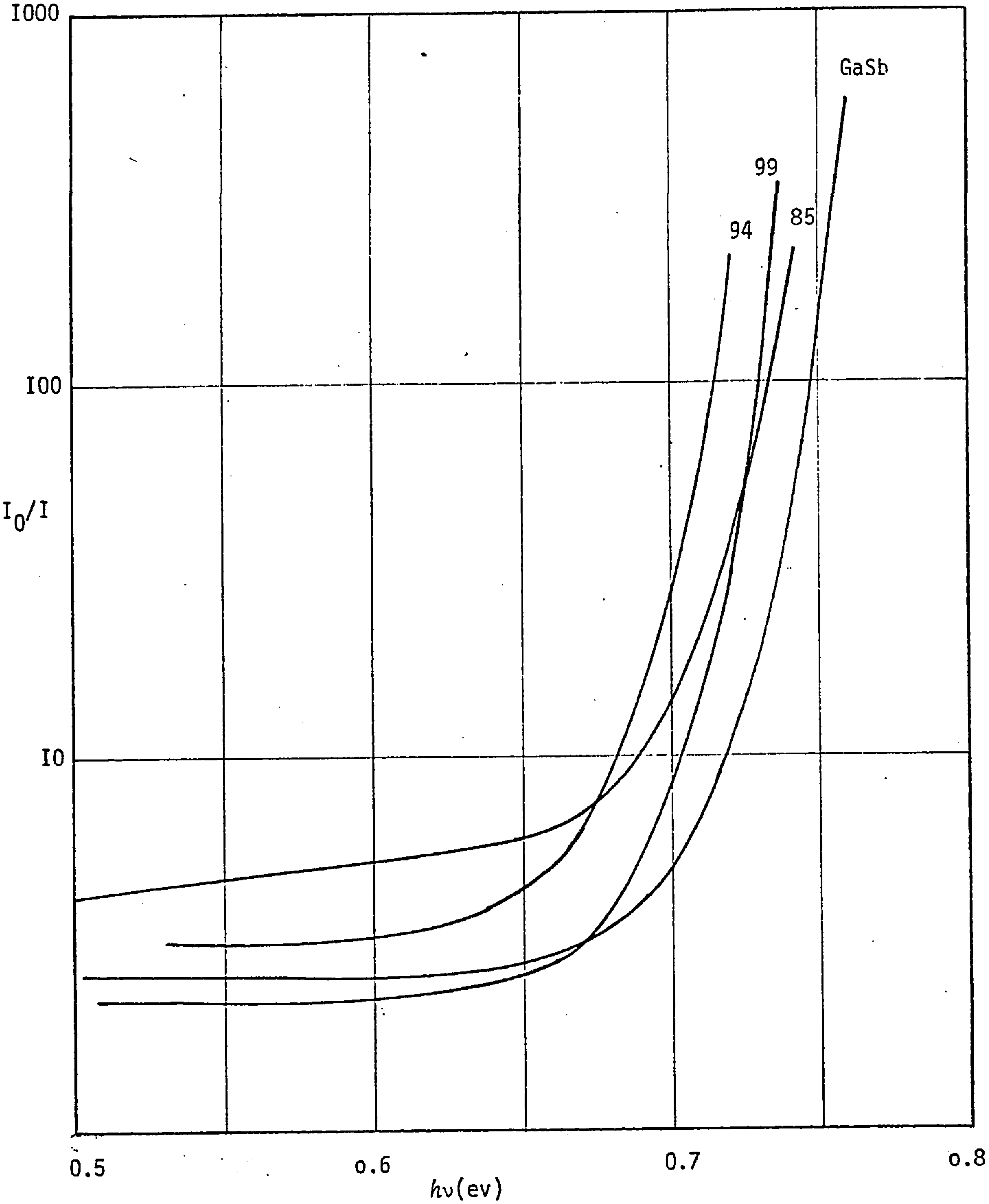

Fig.(3;8a) Absorption curves for $GaAs_xSb_{(I-x)}$ alloys

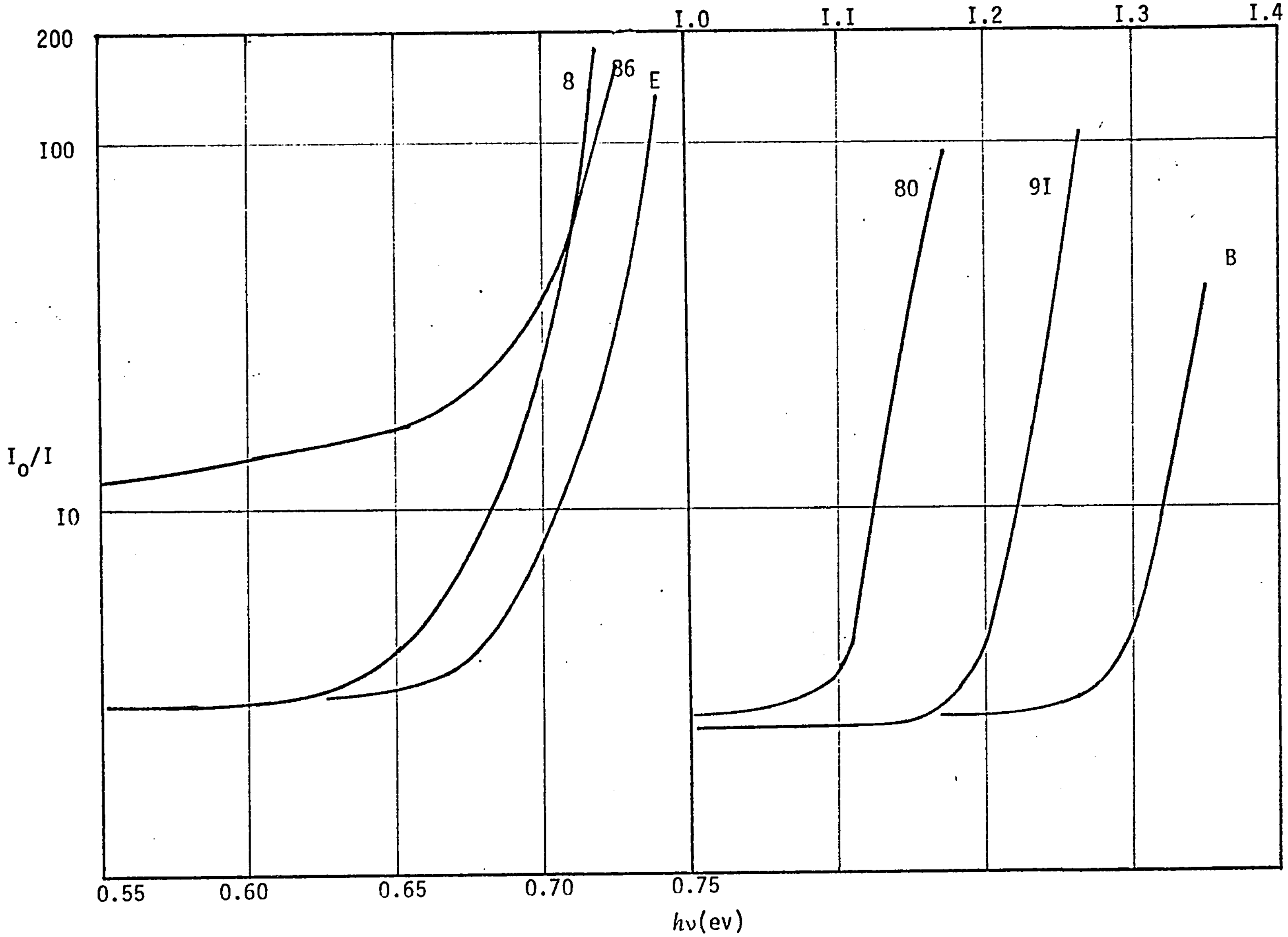

Fig.(3:8b) Absorption curves for $GaAs_xSb_{(I-x)}$ alloys

Ingot	Distance along the ingot (cms)	Specimen #	x	Thickness (microns)	$E_0(300)$ (ev)	$E_0(150)$ (ev)	$E_0(\alpha^2$ vs $h\nu)$ (ev)
-	-	GaSb	0.00	155	0.753	0.736	0.736
T.F.F-1	4.75	E	0.015	148	0.745	0.724	0.725
T.F.F-1	3.7	8	0.10	137	0.719	0.699	0.696
T.Z.F-2	6.95	99	0.17	58	0.708	0.690	0.696
T.Z.F-2	5.6	94	0.26	91	0.705	0.685	0.696
T.Z.F-2	3.55	85	0.34	109	0.732	0.710	0.725
T.Z.F-2	3.8	86	0.355	67	0.730	0.690	0.714
T.Z.F-2	1.6	80	0.85	72	1.140	1.125	1.130
T.Z.F-2	1.05	91	0.89	52	1.222	1.205	1.206
T.F.F-1	2.65	B	0.94	67	1.335	1.313	1.301
-	-	GaAs	1.00	80	1.390	1.377	1.372

Table (3,5) Absorption data for $GaAs_xSb_{(1-x)}$ alloys

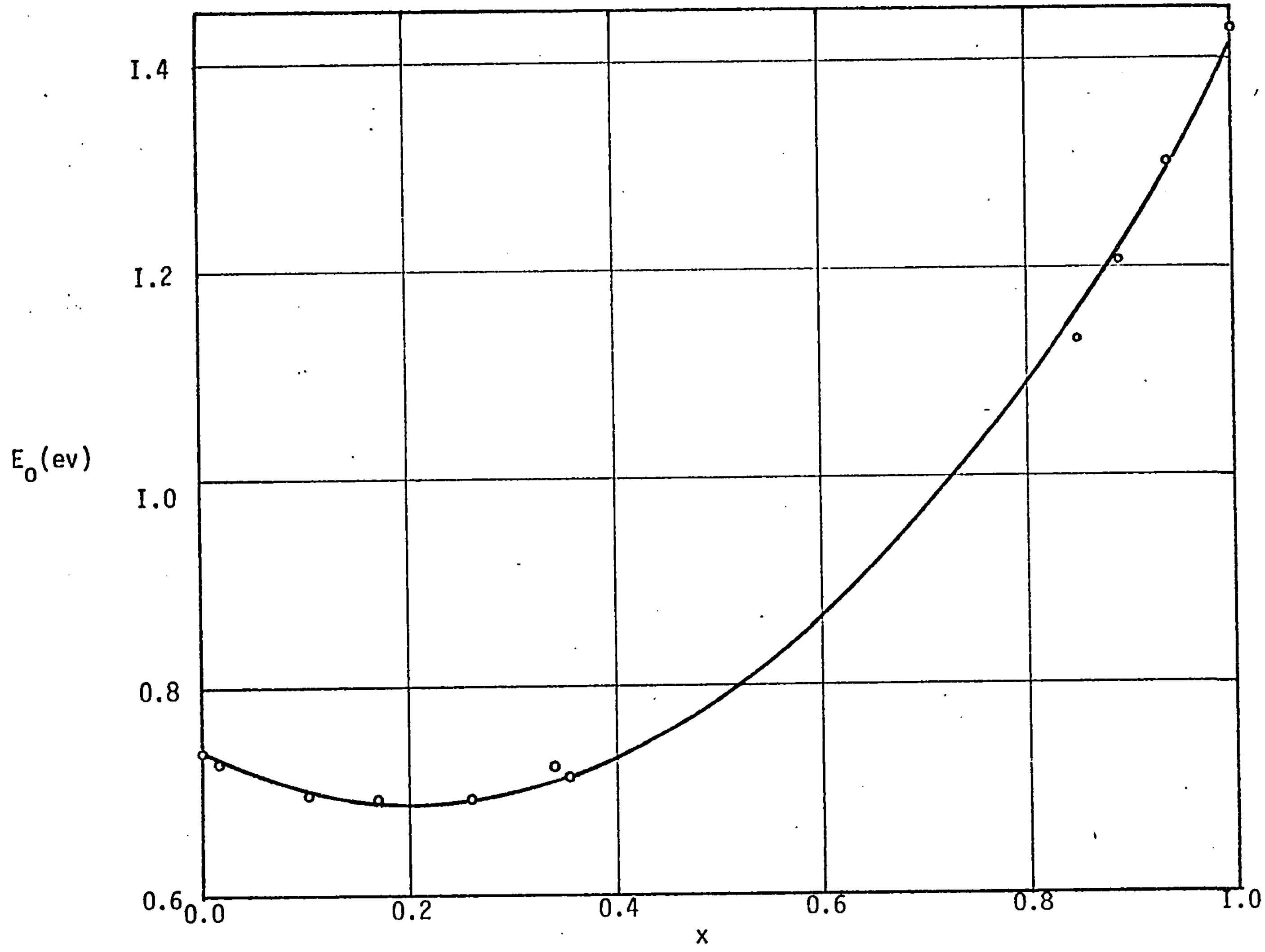

Fig.(3:9) Values of energy gap as a function of composition for $GaAs_xSb_{(I-x)}$ alloys

CHAPTER IV

PLASMA REFLECTION

4.1 Introduction

In this chapter, first a phenomenological development of the theory of infrared reflectivity is given. M.K.S units are used throughout this treatment. Next the experimental techniques and the method of analysis of data are discussed. Finally the data are presented and analysed in two ways according to the degree of degeneracy of the samples. The main attempt has been to calculate the bottom of the band effective mass values in three alloy systems, assuming Kane model.

It was mentioned in section 3.1 that the optical constants η and κ can be determined from reflectivity measurements. There are several methods of approach employed to determine the optical constants from reflectivity measurements. The approach most commonly used in III - V compounds in the infrared range involves measurement of the reflection spectrum at near normal incidence over a wide spectral range, followed by an attempt to fit the observed data by classical dispersion relations. Similar to the absorption spectrum, the reflection spectrum will also show the characteristic behaviour due to interband transition (valence to conduction band), free carrier effect and lattice dispersion, at the appropriate frequencies. Since the first process takes place only at wavelengths shorter than that corresponding to the energy gap there will be no contribution to the reflection spectrum due to this process at longer wavelengths. Hence, only the other two processes need to be considered at longer wavelengths.

4.2 Classical theory of infrared reflectivity

a) Plasma reflection

The characteristic nature of the reflectivity spectrum produced by the free carrier effect is called plasma reflection. It has been stated in section 3.1a that the dynamics of electrons under the influence of an electromagnetic field can be treated classically and the real and imaginary parts of the dielectric constant are given by equations [3:3] and [3:4]. The relaxation time τ_j is given by

$$\frac{1}{\tau_j} = \frac{e}{m_j^* \mu_j} \qquad \text{.................[4:1]}$$

where e is the electronic charge, m_j^* is the effective mass of the carriers and μ_j is the optical mobility. Equations [3:3] and [3:4] may be written as

$$\varepsilon_1 = \varepsilon_\infty - \sum_j \varepsilon_\infty \left\langle \frac{\omega_{p,j}^2 \tau_j^2}{(1+\omega^2 \tau_j^2)} \right\rangle \qquad \text{.........[4:2]}$$

$$\varepsilon_2 = \sum_j \frac{\varepsilon_\infty}{\omega} \left\langle \frac{\omega_{p,j}^2 \tau_j}{(1+\omega^2 \tau_j^2)} \right\rangle \qquad \text{.........[4:3]}$$

Here $\omega_{p,j}$ is the plasma frequency defined by

$$\omega_{p,j} = \left[\frac{n_j e^2}{m_j^* \varepsilon_0 \varepsilon_\infty} \right]^{\frac{1}{2}} \qquad \ldots\ldots\ldots\ldots\ldots\ldots[4:4]$$

where n_j is the carrier concentration and m_j^* is the susceptibility effective mass of the carriers of the type j. Equations [4:2] and [4:3] are the most general equations based on classial theory and these equations should be used as it is in general cases. However, various approximations can be made in practical cases. If there is only one type of carriers involved the summation in the equations can be neglected. Four possible approximations together with numerical integrations of the equations have been compared with experimental data for n and p-type materials, by Schumann and Phillips (67S2). Suitable approximations applicable to high and low mobility semiconductors have been developed by Lyden (64L1) and Murray et al (66M1) respectively. If any of these approximations can not be made the various parameters of the classical theory can be determined by curve fitting to the experimental reflectivity spectrum (65R1, 67R1).

Case when $\omega^2 \tau^2 >> 1$

For all the III - V compounds considered in this thesis mobility of electrons is large enough, so that the above condition is well satisfied for n-type materials and for wavelengths lower than about 50μ. In this case the quantity 1 in the denominator of equations [4:2] and [4:3] may be neglected and for one type of carriers the equations become

$$\varepsilon_1 = \varepsilon_\infty \left[1 - \frac{<\omega_p^2>}{\omega^2} \right] \qquad \text{...........[4:5]}$$

and
$$\varepsilon_2 = \varepsilon_\infty \frac{1}{\omega^3} < \frac{\omega_p^2}{\tau} > \qquad \text{...........[4:6]}$$

However, for degenerate samples the averages may be neglected. When $\omega >> \omega_p$ the imaginary part of the dielectric constant becomes very small and the real part is dominant. It is also seen that as ω approaches ω_p the real part of the dielectric constant decreases and when $\omega = \omega_p$ it reaches a minimum. For $\omega < \omega_p$ the real part of the dielectric constant is negative and the imaginary part of the dielectric constant will be greater than the real part.

For near normal incidence the reflectivity R in terms of the index of refraction η and the extinction coefficient κ is given by

$$R = \frac{(\eta - 1)^2 + \kappa^2}{(\eta + 1)^2 + \kappa^2} \qquad \text{..........[4:7]}$$

where η and κ in terms of ε_1 and ε_2 are given by

$$\varepsilon_1 = \eta^2 - \kappa^2 \qquad \text{......................[4:8]}$$

$$\varepsilon_2 = 2\,\eta\,\kappa \qquad \text{......................[4:9]}$$

From these equations it may be seen that, as the dielectric constant undergoes a minimum the reflectivity also goes through a minimum. This minimum, referred to as the plasma minimum, occurs when $\eta \simeq 1$ and then the reflectivity rises very rapidly. Substituting from equation [4:4], equation [4:5] may be written (from here on ε is used instead of ε_1 for the real part)

$$\varepsilon = \varepsilon_\infty - \frac{n\,e^2}{4\pi^2 c^2 \varepsilon_0 m^*}\,\lambda^2 \qquad \text{.........[4:10]}$$

where n is the carrier concentration and m^* is the susceptibility effective mass. According to equation [4:10] a plot of ε vs λ^2 should be a straight line. The second term in the equation is the free carrier contribution to the dielectric constant and may be denoted by ε_{FC}

$$\varepsilon_{FC} = - \frac{n e^2}{\omega^2 \varepsilon_0 m^*} \qquad \text{................[4:11]}$$

b) Lattice reflection

The lattice contribution to the dielectric constant is no longer constant at long wavelength lattice frequencies. Near the reststrahlen frequencies the lattice dispersion has a strong contribution to the dielectric constant. The spectral region of this influence is in the region of 15 to 60 microns for most of the III - V compounds. The contribution of the complex dielectric constant due to lattice dispersion for a diatomic cubic crystal has been calculated by Born and Huang (54B1)

$$\text{ie} \qquad \tilde{\varepsilon}_{LV} = \frac{(\varepsilon_s - \varepsilon_\infty)\, \omega_t^2}{\omega_t^2 - \omega^2 - i\, \gamma_{lv}\, \omega} \qquad \text{...........[4:12]}$$

and $$\frac{\varepsilon_s}{\varepsilon_\infty} = \frac{\omega_l^2}{\omega_t^2} \quad \text{.................[4:13]}$$

where ε_s is the static dielectric constant, ω_l and ω_t are the longitudinal and transverse optical phonon angular frequencies respectively and γ_{lv} is the characteristic damping frequency of the ions. Using equation [4:13] in [4:12] we have

$$\tilde{\varepsilon}_{LV} = \frac{\varepsilon_\infty \; (\omega_l^2 - \omega_t^2)}{\omega_t^2 - \omega^2 - i \; \gamma_{lv} \; \omega} \quad \text{..................[4:14]}$$

The real part is given by

$$\varepsilon_{LV} = \frac{\varepsilon_\infty \; (\omega_l^2 - \omega_t^2) \; (\omega_t^2 - \omega^2)}{(\omega_t^2 - \omega^2)^2 + \gamma_{lv}^2 \; \omega^2} \quad \text{................[4:15]}$$

4.3 Statistical theory of free carrier reflection

a) Free carrier susceptibility

The refractive index η and the extinction coefficient κ that characterise the optical properties are related to the conductivity σ and the electric susceptibility χ of the material by the following equations from classical electromagnetic theory

$$\varepsilon = \eta^2 - \kappa^2$$

$$\varepsilon_2 = 2\eta\kappa = \frac{\sigma}{\omega\,\varepsilon_0}$$

$$\varepsilon = 1 + \chi$$

In a radiation field, the current due to the carriers has a component in phase and a component out of phase with the electric field. The in-phase current contributes to the conductivity and the out of phase component contributes to the electric susceptibility. The total current density can be calculated using Boltzmann equation, and the free carrier conductivity and susceptibility may be expressed in terms of the band structure of the semiconductor. The current density per unit volume is given by (61S1)

$$J = -e \int n(k)\,\Delta f\ v\ d\Omega_k$$

where $n(k) = \frac{2}{(2\pi)^3}$ is the number of states per unit volume, Δf is the change in the Fermi distribution function, v is the velocity of the carriers and $d\Omega_k$ is the volume element in k-space.

$$J = -\frac{2}{(2\pi)^3} e \int \Delta f \; v \; d\Omega_k$$

The Boltzmann transport equation is given by

$$\frac{1}{\hbar} \frac{df}{dE} (F \cdot \nabla_k E) = - \frac{f - f_0}{\tau} \qquad \text{................[4:16]}$$

where F is the external field, f_0 and f are the Fermi distribution functions before and after the disturbance and τ is the relaxation time. Assuming the disturbance is small $\frac{df}{dE}$ can be replaced by $\frac{df_0}{dE}$ and $f - f_0 = \Delta f$

$$F = -e\,\mathcal{E}$$

where $\mathcal{E}$ is the applied electric field.

$$\Delta f = \frac{e}{\hbar} \tau \, \mathcal{E} \, \frac{df_0}{dE} \quad \nabla_k \; E$$

When the disturbance is produced by an alternating electric field applied in the x-direction given by $E_x = E_0 \, exp\,(i\omega\, t)$, Δf has to be replaced by Δf_1 given by

$$\Delta f_1 = \frac{1}{1 + i\omega\tau} \Delta f$$

For crystals with cubic symmetry the current will be in the same direction as the applied field. Hence we may write

$$J_x = -\frac{2}{(2\pi)^3} \frac{e^2}{\hbar} \int E_x \frac{\tau\, v_x}{1+i\omega\tau} \frac{\partial E}{\partial k_x} \frac{\partial f_0}{\partial E} d\Omega_k$$

$$\text{or} \quad J_x = -\frac{2}{(2\pi)^3} \frac{e^2}{\hbar} \int E_x \frac{\tau v_x}{1+i\omega\tau} \frac{\partial f_0}{\partial k_x} d\Omega_k$$

Separating the real and imaginary parts and using the substitution given by

$$\frac{\partial E_x}{\partial t} = i \; E_0 \, \omega \; exp\,(i\omega t) = i\omega E_x$$

$$J_x = -\frac{2}{(2\pi)^3} \frac{e^2}{\hbar} \left[E_x \int \frac{\tau\, v_x}{1+\omega^2\tau^2} \frac{\partial f_0}{\partial k_x} d\Omega_k - \frac{\partial\, E_x}{\partial\, t} \int \frac{\tau^2 v_x}{1+\omega^2\tau^2} \frac{\partial f_0}{\partial k_x} d\Omega_k \right] \quad \text{..............[4:17]}$$

The first term of this equation which is the in-phase component corresponds to a continuous current and the second term which is the out of phase component corresponds to a displacement current. Hence the equation [4:17] can be written

$$J_x = \sigma E_x + \chi \frac{\partial E_x}{\partial t}$$

where σ is the conductivity and χ is the electric susceptibility contribution of the carriers.

$$\text{ie} \quad \chi_{FC} = \frac{2}{(2\pi)^3} \frac{e^2}{\hbar} \int \frac{\tau^2 v_x}{1+\omega^2\tau^2} \frac{\partial f_0}{\partial k_x} d\Omega_k \qquad \ldots\ldots\ldots\ldots.[4:18]$$

Case when $\omega^2\tau^2 >> 1$

When this condition is satisfied the term 1 in the denominator of equation [4 :18] can be neglected and it may be written

$$\chi_{FC} = \frac{2}{(2\pi)^3} \frac{e^2}{\hbar\,\omega^2} \int v_x \frac{\partial f_0}{\partial k_x} d\Omega_k \qquad \ldots\ldots\ldots\ldots\ldots.[4:19]$$

The free carrier susceptibility is independent of τ and depends solely on the structure of the energy band, aside from carrier concentration. Integrating by parts the integral in equation [4:19] becomes

$$= \int \left[\, v_x \, f_0 \,\right]_{k_x = -\infty}^{k_x = +\infty} dk_y \, dk_z \;-\; \int \frac{\partial v_x}{\partial k_x} \, f_0 \, d\Omega_k$$

The first term is zero. For a band with spherical energy surfaces

$$v_x = \frac{1}{\hbar} \, \frac{\partial E}{\partial k_x}$$

$$\text{and} \qquad \chi_{FC} = \frac{2}{(2\pi)^3} \, \frac{e^2}{\hbar^2 \omega^2} \int \frac{\partial^2 E}{\partial k_x^2} \, f_0 \, d\Omega_k$$

For crystals with cubic symmetry the susceptibility is independant of the direction and hence it may be written

$$\chi_{FC} = \frac{2}{(2\pi)^3} \, \frac{e^2}{\hbar^2 \omega^2} \int \frac{1}{3} \left(\frac{\partial^2 E}{\partial k_x^2} + \frac{\partial^2 E}{\partial k_y^2} + \frac{\partial^2 E}{\partial k_z^2} \right) f_0 \, d\Omega_k$$

$$\text{or} \quad \chi_{FC} = \frac{1}{3} \, \frac{2}{(2\pi)^3} \, \frac{e^2}{\hbar^2 \omega^2} \int \nabla_k^2 E \; f_0 \, d\Omega_k \qquad \ldots\ldots\ldots\ldots\ldots\ldots\ldots [4:20]$$

The terms inside the integral can be expanded in spherical polar co-ordinates. Since there is spherical symmetry the angular terms vanish and we have

$$\chi_{FC} = \frac{1}{3\pi^2} \frac{e^2}{\hbar^2 \omega^2} \int_0^{\infty} \frac{\partial}{\partial k} \left(k^2 \frac{\partial E}{\partial k} \right) f_0 \, dk$$

Integrating by parts

$$\chi_{FC} = \frac{1}{3\pi^2} \frac{e}{\hbar^2 \omega^2} \left\{ \left[f_0 \, k^2 \frac{\partial E}{\partial k} \right]_{k=0}^{k=\infty} - \int_0^{\infty} \frac{\partial f_0}{\partial k} \, k^2 \, \frac{\partial E}{\partial k} \, dk \right\}$$

The first term is zero and changing the integration variable in the second term we have

$$\chi_{FC} = - \frac{1}{3\pi^2} \frac{e^2}{\hbar^2 \omega^2} \int_0^{\infty} k^2 \frac{\partial E}{\partial k} \frac{\partial f_0}{\partial E} \, dE \qquad \text{..........[4:21]}$$

So the free carrier contribution to the real part of the dielectric constant is given by

$$\varepsilon_{FC} = \frac{\chi_{FC}}{\varepsilon_0} \qquad \text{..................[4:22]}$$

Thus the total dielectric constant (real part) of the crystal in the spectral region of interest is given by

$$\varepsilon = \varepsilon_\infty + \varepsilon_{FC} + \varepsilon_{LV} \qquad \text{..................[4:23]}$$

b) Carrier concentration

The carrier concentration in a band in terms of the density of states may be written as

$$n = \int_0^\infty n(k) \; f_0 \; d\Omega_k$$

where $n(k) = \frac{2}{(2\pi)^3}$ and $d\Omega_k = 4\pi \; k^2 \; dk$

Hence we have

$$n = \frac{1}{\pi^2} \int_0^\infty f_0 \, k^2 \, dk$$

Integrating by parts

$$n = \left[\frac{1}{\pi^2} \; f_0 \; \frac{k^3}{3} \right]_{k=0}^{k=\infty} - \frac{1}{3\pi^2} \int_0^\infty k^3 \; \frac{\partial f_0}{\partial k} \; dk$$

The first term is zero and changing the variable of integration in the second term from dk to dE

$$n = \frac{1}{3\pi^2}\int_0^\infty k^3 \quad \frac{\partial f_0}{\partial E} \quad dE \qquad \text{...............[4:24]}$$

For a degenerate semiconductor the upper limit of integration can be replaced by E_F. Then $\frac{\partial f_0}{\partial E}$ vanishes everywhere except $E \simeq E_F$. Hence evaluating the equation at E_F

$$n = \frac{k_F^3}{3\pi^2} \qquad \text{................[4:25]}$$

c) Effective mass

It is seen that ϵ_{FC} in equation [4:11]contains m^*. Hence measurement of the free carrier contribution to the dielectric constant (or susceptibility) enables us to calculate the effective mass, if n is known. This method was first used by Spitzer and Fan (57S1) to determine the effective mass of the carriers in a semiconductor. The meaning of the effective mass for different cases of electron degeneracy has been discussed in section 1.6. Thus for degenerate semiconductor m^* given by equation [4:11] is the effective mass at the Fermi level.

Comparing equation [4:11],[4:22] and [4:21], and changing the upper limit of integration to E_F we have

$$\frac{1}{m^*} = \frac{1}{3\pi^2 \hbar^2 n}\int_0^{E_F} k^2 \quad \frac{\partial E}{\partial k} \quad \frac{\partial f_0}{\partial E} \quad dE$$

Evaluating the integral in a manner similar to that applied to obtain equation [4:24]

$$\frac{1}{m^*} = \frac{k_F^2 \left.\frac{dE}{dk}\right|_F}{3\pi^2 \hbar^2 n}$$

Substituting for n from equation [4:25]

$$\frac{1}{m^*} = \frac{1}{\hbar^2 k_F} \left.\frac{dE}{dk}\right|_F \qquad \text{................[4:26]}$$

Thus the effective mass one obtains in a degenerate case is the cyclotron effective mass at the Fermi level.

However, when the condition of full degeneracy $E_F >> KT$ is not satisfied, all the electrons in the band make contribution to the free carrier susceptibility which give rise to ε_{FC}. In such a case the effective mass has no specific meaning and can not be defined in a simple way. Then the exact expressions for susceptibility χ_{FC} given by equation [4:21] in terms of the electron distribution in k-space should be used in order to obtain the correct information about the band structure.

4.4 Review of Previous work in III - V materials

The first measurements of plasma edge reflectivity for the determination of effective mass were carried out by Spitzer and Fan (57S1). They determined the effective mass values of carriers in n and p-type Ge, Si, n and p-type InSb and n type InAs. Their results showed good agreement with the values obtained from other measurements. It was also reported that for n-type InSb and InAs, with increasing carrier concentration, the plasma edge shifts towards shorter wavelengths and the effective mass increases. The increase in effective mass was explained by its energy dependence, and making adegenerate approximation E vs k curve for the conduction band was obtained. Measurements on n-type GaAs doped from 5×10^{20} to 5×10^{24} m^{-3} were made by Spitzer and Whelan (59S2). Cardona (61C1) compared, the effective mass values for InAs obtained by Spitzer and Fan and that obtained by him from Faraday rotation measurements, with Kane's theory. The agreement was quite satisfactory. Some recent measurements on doped InAs samples have been reported by Nemelova and Coworkers (68N1). Reflection measurements on InP samples and the effective mass values have been reported by Newman (58N1) and Cardona (61C2).

Becker et al (61B1) and Cardona (61C3) conducted a thorough analysis of the data from plasma reflection measurement in n-type GaSb in conjunction with electric and galvenomagnetic data and interpreted the conduction band structure. Liang et al (68L1) have determined the conduction band structure of GaSb combining infrared reflectivity and Faraday rotation measurements. Light and heavy hole masses in GaAs and GaSb have also been determined by reflectivity measurements (68W1).

The only measurements in III - V alloys yet reported are those made on evaporated layers of $InAs_xSb_{(1-x)}$ alloys by Potter and Kretschmar (64P2) and the measurements made on two compositions of $Ga_xIn_{(1-x)}As$ alloys by Hockings et al (66H1).

4.5 Reflectivity measurements

a) Sample preparation

Preparation of alloys in ingot form has been described in section 2.6. The ingots were glued on long arborite blocks using glyptol. Cross-sectional slices of 1mm thick were cut from various positions along the length of the ingot using a 0.008" carborundum saw. The slices had varying composition and carrier concentration. These slices were glued on to small arborite blocks and were cut to be rectangular of approximate dimensions 12 x 3 mm. The small pieces cut out from the sample were used for x - ray powder photographs and hence the exact composition of each sample was determined. The rectangular slices were removed from the arborite block using acetone. These samples were carefully lapped using an adjustable lapping block on a glass plate covered with a mixture of distilled water and 600 grit lapping powder. The lapping was performed until about a 0.5mm thick sample was produced, making sure that the faces and the two longer sides were parallel. Then the sample was mounted flat on a specimen holder using glyptol. The face of the sample was then mechanically polished,using successively alumina powders of 5, 1, 0.3 and 0.05 μ grain size, on cloth covered wheels. The sample was removed from the holder using acetone. The other side of the sample was left unpolished in order to eliminate any effect of multiple reflection. These specimens were suitable for both reflectivity and Hall effect measurements.

Each sample was etched immediately before the reflectivity measurement. For InAs - GaAs alloys Wolsky etch (1 part HNO_3 + 7 part HCl + 8 part CH_3COOH) was used. For all other alloy systems a solution of 1 part HNO_3 plus 7 parts HCl was used. The sample was dipped in the etching solution with a tweezer only for few seconds and then washed in alcohol. In order to test this polishing technique initially two high resistivity samples of InSb and GaAs were prepared as described. The measured reflectance was found to show good agreement with previously published data (54O1, 59S2).

b) Optical system

The method of measuring reflectivity near normal incidence was similar to that used by other workers (60C2). The monochromator described in section 3,5a was used to obtain monochromatic beam. A convenient wavelength range, from 2 to 23 μ , was obtained by using an NaCl prism for the shorter wavelengths and a KB_r prism for the longer wavelengths. The exit optics were designed as shown in Fig. (4:1). The monochromatic beam from the exit slit filled a concave mirror M_1 of 4" diameter and 20.7cms focal length. The concave mirror produced an image of the exit slit on a plane where the sample was to be placed. The image was of approximate dimensions 10 x 1mm. A sample holder was designed to bring the sample and a reference mirror to the position of the image, alternately . A sketch of the holder is shown in Fig. (4:2). A rectangular brass plate was fixed to the axis of an aluminum rod and two identical holes were made on the plate, symmetrically on either side of the axial rod. A small aluminised plane mirror was held against one hole and a small rectangular brass plate,which served to mount the sample, was held against the other hole by means of screws. The axial rod was mounted on a circular gear wheel coupled to a screw thread. By turning the screw the sample or the reference mirror could be brought to the plane of the image. The light beam reflected by the sample or the reference mirror was focussed by a concave mirror M_2 of focal length 5.8cms on to the sensitive element of the bolometer detector. The mirrors M_1 and M_2 were fixed as close as possible so that the angle of incidence of the beam on the sample was always

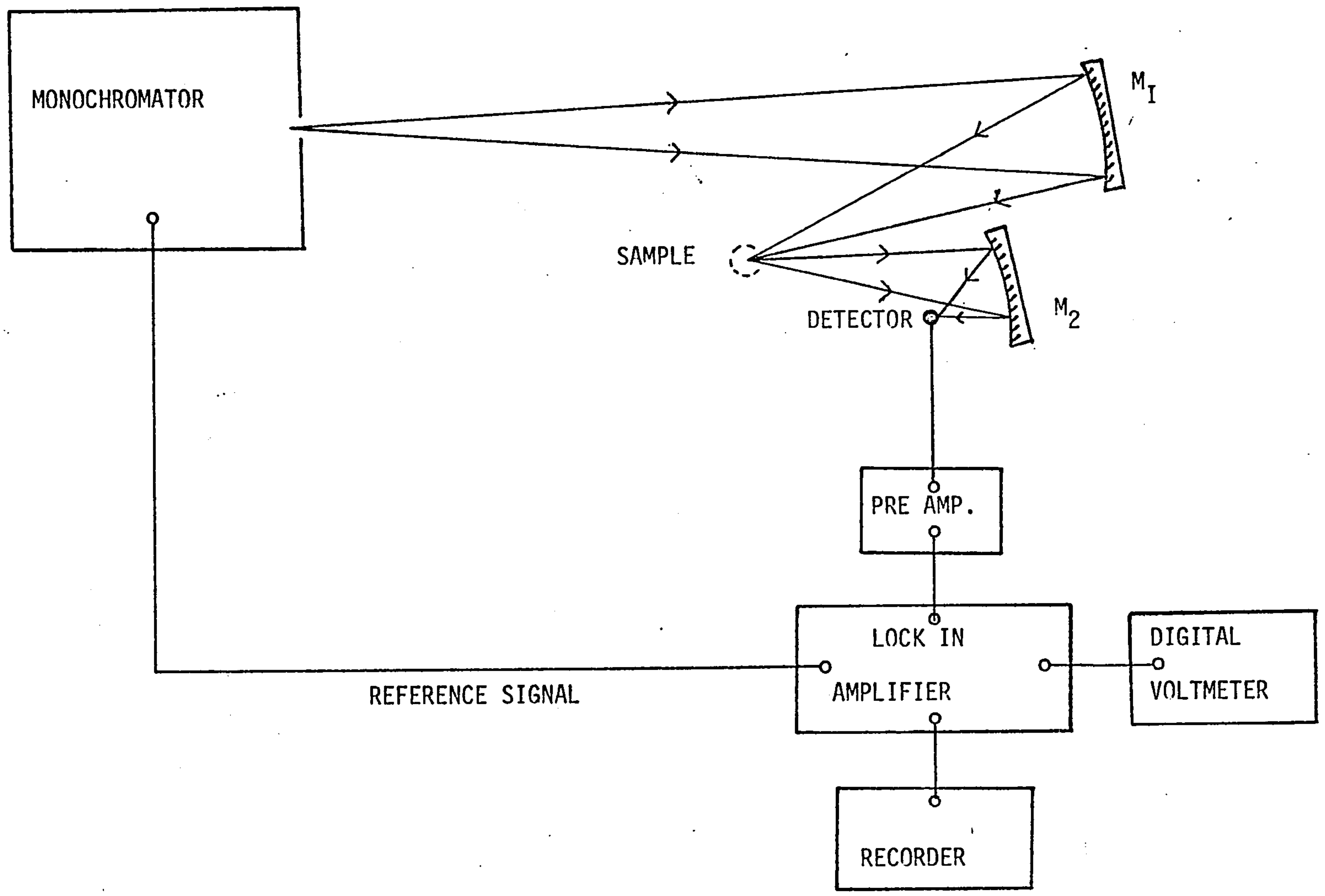

Fig.(4:I) Electro-Optical system for infrared reflectiviy measurement

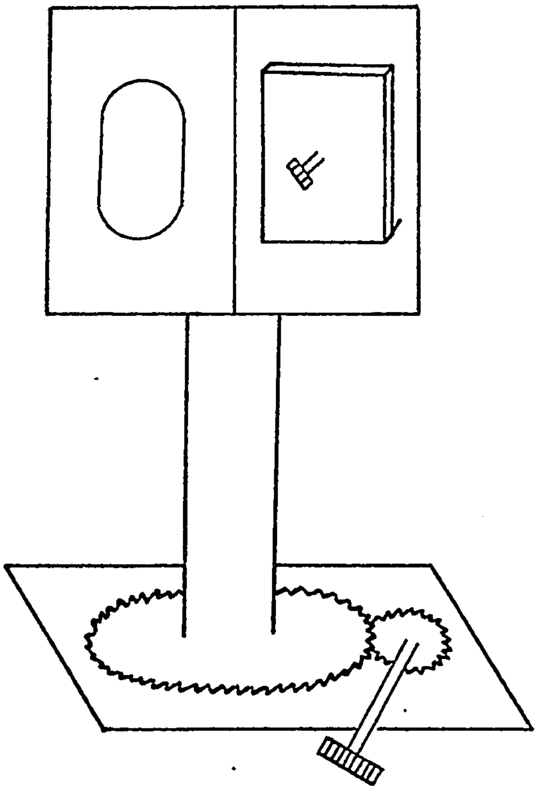

Fig.(4:2) Specimen holder for reflectivity measurement

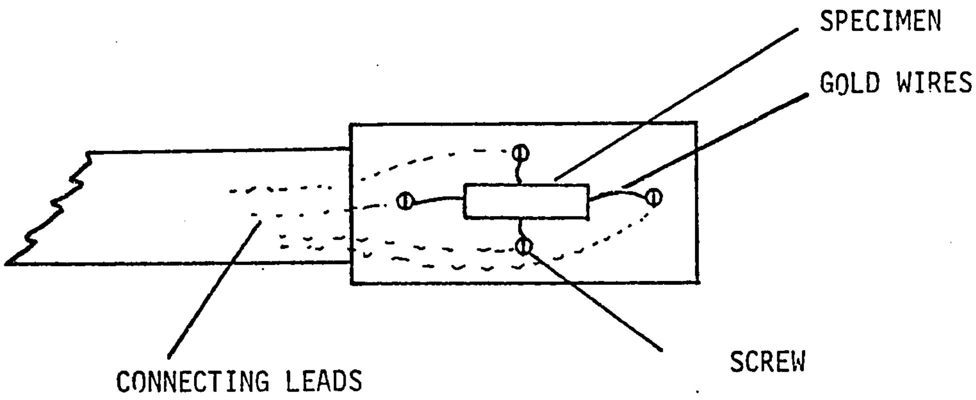

Fig.(4:3) Hall probe

less than 10°. The angle of incidence on mirrors M_1 and M_2 was also made as small as possible in order to minimise the distortion of the image. All the mirrors could be tilted in vertical and horizontal planes by the screws at the back of the mirrors. The mirrors were aluminised and coated with silicon monoxide to prevent deterioration of the surface.

The output of the detector was first amplified by a preamplifier and then by a Model 120 P.A.R. lock-in amplifier. The lock-in amplifier was operated in the selective external mode as described in section 3.5a. The output of the amplifier was fed into a Phillips chart recorder and was also displayed on a digital voltmeter. An input signal of one microvolt could be easily measured above the noise level.

c) Alignment procedure

The exit optics were aligned using a mercury vapour lamp in place of the globar source. The power for the monochromator and the electronic instruments were turned on and the green line of the mercury spectrum was brought at the exit slit by adjusting the wavelength cam lever. The sample was mounted on the brass plate with the polished surface facing outwards. Then the plate containing the sample was placed on the sample holder so that the sample was at the centre of the opening. The holder was then rotated so that the sample was facing M_1 , and then M_1 was adjusted so that the image of the exit slit was formed at the centre of the sample. The sample holder was slowly rotated so that the reflected beam was completely falling on M_2. Finally M_2 was aligned so that the focussed beam was falling on the proper position of the detector face in order to have maximum signal output as shown by the digital voltmeter. The reference mirror was brought to the position of the image by rotating the holder through 180° and the previous alignment procedure was repeated. Reference marks were made corresponding to the position of the sample and the reference mirror so that they can be brought in position without the aid of visible light. However, for each sample, small adjustments were necessary to optimise the signal. Since the measurement of absolute reflectivity was involved the correct alignment of the system before each measurement was important.

d) Measurement procedure

The mercury lamp was removed and the globar was replaced. The water supply for the globar cooling system was turned on and few minutes were allowed to reach steady conditions. The reflected intensity from the sample was observed on the digital voltmeter and small adjustments of the mirrors were made to optimise the signal. First a quick run of the spectrum was taken to determine the position of plasma minimum. Then a slow run of the appropriate region of the spectrum was made and the spectrum was recorded on the chart. The chart could be read and the values of I_r corresponding to different values of the wavelength could be obtained. The same procedure was repeated with the reference mirror in position and a chart record of I_0 vs λ in the same spectral region was obtained. Values of I_r and the corresponding values of I_0, at 0.2 micron intervals were read from the chart. The ratios I_r/I_0 were determined. Thus values of R as a function of λ were obtained, assuming the reflectivity of aluminum to be equal to one.

4.6 Hall effect measurements

a) Equipment

A four point probe as shown in Fig. (4:3) was used for Hall effect measurements. Sample contacts were made by small gold wires held by small screws on to the end base of the probe. Current and voltage leads were taken from the screws along the length of the probe. The circuit used for Hall measurement is shown in Fig. (4:4). All the wires from the probe to the control panel were shielded. A back off system was used to balance the zero field D.C. voltage between the Hall contacts. The voltage contribution due to magnetoresistance was eliminated by measuring the Hall voltage in normal and reverse magnetic fields and taking the average of the two.

b) Measurement

The sample, after reflectivity measurement, was placed on the Hall probe and the gold wires were spark welded to obtain ohmic contacts of low resistance of the order of 1 or 2 ohms. The probe was mounted between the pole pieces of an electromagnet, so that the sample faces were normal to the field direction. The magnet was a Magnion - Harvey Wells 15 inch electromagnet with a pole gap of 1¼" and a maximum field of $3.2 Wb/m^2$.

The leads from the probe were connected to the control panel. The current through the sample and the back-off emf were supplied by two 12 volt automobile batteries. The current through the sample was adjusted to be approximately 80ma by a variable resistor in series with the specimen. The current was determined from the potential drop across a 1 ohm standard resistance measured with a Rubicon potentiometer. The voltage across the Hall probes was amplified by an Artrodata Nanovolt amplifier model 120 and the output was displayed on a Hewlett Packard digital voltmeter. The zero field voltage was nulled by adjusting the resistance in the back off system. Fields from 1to 3.2W/m^2 were applied and the corresponding voltages were measured for either direction of the field. The average value of the Hall voltage for each value of the magnetic field was determined.

After the Hall measurement the sample was taken out from the probe; the thickness was measured at different places using a micrometer screw and an average value of the thickness was determined.

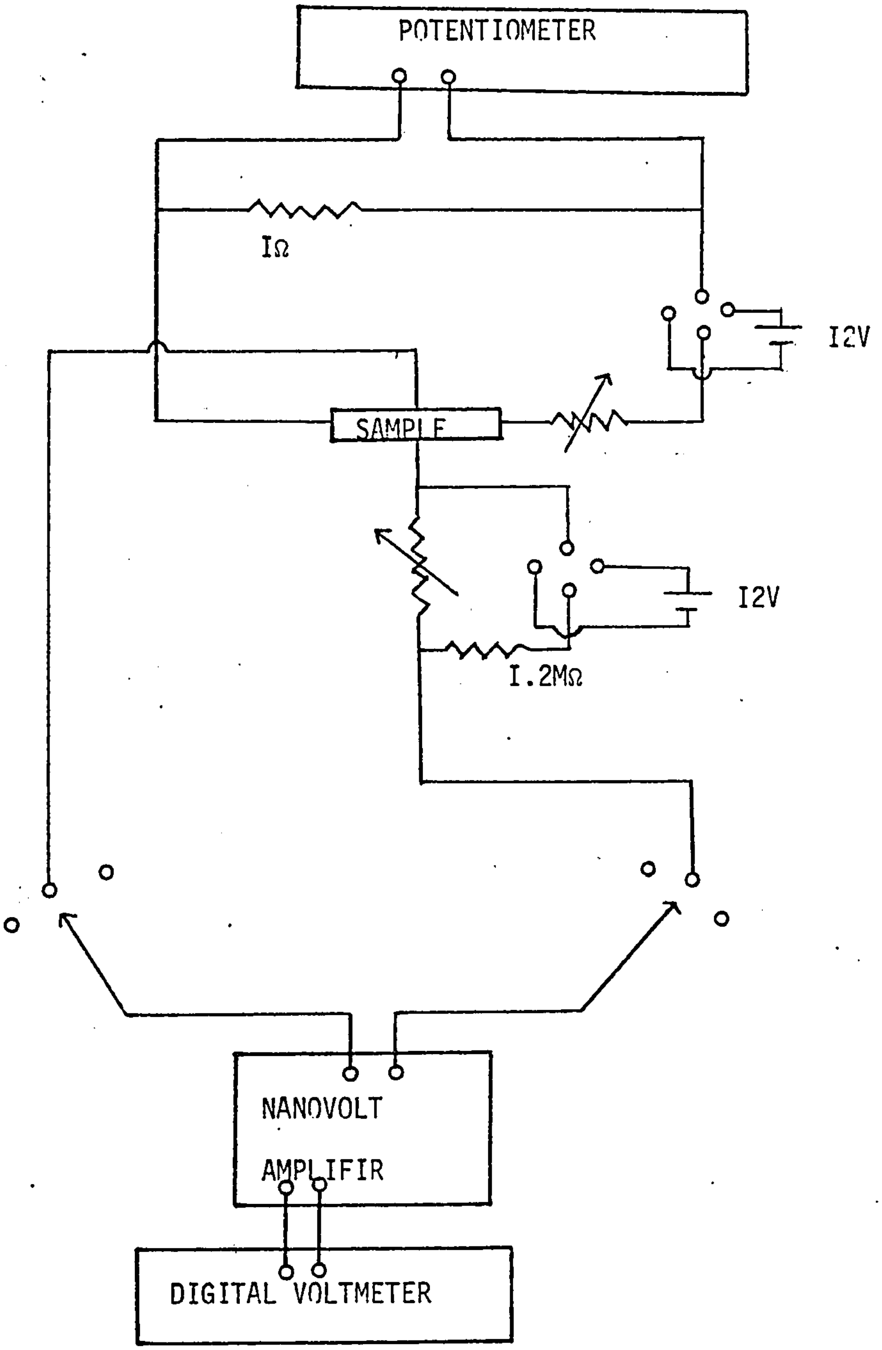

Fig.(4:4) Electrical circuit for Hall effect measurement

4.7 Method of analysis of data

Experimental data have been obtained on three alloy systems $Ga_xIn_{(1-x)}Sb$, $Ga_xIn_{(1-x)}As$ and $InAs_xSb_{(1-x)}$. Since the method of analysis of the data is only dependent on the degree of degeneracy of the samples and not on the alloy system considered, first the procedure of analysis for various cases is discussed before the data for each alloy system are presented.

For all the alloy systems considered here there are electrons only in the (000) band and the mobility values are high so that the condition $(\omega\tau)^2 >> 1$ is always satisfied in the infrared range. Under this condition equations [4:10], [4:22] and [4:23] are valid. For $\lambda < \lambda_{min}$ the imaginary part of the dielectric constant is small and hence κ is very small compared to η according to equation [4:9]. So κ^2 can be neglected in equation [4:7] and [4:8] so that

$$R = \frac{(\eta - 1)^2}{(\eta + 1)^2} \qquad \text{.................[4:27]}$$

and

$$\varepsilon = \eta^2 \qquad \text{.................[4:28]}$$

Thus, for wavelengths less than the plasma minimum the dielectric constant can be calculated from the measured value of R only.

a) Degenerate case ie $E_F >> KT$

If ε_{LV} is negligible, for $\lambda < \lambda_{min}$ equation [4:23] reduces to equation [4:10] and m^* can be calculated from the slope of ε vs λ^2 graph knowing n. The intercept on the ε axis gives the value of ε_∞. However, if the value of reflectivity at the minimum is very low so that $R \simeq 0$, m^* can be easily estimated from λ_{min} only. In such a case $\eta=1$ and $\varepsilon=1$. Hence equation [4:10] can be written

$$\left(\frac{m^*}{m} \right) = \frac{ne^2}{4\pi^2 c^2 m \varepsilon_0 (\varepsilon_\infty - 1)} \lambda^2_{min}$$

and $\frac{m^*}{m}$ can be easily calculated knowing λ_{min} and n. This method has been previously used for determining the electron effective mass values in GaAs (59S2), InP (58N1) and in some other compounds. However, for the alloys considered here values of ε_∞ were not known and values of R_{min} were not always sufficiently low and hence the above method was not used.

The effective mass at the bottom of the (000) band can be calculated assuming that the E - k relation for the band is given by the Kane equation [1:8], and using the experimental effective mass value.

Differentiating equation [1:8]

$$\left.\frac{dE}{dk}\right|_{E=E_F} = 2a\,k_F\left\{1+\left[1+\frac{4a}{E_0^*}\left(\frac{m}{m_0^*}-1\right)k_F^2\right]^{-\frac{1}{2}}\left(\frac{m}{m_0^*}-1\right)\right\}\text{......[4:29]}$$

Substituting $a = \frac{\hbar^2}{2m}$ and k_F from equation [4:25] in equation [4:26] it can be shown

$$\left(\frac{m}{m^*}\right) = 1+\left(\frac{m}{m_0^*}-1\right)\left[1+\frac{4a}{E_0^*}\left(\frac{m}{m_0^*}-1\right)(3\pi^2 n)^{2/3}\right]^{-\frac{1}{2}}\quad\text{.....[4:30]}$$

where E_0^* is the effective mass band gap, and m_0^* is the bottom of the band effective mass. For each sample m^*/m can be calculated from reflectivity measurement and n can be calculated from Hall effect measurement. Then, if E_0^* is knownm_0^*/m can be easily calculated from equation [4:30]. Since no experimental data for E_0^* values for the alloys have been reported and the value for InSb (62S1) has been shown to be the mean of room temperature and absolute zero values of the energy gap, it has been arbitrarily assumed that E_0^* values for alloys can also be taken in the same way. However, from test calculations, it has been found that the effect of changing E_0^* between the room temperature and absolute zero values of the energy gap produced only very little effect on the m_0^* values calculated. For each specimen m_0^*/m can be obtained from the experimental values of n and m^*/m by an iterative solution of equation [4:30]. The value of the Fermi energy for each sample can also be obtained by evaluating equation [1:8] at $E = E_F$.

b) Case of general degeneracy

When the fully degenerate condition ($E_F >> KT$) is not satisfied the general equations given by [4:23] and [4:22] were used. Equation [4:23] can be written

$$\varepsilon = \varepsilon_\infty - \lambda^2 \left(\frac{e^2}{12\pi^4 C^2 \hbar^2 \varepsilon_0} \right) I + \varepsilon_{LV} \qquad \text{..............[4:31]}$$

$$\text{where } I = \int_0^\infty k^2 \frac{dE}{dk} \frac{df_0}{dE} \, dE \qquad \text{..............[4:32]}$$

Again a Kane band model is assumed. Differentiating Kane equation [1: 8]

$$\frac{dE}{dk} = 2ak \left\{ 1 + \left[1 + \frac{4a}{E_0^*} \left(\frac{m}{m_0^*} - 1\right) k^2 \right]^{-\frac{1}{2}} \left(\frac{m}{m_0^*} - 1\right) \right\} \text{...[4:33]}$$

$$f_0 = \frac{1}{1 + exp\left(\frac{E-E_F}{KT}\right)}$$

$$\frac{df_0}{dE} = \frac{1}{KT} \qquad \frac{1}{2 + exp\left(\frac{E-E_F}{KT}\right) + exp\left(\frac{E_F-E}{KT}\right)} \qquad \text{..........[4:34]}$$

Using equation [4:33] and [4:34], equation [4:32] becomes

$$I = \frac{2a}{KT} \int \frac{k^3 \left\{1 + \left(\frac{m}{m_0^*} - 1\right)\left[1 + \frac{4a}{E_0^*}\left(\frac{m}{m_0^*} - 1\right) k^2\right]^{-\frac{1}{2}}\right\}}{2 + exp\left(\frac{E-E_F}{KT}\right) + exp\left(\frac{E_F-E}{KT}\right)} dE \qquad \text{...[4:35]}$$

For all III - V compounds the term ak^2 in equation [1:8] may be neglected, since it is much smaller than the second term. Hence an expression for k in terms of E can be obtained and is given by

$$k = \left[\frac{E\,(E + E_0^*)}{a\,E_0^*\left(\frac{m}{m_0^*} - 1\right)}\right]^{\frac{1}{2}} \qquad \text{......................[4:36]}$$

Substituting for k in equation [4:35] we have

$$I = \frac{2a}{KT} \int_0^\infty \frac{\left[\frac{E\,(E + E_0^*)}{aE_0^*\left(\frac{m}{m_0^*} - 1\right)}\right]^{3/2} \left\{1 + \left(\frac{m}{m_0^*} - 1\right)\left[1 + \frac{4E}{E_0^{*2}}(E+E_0^*)\right]^{-\frac{1}{2}}\right\}}{2 + exp\left(\frac{E-E_F}{KT}\right) + exp\left(\frac{E_F-E}{KT}\right)} dE \qquad \text{..[4:37]}$$

Since the reflectivity measurements were made at frequencies much higher than the reststrahlen frequency, $\omega^2 >> \omega_t^2, \gamma_{lv}^2$. Hence neglecting ω_t^2 and γ_{lv}^2 compared to ω^2 in equation [4:15], it may be written

$$\varepsilon_{LV} = - \varepsilon_\infty \; (\nu_l^2 - \nu_t^2) \; \lambda^2 \qquad \ldots\ldots\ldots\ldots.[4:38]$$

where ν_l and ν_t are the longitudinal and transverse optical phonon frequencies expressed in wave numbers. Using equation [4:37] and [4:38], equation [4:31] can be written

$$\varepsilon = \varepsilon_\infty - S \; \lambda^2 \qquad \ldots\ldots\ldots\ldots\ldots\ldots.[4:39]$$

where $S = S_{FC} + S_{LV}$ ....[4:40]

$$S_{FC} = \frac{e}{6KT \; a^{\frac{1}{2}} \; \pi^4 \; c^2 \; \hbar^2 \; \varepsilon_0} \left[\frac{1}{E_0^* \; (\frac{m}{m_0^*} - 1 \;)} \right]^{3/2}$$

$$x \int_0^\infty \frac{[E \; (E + E_0^*) \;]^{3/2} \left\{ 1 + (\frac{m}{m_0^*} - 1) \; \left[1 + \frac{4E}{E_0^{*2}} \; (E + E_0^*) \right]^{-\frac{1}{2}} \right\}}{2 + \; exp \; (\frac{E-E_F}{KT}) + \; exp \; (\frac{E_F-E}{KT})} dE \; ..[4:41]$$

$$S_{LV} = \varepsilon_\infty \left(\nu_l^2 - \nu_t^2\right) \qquad \text{......................[4:42]}$$

According to equation [4:39] independent of the degree of degeneracy of the sample, always a plot of ε against λ^2 gives a straight line of slope S. If S_{LV} is calculated using equation [4:42] the experimental value of S_{FC} can be obtained. Using equation [4:34] and [4:36] in equation [4:24] the expression for carrier concentration in a general case is given by

$$n = \frac{1}{3\pi^2 \quad KT} \quad \frac{1}{\left[a\ E_0^* \left(\frac{m}{m_0^*} - 1\right) \right]^{3/2}}$$

$$\times \int_0^\infty \frac{\left[E\ (E + E_0^*) \right]^{3/2}}{2 + \exp\left(\frac{E-E_F}{KT}\right) + \exp\left(\frac{E_F-E}{KT}\right)}\ dE \qquad \text{......[4:43]}$$

Equation [4:41] and [4:43] contain two experimentally measured parameters S_{FC} and n, and three unknown parameters E_0^*, E_F and m_0^*. Again E_0^* values were assumed as mentioned earlier. Then the two equations can be solved to give values of $\frac{m_0^*}{m}$ and E_F. Numerical integration methods were used on an IBM 360 computer in order to compute the integrals involved in the equations. The computer program is given in Appendix I. For a series of values of E_F, the corresponding values of $\frac{m_0^*}{m}$ consistent with equation [4:41] can be obtained. Thus a curve of E_F vs $\frac{m_0^*}{m}$ can be plotted and this curve gives the different possible solutions of equation [4:41]. Similarly, for the same values of E_F, the corresponding values of m_0^*/m consistent with equation [4:43] can be obtained. These values of m_0^*/m can also be plotted against E_F and this curve gives the possible solutions consistent with equation [4:43]. The intersection of the two curves will give the value of m_0^*/m and E_F for the specimen.

c) Determination of τ , μ_{opt} and σ

Using the value of reflectivity at the plasma minimum it is possible to make a direct determination of the relaxation time of the carriers. Making use of the condition that R should be a minimum at λ_{min} and under the approximation $\omega^2 \tau^2 >> 1$ an expression for the absorption index κ in terms of η at the minimum can be obtained (68M1)

$$\kappa_{min} = \frac{(\varepsilon_\infty - 1)(\eta_{min}^2 - 1)}{(5\,\eta_{min}^2 + 3\,\varepsilon_\infty - 2)} \qquad \text{...............[4:44]}$$

For large values of $\omega_p\tau$, the following approximate expressions have also been obtained (68M1)

$$\left.\begin{aligned} \kappa^2_{min} &= 4\ R_{min} \\ \eta_{min} &= 1 + 5\ R_{min} \\ \omega^2_p &= \left(1 - \frac{\eta^2_{min}}{\varepsilon_\infty}\right) \omega^2_{min} \end{aligned}\right\} \qquad \text{.........[4:45]}$$

$$\tau = \frac{1}{\omega_{min}} \left(\frac{\varepsilon_\infty - \eta^2_{min} - \kappa^2_{min}}{2\ \eta_{min}\ \kappa_{min}} \right) \qquad \text{.........[4:46]}$$

$$\mu_{opt} = \frac{e\tau}{m^*} \qquad \text{.........[4:47]}$$

$$\sigma = n\ e\ \mu_{opt} = \varepsilon_\infty\ \varepsilon_0\ \omega^2_p\ \tau \qquad \text{.........[4:48]}$$

Thus τ , μ_{opt} and σ can be calculated from plasma reflection data at the minimum.

4.8 Data, Results and Discussion

a) $Ga_xIn_{(1-x)}Sb$ alloys

Samples of this alloy system were taken from ingots D.F.A-8, T.F.A-3 and T.F.A-2. Reflectance measurements were made on 13 specimens in the composition range $0 < x < 0.82$. Curves for R against λ were plotted and typical curves are shown in Fig. (4:5). All the curves show the characteristic plasma reflection edge. For wavelengths less than the plasma minimum the dielectric constant values were calculated and plotted against λ^2. The resulting graphs for the specimens in Fig. (4:5) are shown in Fig. (4:6). All the graphs are straight lines as expected from the theory. Values of ε_∞ for each specimen were obtained from the intercept on the ε axis. The slopes of the lines corresponding to each of the samples were also calculated. Typical Hall data for a sample is shown in Table (4,1). The carrier concentration was calculated from the saturation value of the Hall coefficient R_∞ at high fields. Under this condition the Hall scattering factor is equal to one independant of the scattering mechanism and degree of degeneracy, so that $n = 1/eR_\infty$. For all samples the Hall coefficient reached saturation below the field $3Wb/m^2$. All the relevant data for the samples are recorded in Table (4,2). Since all the samples had electron concentration greater than $10^{24}/m^3$ degenerate condition was assumed and the suceptibility effective mass values and the corresponding effective mass values at the bottom of the band were calculated by the method described for the degenerate case in section 4.7a. The calculated values are given in Table (4,3). From the values of the Fermi energy, it is easily seen that the above assumption is valid. The effect on the slope of the ε vs λ^2 line due to the lattice dispersion was calculated from equation [4:42] and for all samples the effect was estimated to be less than 2%.

Since this is within experimental error here, the correction was neglected in calculating the final values of m_0^*/m. Fig.(4:7) shows the variation of m_0^*/m as a function of x. The values obtained by Faraday rotation and magnetothermoelectric power measurements (69A1) are also shown in the same figure for comparison. It is seen that the results are in good agreement with one another. The variation of ε_∞ as a function of x is plotted in Fig. (4:8) and it is seen that with in the limits of experimental error the variation is linear with x between the values for the two compounds (16.9 for InSb and 15.2 for GaSb), the individual values showing a scatter about the straight line of up to 7%.

As indicated by the dashed part of curve in Fig. (4:7), in the range $0.85 < x < 1.0$ no experimental measurement was made. In this region there will be electrons in the (000) band and the <111> minima even at low levels of doping. Hence the method of analysis developed for single band in the previous section is no longer valid and the data can be interpreted only with some aditional measurements as carried out by Liang et al (68L1). Such a complicated procedure was not carried out. However it is seen that an extrapolation of the data gives a value of 0.045 for the effective mass at the bottom of (000) band for GaSb. For InSb a value of 0.013 is obtained. These values for the compounds are in good agreement with the values obtained from other experimental measurements (62D1).

Woolley and Thompson (64W2) attempted to predict the variation of the effective mass m_0^* with x at the bottom of (000) conduction band, using Kane model modified by Cardona for higher band interactions, and the available band gaps at the Γ point. The values of m_0^*/m given in Fig. (4:7) are, over most of the composition range, smaller than the values predicted. This is mainly due to the choice of a constant value of 23 ev for P^2 at all values of x, in the calculation. Another reason could be the fact that a modified form of the Kane equation was used by Woolley and Thompson.

From the value of reflectivity at the plasma minimum values of τ, ω_p, μ_{opt} and σ for all the samples were calculated using equations [4:45], [4:46], [4:47] and [4:48]. These results are recorded in Table (4,4). The relaxation time is a direct measurement from plasma minimum. The values of τ , μ_{opt} and σ are all in the right order of magnitude. Since the samples are different in composition and carrier concentration it is difficult

Thickness t (mm)	Current I (ma)	Set field B_s (Wb/m^2)	V ($\times 5 \times 10^{-4}$ volts)	$V-$ ($\times 5 \times 10^{-4}$ v.)	Hall Voltage V ($\times 5 \times 10^{-4}$ volts)	Correct B field (Wb/m^2)	$\frac{V}{B}$ ($\times 10^{-4}$)
0.718	81.41	1	0.794	0.878	0.836	1.0611	3.9390
0.719	81.22	1.6	1.241	1.438	1.340	1.7003	3.9405
0.716	81.10	2.0	1.553	1.823	1.688	2.1398	3.9443
0.718		2.2	1.689	2.005	1.847	2.3562	3.9194
0.718		2.4	1.824	2.175	2.000	2.5580	3.9093
		2.6	1.954	2.339	2.147	2.7558	3.8954
		2.8	2.085	2.505	2.295	2.9518	3.8874

Average t = 0.718 , Average I = 81.24 ma

$$R_\infty = \frac{V}{B} \cdot \frac{t}{I} = 3.4357 \times 10^{-6} \; m^3/\,\text{Coulomb}$$

$$n = 1.8168 \times 10^{24} \; /m^3$$

Table (4,1) Typical Hall data (Sample T.F.A-3, 204)

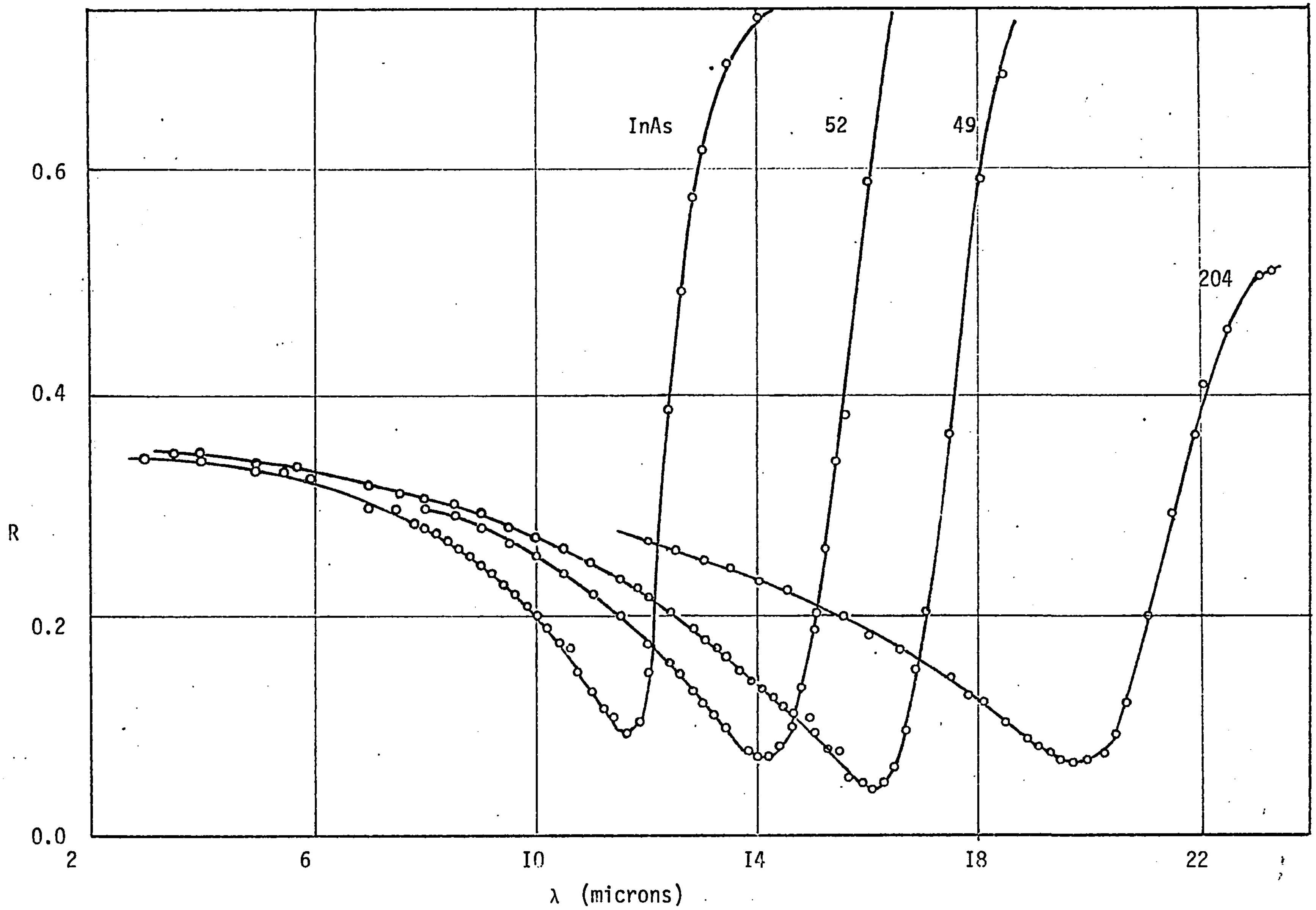

Fig.(4:5) Typical plasma reflection curves for $Ga_xIn_{(I-x)}Sb$ alloys

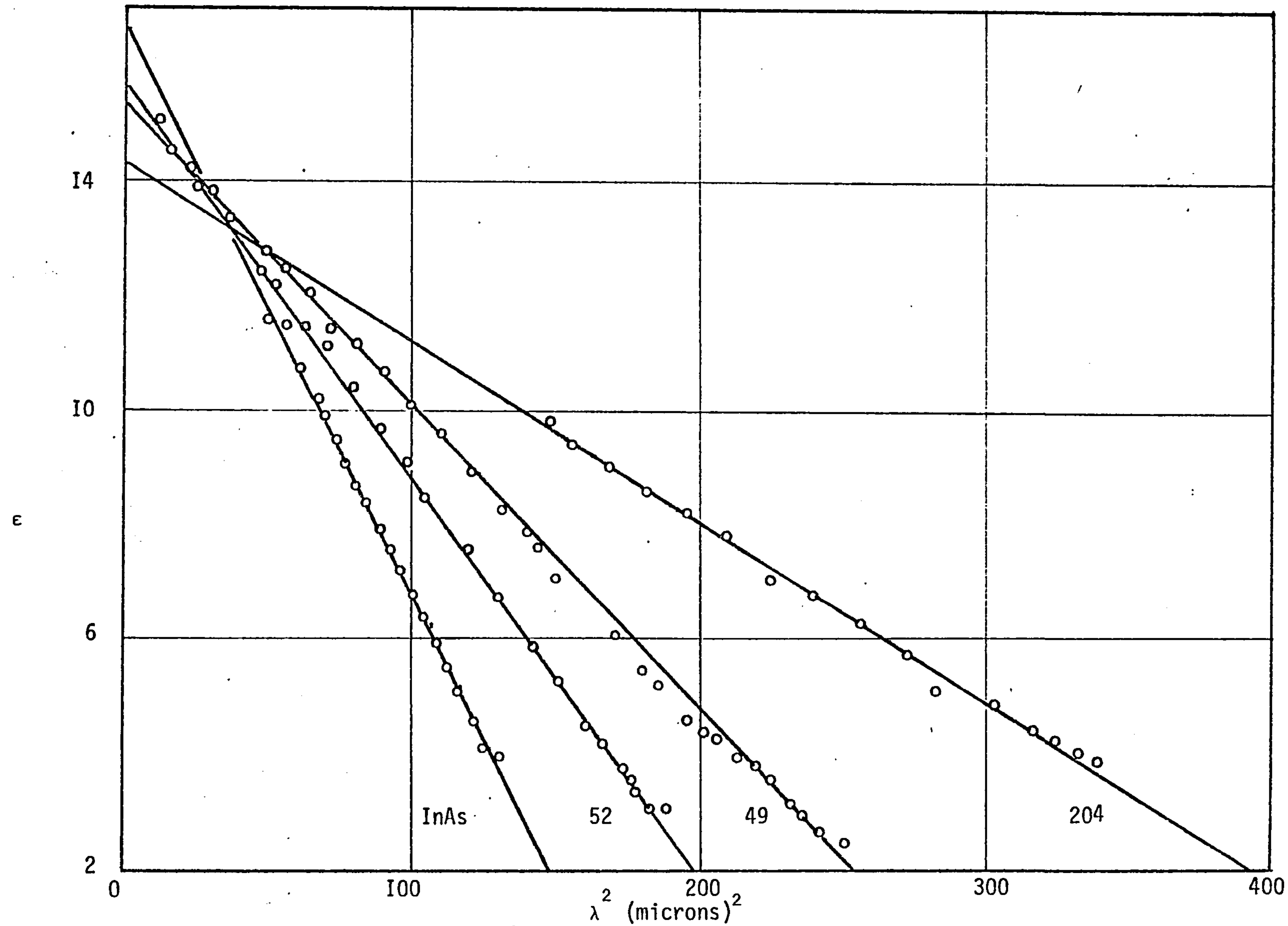

λ^2 (microns)^2

Fig.(4:6) Typical graphs of ε vs λ^2 for $Ga_xIn_{(I-x)}Sb$ alloys

Ingot	Code No of Specimen	Distance along the ingot (cms)	x	Thickness (mm)	n ($\times 10^{24}/m^3$)	slope ($\times 10^{-2}/m^2$)
-	InSb	-	0.000	0.389	6.278	10.1200
D.F.A-8	E25-12	12.6	0.100	0.509	1.385	3.3227
D.F.A-8	E25-31	11.0	0.170	0.543	1.292	3.1364
T.F.A-2	52	5.95	0.300	0.466	3.696	6.8965
T.F.A-2	51	5.45	0.355	0.565	3.535	6.4680
T.F.A-2	50	5.05	0.395	0.652	3.242	6.2220
T.F.A-2	49	4.55	0.440	0.528	2.653	5.3103
T.F.A-2	48	4.2	0.485	0.534	2.588	4.7452
T.F.A-2	44	3.45	0.580	0.529	2.169	4.3093
T.F.A-2	46	3.05	0.605	0.509	2.210	4.3617
T.F.A-2	45	2.4	0.645	0.718	1.900	3.8515
T.F.A-3	204	2.25	0.775	0.191	1.817	3.2151
T.F.A-3	205	0.85	0.820	0.627	1.578	2.7800

Table (4,2) Experimental data for $Ga_xIn_{(1-x)}Sb$ alloys

Code No of Specimen	x	ε_∞	E_0^* (ev)	$\frac{m^*}{m}$	$\frac{m_0^*}{m}$	E_F (ev)
InSb	0.000	16.9	0.205	0.05564	0.0133	0.3567
E25 - 12	0.100	14.5	0.225	0.03738	0.0154	0.1712
E25 - 31	0.170	13.8	0.245	0.03694	0.0165	0.1616
52	0.300	16.0	0.285	0.04807	0.0178	0.2633
51	0.355	15.2	0.305	0.04902	0.0198	0.2449
50	0.395	16.0	0.32	0.04674	0.0196	0.2400
49	0.44	15.4	0.345	0.04481	0.0209	0.2126
48	0.485	14.9	0.360	0.04893	0.0251	0.1856
44	0.580	15.6	0.415	0.04514	0.0255	0.1730
46	0.605	16.4	0.43	0.04546	0.0261	0.1729
45	0.645	16.6	0.46	0.04425	0.0271	0.1570
204	0.775	14.5	0.56	0.05069	0.0360	0.1254
205	0.820	14.5	0.60	0.05091	0.0381	0.1112

Table (4,3) Computed values for $Ga_xIn_{(1-x)}Sb$ alloys

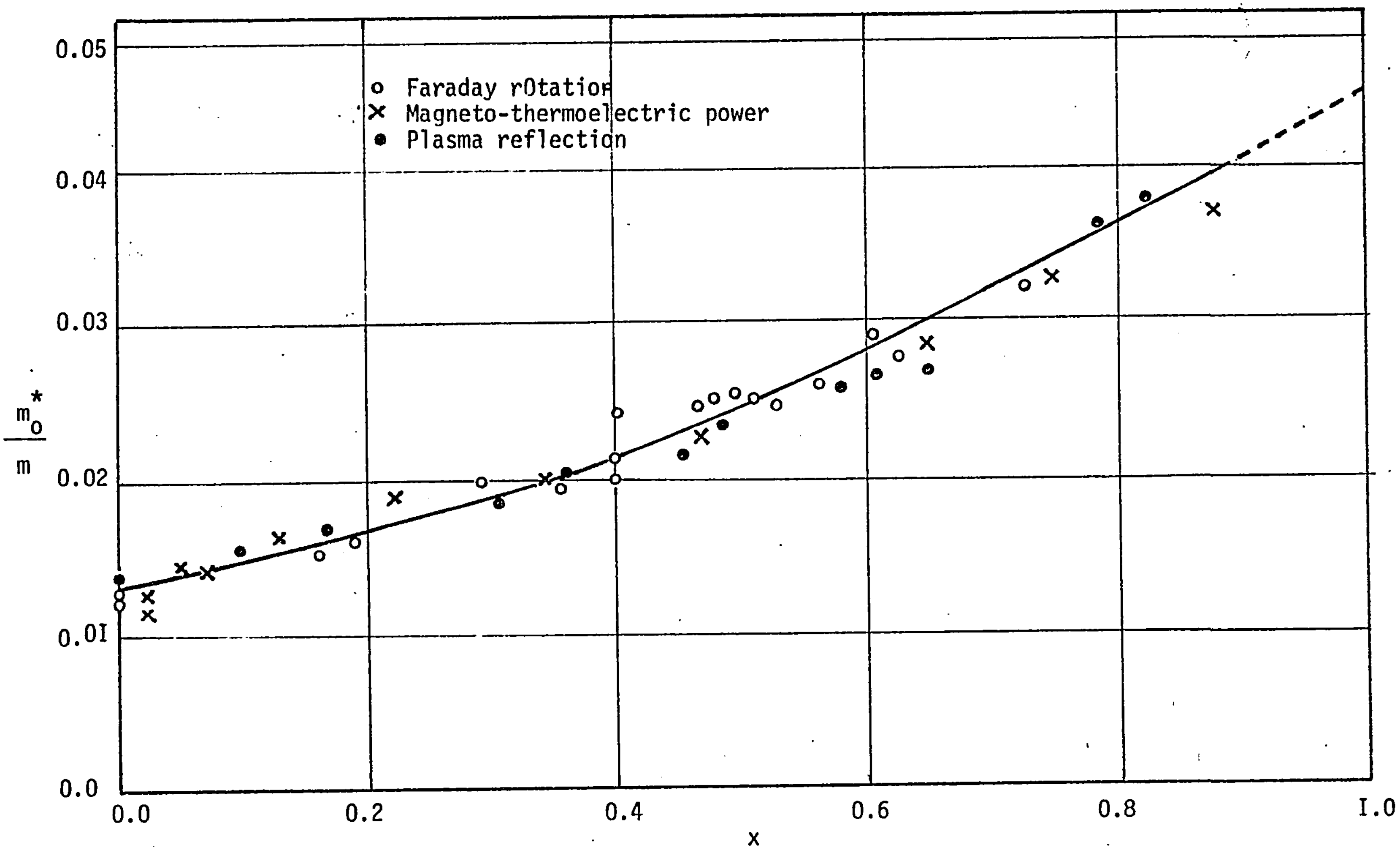

Fig.(4:7) Variation of m_o^*/m with composition for $Ga_xIn_{(I-x)}Sb$ alloys

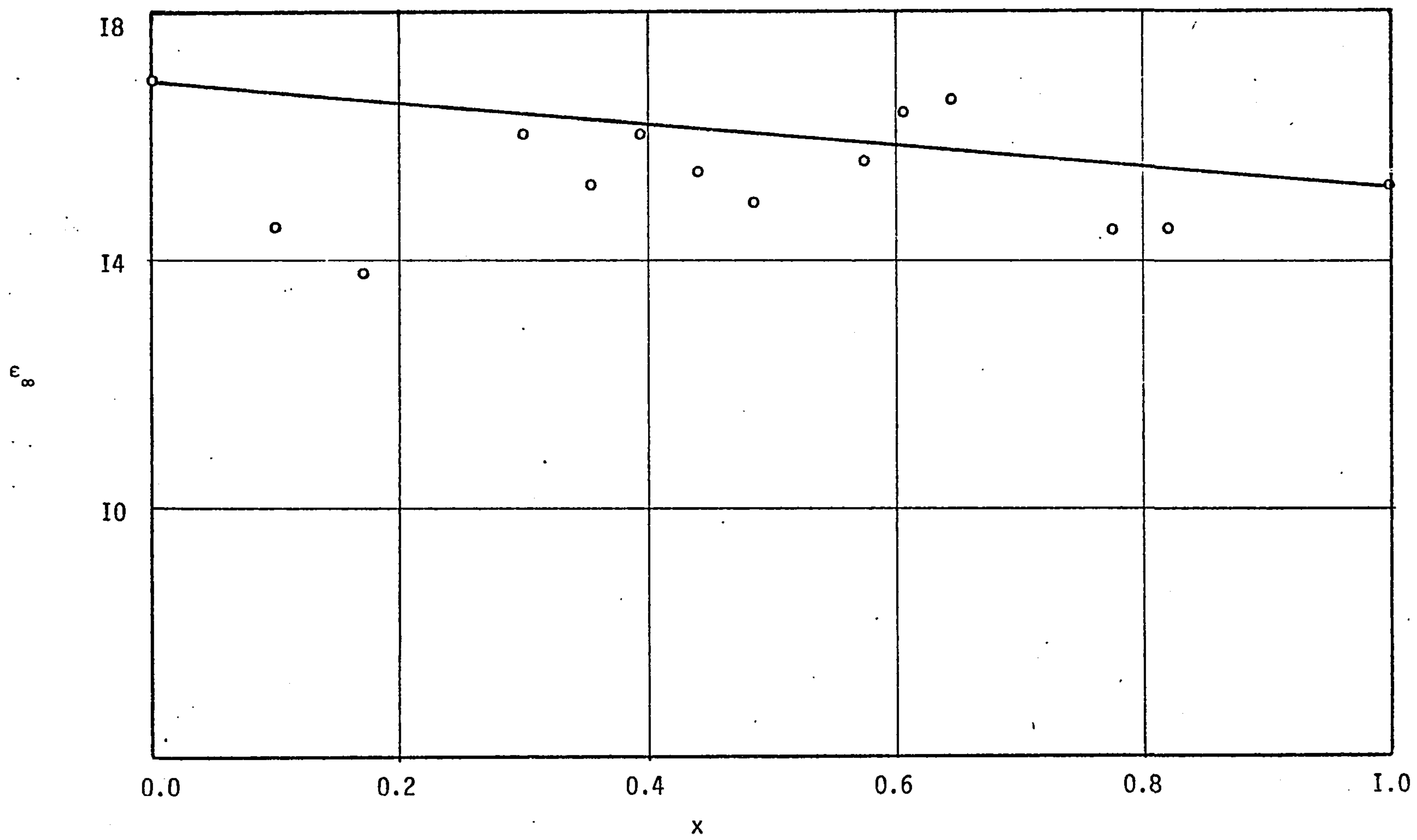

Fig.(4:8) Variation of ε_∞ with composition for $Ga_xIn_{(I-x)}Sb$ alloys

Code NO of Specimen	x	R_{min}	λ_{min} (microns)	τ $(x10^{-13}sec)$	ω_p $(x10^{14}/sec)$	μ_{opt} $(m^2/Volt.sec)$	σ $(x10^5\Omega^{-1}m^{-1})$
InSb	0.000	0.095	11.6	0.5195	1.5157	0.1642	1.7850
E25-2	0.100	0.110	18.8	0.6194	0.9152	0.2915	0.6651
E25-31	0.170	0.086	19.4	0.7578	0.8961	0.3608	0.7432
52	0.300	0.052	14.2	0.9753	1.2589	0.3569	2.1888
51	0.355	0.040	14.4	1.1473	1.2451	0.4117	2.3927
50	0.395	0.050	14.7	1.0390	1.2172	0.3910	2.1797
49	0.440	0.040	16	1.2706	1.1209	0.4988	2.1756
48	0.485	0.045	16.6	1.1720	1.0760	0.4213	1.7895
44	0.580	0.060	17.8	1.0683	0.9992	0.4163	1.4727
46	0.605	0.095	17.6	0.7626	0.9967	0.2951	1.0995
45	0.645	0.095	18.8	0.8255	0.9340	0.3282	1.0579
204	0.775	0.060	19.9	1.1103	0.8897	0.3828	1.1205
205	0.820	0.099	20.4	0.7422	0.8492	0.2564	0.6868

Table (4,4) Computed values from plasma minimum for $Ga_xIn_{(1-x)}Sb$ alloys to make any quantitativecomparison with theory. The mobility calculated here is the optical mobility and is usually less than the conductivity mobility as reported by other workers (67H1). It is very difficult to make quatitative comparison between the two mobilities. In an electrical measurement the mobility measured is an average for all the free electrons in the bulk sample. However in an optical measurement the mobility of the electrons in the penetration depth of 20 to 30 microns is obtained.

b) $Ga_xIn_{(1-x)}As$ alloys

Samples in the composition range $0.0 < x < 0.5$ were taken from the ingot T.F.B-1 and samples in the range $0.5 < x < 1.0$ were taken from the ingot T.F.B-8. The carrier concentration of the samples was in the range 9×10^{23} to 6×10^{24} m^{-3}. Reflectivity and Hall effect measurements were made on 15 samples over the whole composition range. Plasma reflection curves and the corresponding ε vs λ^2 graphs for few typical samples are shown in Fig. (4:9) and Fig. (4:10) respectively. For a few GaAs rich samples it was not possible to observe the plasma minimum, since the minimum was beyond the range of the monochromator. ε vs λ^2 graphs for all samples were straight lines indicating the validity of equations [4:10]and [4:39] . The values of ε_∞ obtained are plotted as a function of x in Fig. (4:11) and they show linear variation between the values of

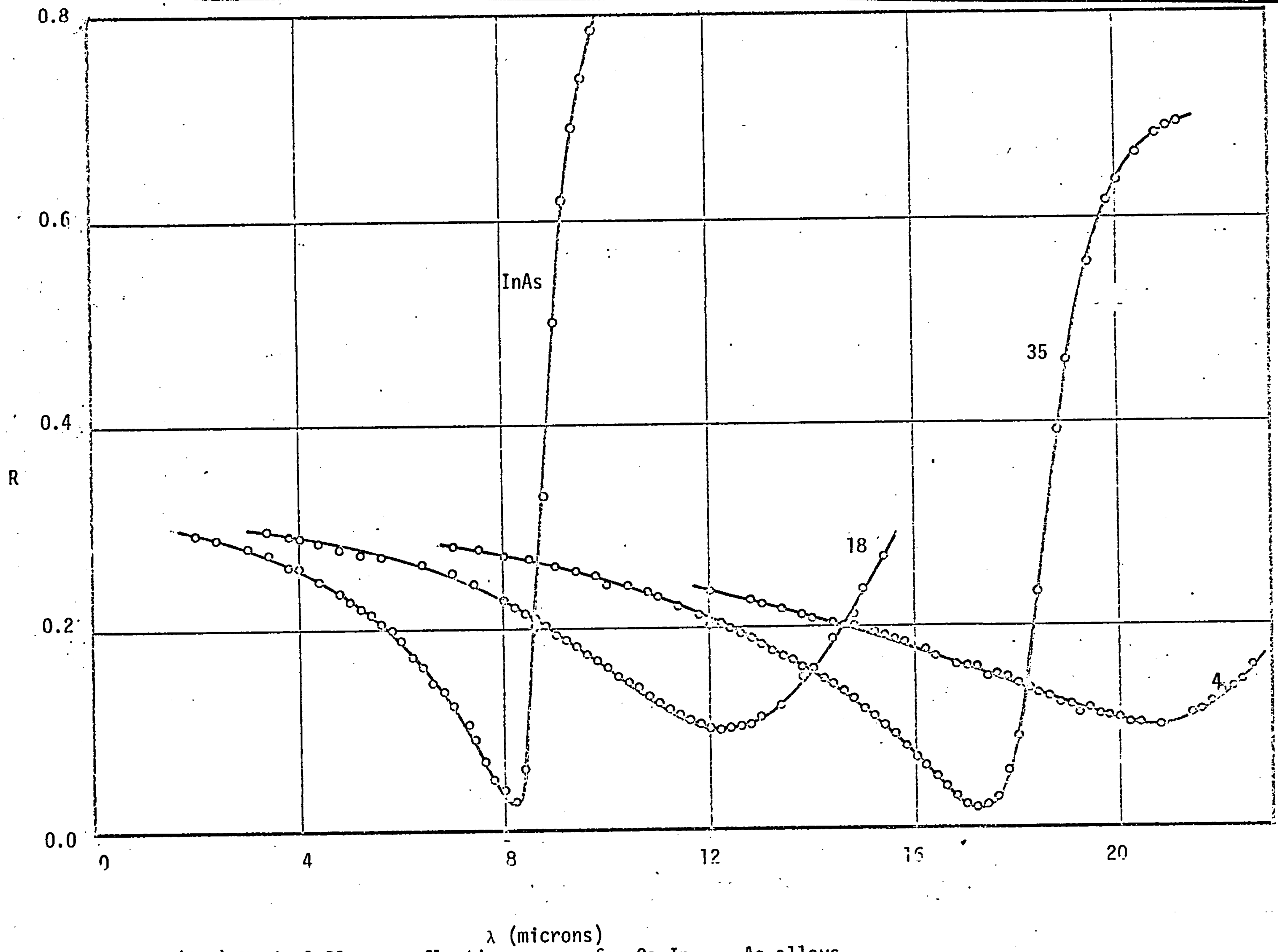

Fig. (4:9) Typical Plasma reflection curves for $Ga_xIn_{(1-x)}As$ alloys

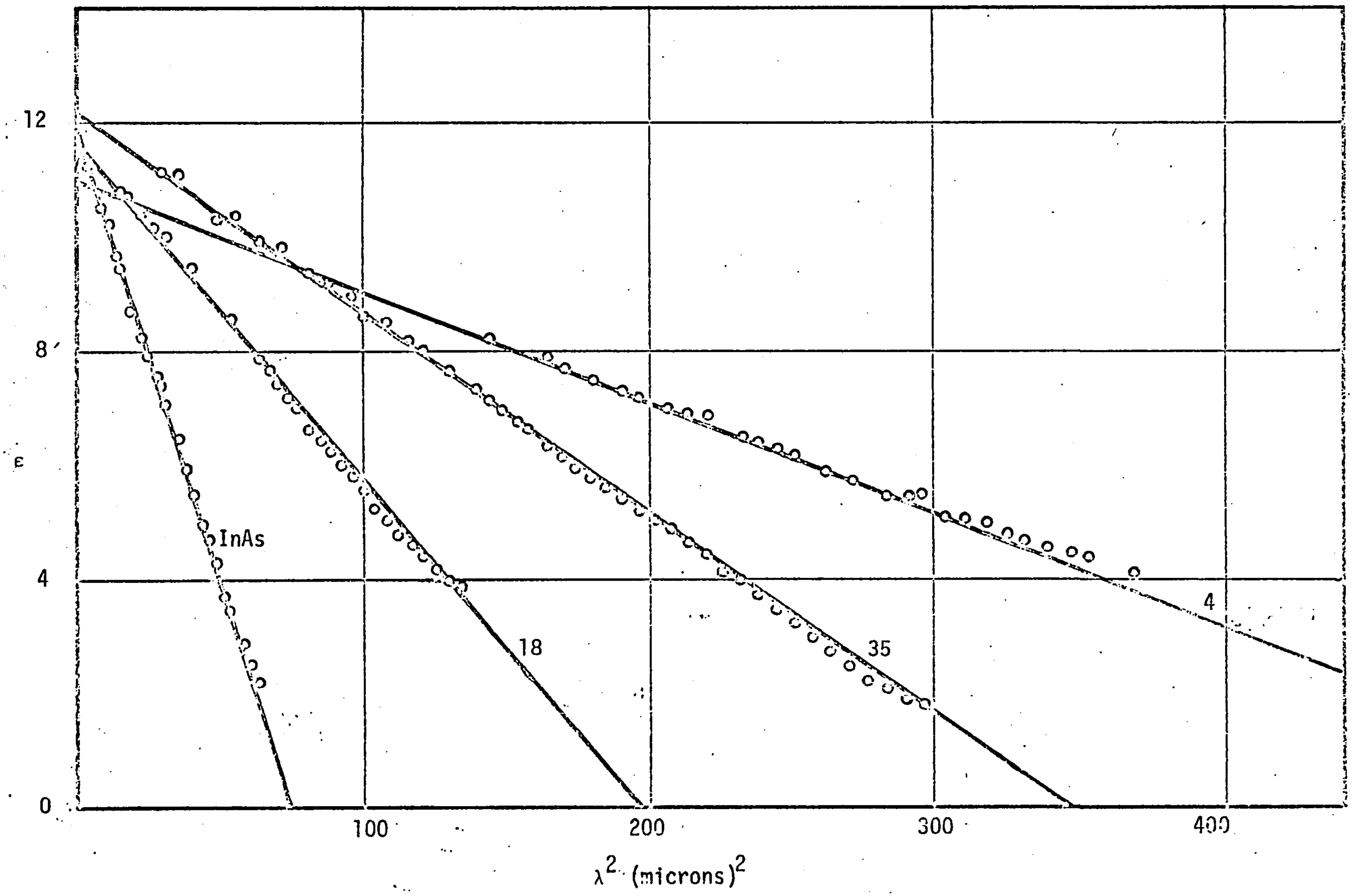

Fig. (4:10) Typical graphs of ε vs λ^2 for $Ga_xIn_{(1-x)}As$ alloys

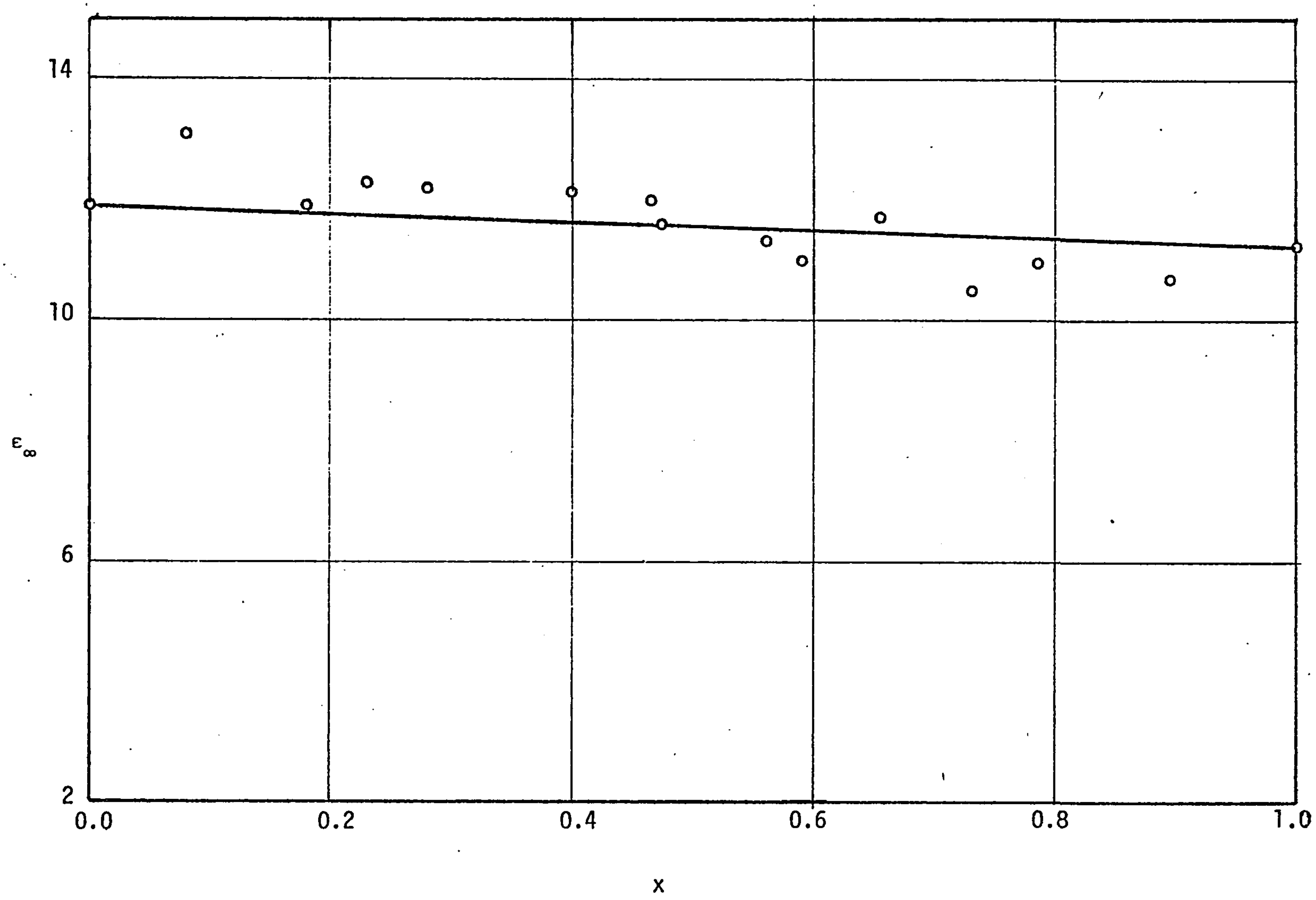

Fig. (4:II) Varation of ε_∞ with x for $Ga_xIn_{(1-x)}As$ alloys

Ingot	Code No of Specimen	Distance along the ingot (cms)	x	Thickness (mm)	n ($\times 10^{24}/m^3$)	S ($\times 10^{-2}/m^2$)	S_{LV} ($\times 10^{-2}/m^2$)	S_{FC} ($\times 10^{-2}/m^2$)
T.F.B-1	InAs	-	0.000	-	12.030	15.455	-	15.455
T.F.B-1	30	11.15	0.080	0.543	2.394	4.440	-	4.440
T.F.B-1	33	8.85	0.180	0.544	2.104	3.914	-	3.914
T.F.B-1	50	8.3	0.230	0.653	2.095	3.942	-	3.942
T.F.B-1	35	7.5	0.280	0.331	1.886	3.517	-	3.517
T.F.B-1	AT-417	6.6	0.400	0.432	1.604	2.909	-	2.909
T.F.B-1	81	-	0.465	0.655	1.361	2.280	-	2.280
T.F.B-8	17	6.45	0.475	0.465	6.338	8.657	-	8.657
T.F.B-1	52	4.95	0.560	1.004	1.118	1.685	-	1.685
T.F.B-8	15	6.15	0.590	0.469	5.483	7.383	-	7.383
T.F.B-8	18	6.25	0.655	0.487	4.318	5.970	-	5.97
T.F.B-8	14	5.8	0.730	0.483	1.992	2.793	0.096	2.697
T.F.B-8	4	4.85	0.785	0.799	1.443	1.977	0.107	1.870
T.F.B-8	16	2.75	0.895	0.337	0.868	1.200	0.128	1.072
-	GaAs	-	1.000	0.686	1.897	2.277	0.14	2.137

Table (4,5) Experimental data for $Ga_x In_{(1-x)} As$ alloys

Code No of Specimen	x	ε_∞	E_0^* (ev)	$(\frac{m^*}{m})$	$(\frac{m_0^*}{m})$	E_F (ev)
InAs	0.000	11.9	0.397	0.06982	0.0250	0.4007
30	0.080	13.1	0.445	0.04836	0.0284	0.1701
33	0.180	11.9	0.510	0.04821	0.0313	0.1506
50	0.230	12.3	0.540	0.04766	0.0315	0.1510
35	0.280	12.2	0.580	0.04809	0.0336	0.1365
AT-417	0.400	12.1	0.690	0.04947	0.0380	0.1144
81	0.465	12.0	0.750	0.05354	0.0438	0.0922
17	0.475	11.6	0.770	0.06567	0.0430	0.2297
52	0.560	10.3	0.850	-	0.0492	0.0588
15	0.590	11.0	0.885	0.06661	0.0478	0.1986
18	0.655	11.7	0.960	0.06488	0.0493	0.1695
14	0.730	10.5	1.060	-	0.0550	0.0826
4	0.785	11	1.130	-	0.0595	0.0582
16	0.895	10.7	1.275	-	0.0645	0.0301
GaAs	1.000	11.25	1.460	-	0.0706	0.0595

Table (4,6) Computed values for $Ga_xIn_{(1-x)}As$ alloys

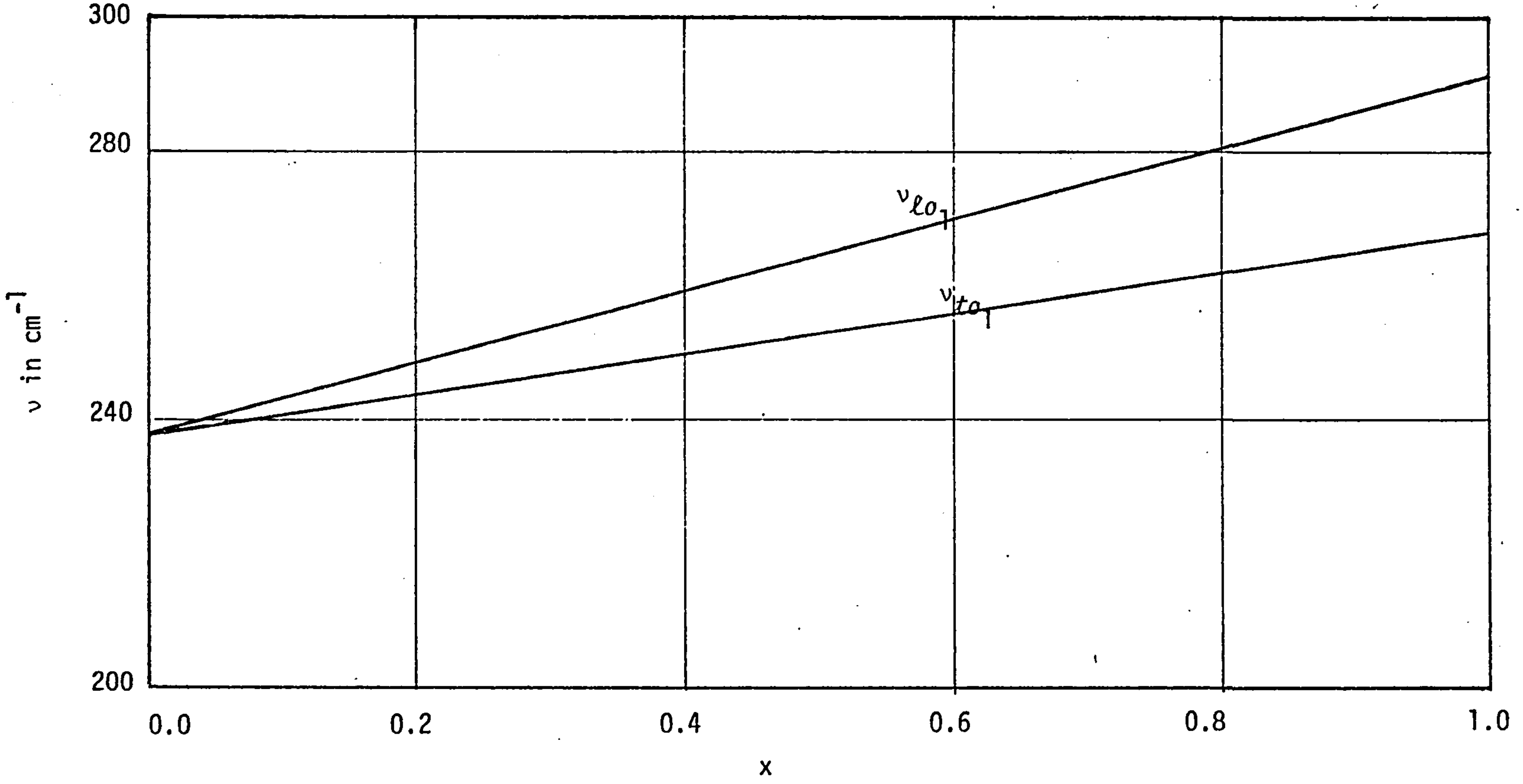

Fig. (4:12) Variation of longitudinal and transverse optical phonon frequencies for $Ga_xIn_{(1-x)}As$ alloys according to reference 68B1

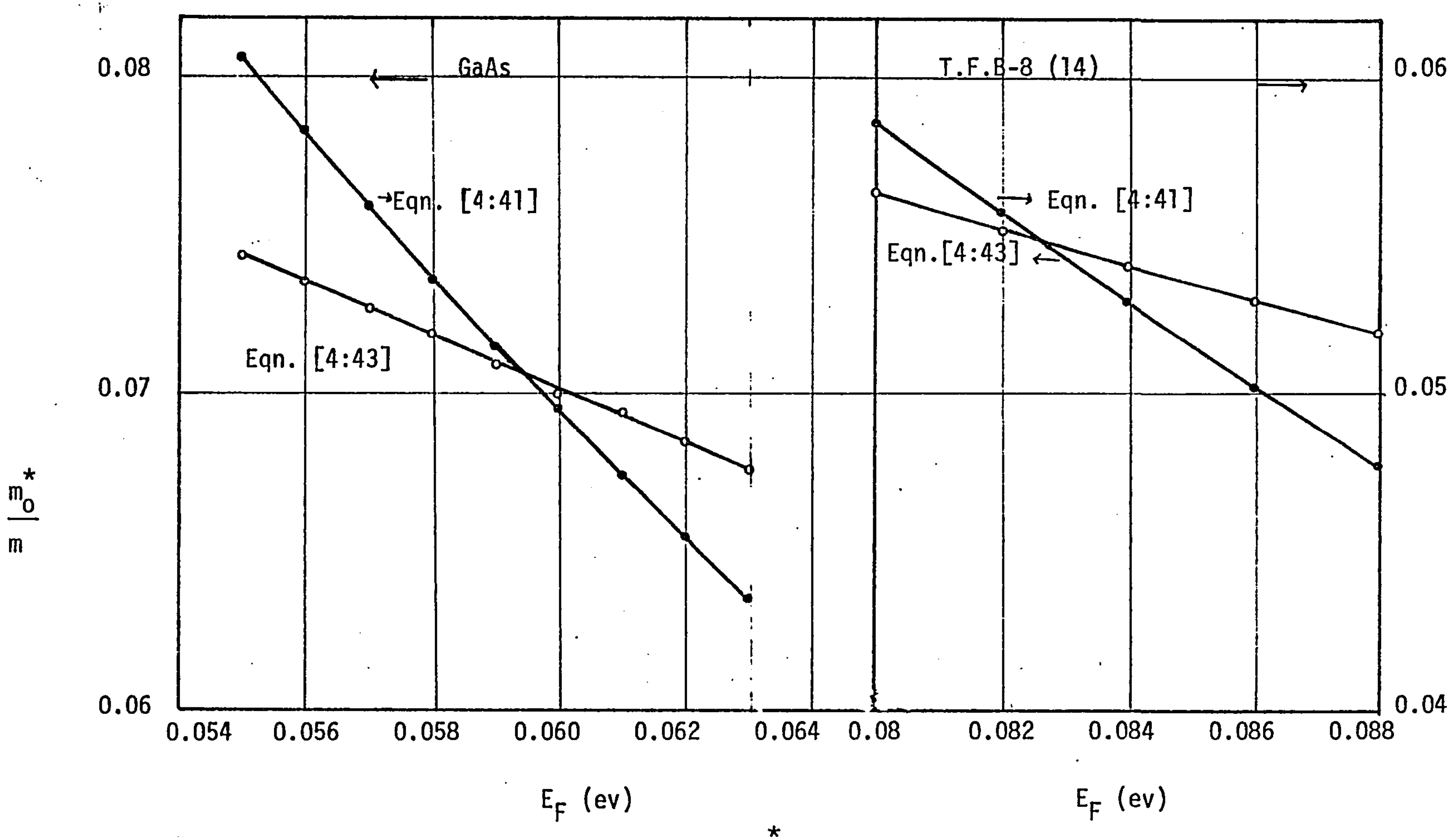

Fig. (4:13) Graphical solution to obtain m_o^*/m and E_F for two typical samples of $Ga_xIn_{(1-x)}As$ alloys

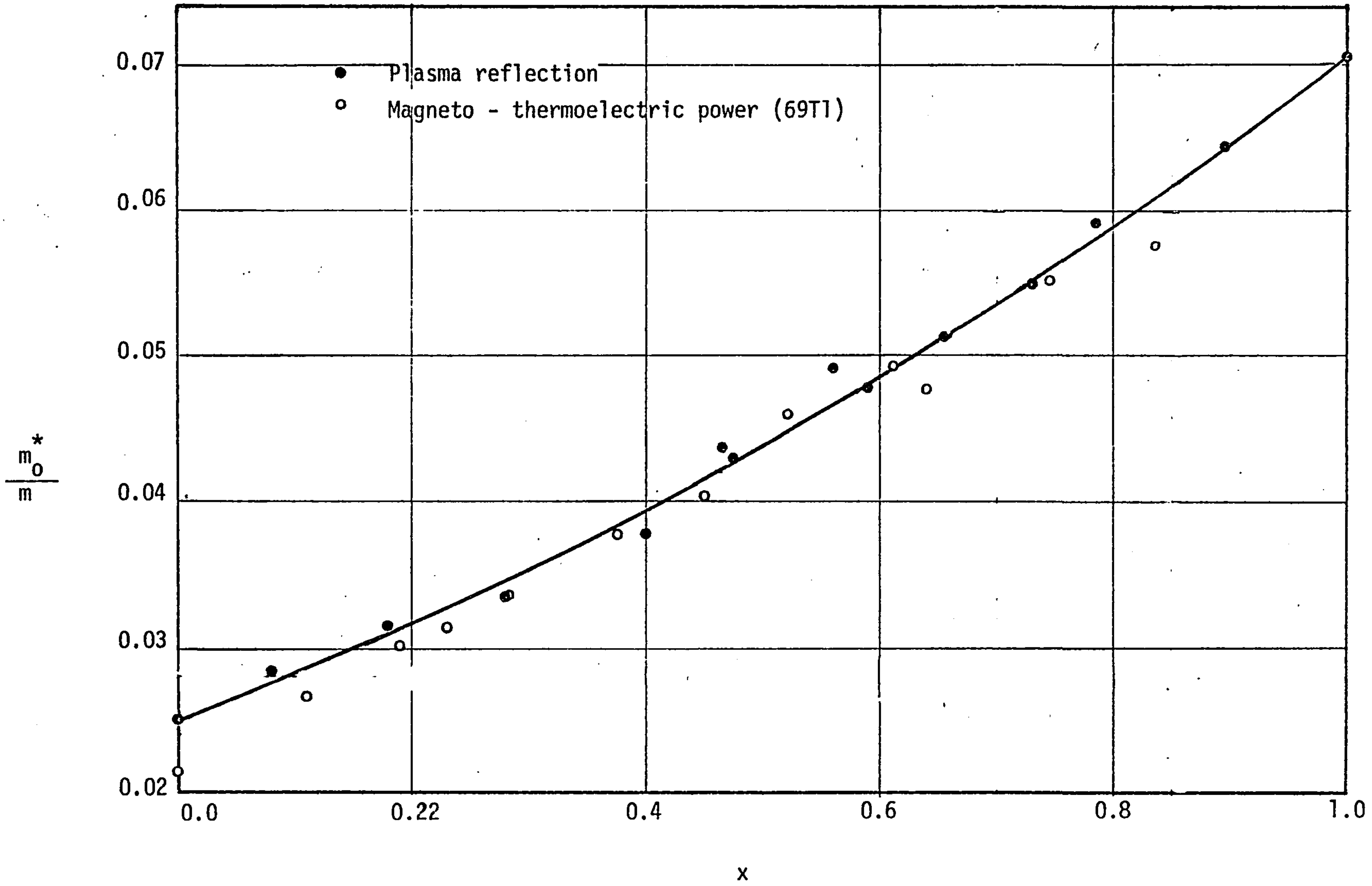

Fig. (4:14) Variation of m_o^*/m with composition for $GaIn_{(1-x)}As$ alloys

Code No of specimen	x	$(\frac{m^*}{m})$	R_{min}	λ_{min} (microns)	τ ($\times 10^{-14}$sec)	ω_p ($\times 10^{14}$/sec)	μ_{opt} (m^2/volt sec)	σ ($\times 10^5 \Omega^{-1} m^{-1}$)
InAs	0.000	0.06982	0.029	8.3	6.175	2.1407	0.1558	2.9802
30	0.080	0.04836	0.064	15.7	7.403	1.1170	0.2693	1.0710
33	0.180	0.04821	0.020	16.4	15.354	1.0886	0.5602	1.9161
50	0.230	0.04766	0.019	16.6	16.607	1.0780	0.6129	2.1006
35	0.280	0.04809	0.022	17.2	15.619	1.0380	0.5713	1.8182
AT 417	0.400	0.04947	0.057	18.6	8.792	0.9411	0.3126	0.8338
81	0.465	0.05354	0.086	20.4	6.806	0.8410	0.2236	0.5112
17	0.475	0.06567	0.016	10.6	11.010	1.6853	0.2948	3.2090
52	0.56	0.05953	0.069	21.6	7.316	0.7918	0.2162	0.4181
15	0.59	0.06661	0.107	10.2	2.507	1.6370	0.6620	0.6540
18	0.655	0.06488	0.099	12.2	3.475	1.3890	0.9421	0.6938
14	0.730	0.06624	0.052	17.8	7.703	0.9749	0.2046	0.6804
4	0.785	0.06921	0.102	20.8	5.357	0.8063	0.1362	0.3390
GaAs	1.000	0.07962	0.076	19.4	6.6646	0.8845	0.1472	0.5169

Table (4,7) Computed values from plasma minimum for $Ga_xIn_{(1-x)}As$ alloys

InAs (11.7) and that of GaAs (11.1) within the limits of experimental error. For sufficiently degenerate samples $E_F >> KT$ the susceptibility effective mass, the Fermi energy and the effective mass at the bottom of the band m_0^*/m were calculated as described in section 4.7a. For these samples the effect of lattice dispersion was estimated to be negligible with in the limits of experimental error and hence it was neglected in the analysis. For low doped samples the more general analysis developed in section 4.7b was used to calculate m_0^*/m and E_F. In order to calculate S_{LV} from equation [4:42] the values of ν_l and ν_t were taken from published data (68B1) shown in Fig. (4:12). E_0^* values were obtained from the room temperature E_0 values determined by the author (section 3.6a) and the absolute zero energy gap values reported by Coderre (69C2). The graphical solution to obtain m_0^*/m for two typical samples is shown in Fig. (4:13). All the relevant data for the samples are recorded in Table (4,5). The calculated values of m_0^*/m and E_F are given in Table (4,6). The values of m_0^*/m are plotted as a function of x in Fig. (4:14). Values obtained from magneto-thermoelectric power measurements (69T1) are also shown in the same figure. There is very good agreement between different methods. Values for InAs and GaAs compare very well with the values quoted in the literature (62D1). The values for two compositions obtained by Hockings et al (66H1) also show reasonable agreement with the present curve.

However, their results could be less accurate due to the fact that they have taken samples with x different as much as ± 0.04 to be of one composition, inorder to extrapolate the effective mass at the bottom of the band. Due to the same reasons pointed out for InSb - GaSb alloys, Woolley and Thompson (64W2) calculated values of m_0^* show considerable disagreement.

Table (4,7) gives the calculated values of τ, ω_p, μ_{opt} and σ from the plasma minimum and the values are in the right order of magnitude. Since it was necessary to have values of m^* for calculating the optical mobilities of nondegenerate samples, it was assumed that the m^* values given by equation[4:11] can be used for the purpose.

c) $\underline{\text{InAs}_x\text{Sb}_{(1-x)}\text{ alloys}}$

Samples were taken from ingots T.F.C-6' and T.F.C-7. The carrier concentrations were in the range 3×10^{24} to $8 \times 10^{24} m^{-3}$. Measurements were made on 12 samples in the composition ranges $0 < x < 0.42$ and $0.7 < x < 1.0$. Plasma reflection curves and the corresponding ε vs λ^2 graph for a few typical samples are shown in Fig. (4:15) and Fig. (4:16) respectively. The method of analysis of the data was the same as that used for $Ga_xIn_{(1-x)}Sb$ alloys. Fig. (4:17) shows the variation of ε_∞ with the molecular composition x and again the variation is linear within the limits of experimental error. E_0^* values have been taken from reference 68V1. Table (4,8) gives the relevant data for all the samples. The calculated values of effective mass and Fermi level are recorded in Table (4,9). The variation of m_0^*/m as a function of x is plotted in Fig. (4:18). The values obtained from free carrier Faraday rotation and magneto-thermoelectric power measurements (68V1) are also shown in the same figure. It is seen that the agreement is good. The m_0^*/m values reported by Potter and Kretschmar (64P2) are much lower than the present values. The reasons for this are not clear. However the present values are very consistent with other measurements. Possibly their values are in error due to the various approximations used. Again there is considerable disagreement with the calculated values of Woolley and Thompson (64W2), andthis may be explained as due to the same reasons pointed out in the other alloy systems.

The calculated values of τ, ω_p, μ_{opt} and σ are recorded in Table (4,10).

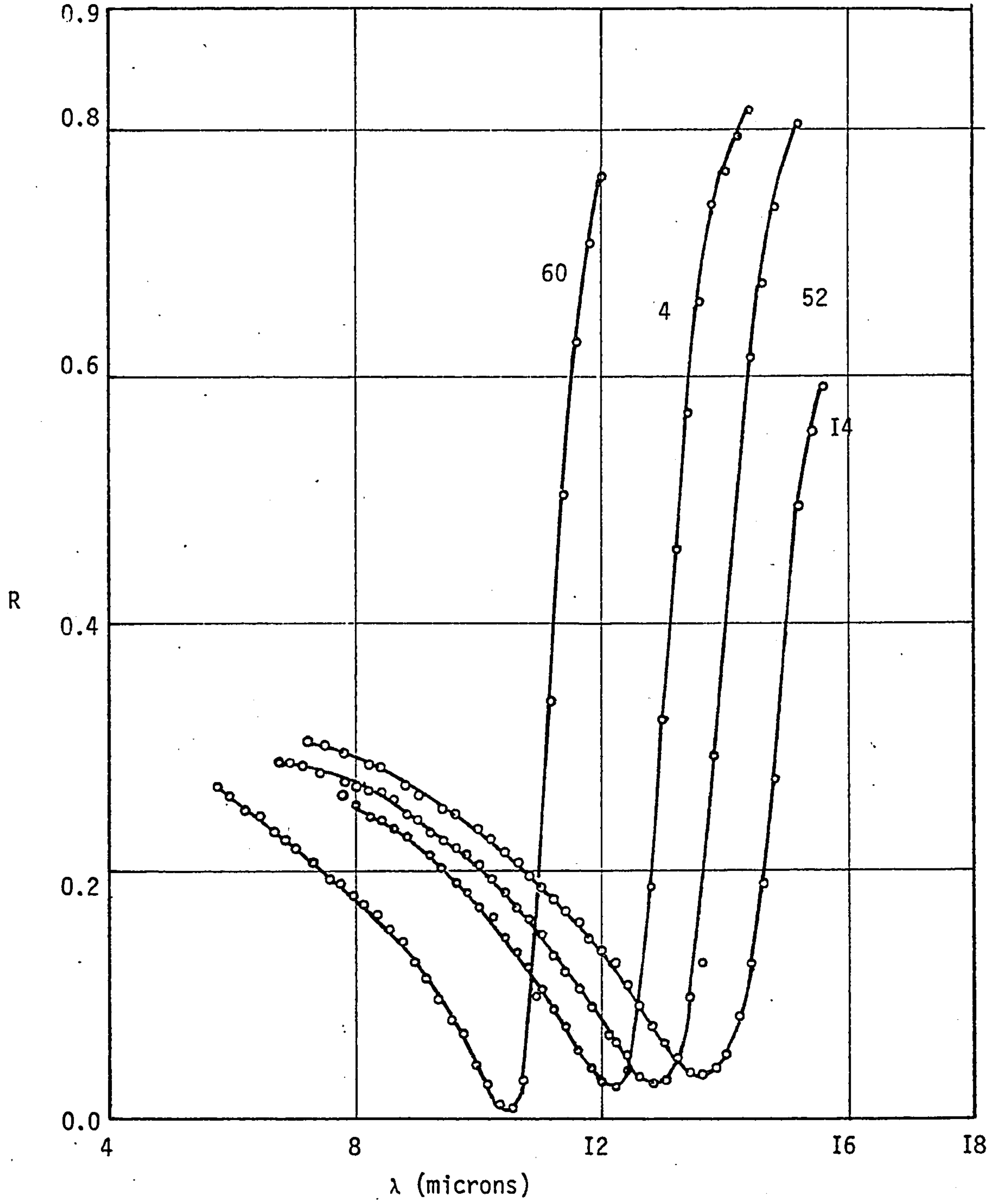

Fig.(4:I5) Plasma reflection curves for $InAs_xSb_{(I-x)}$ alloys

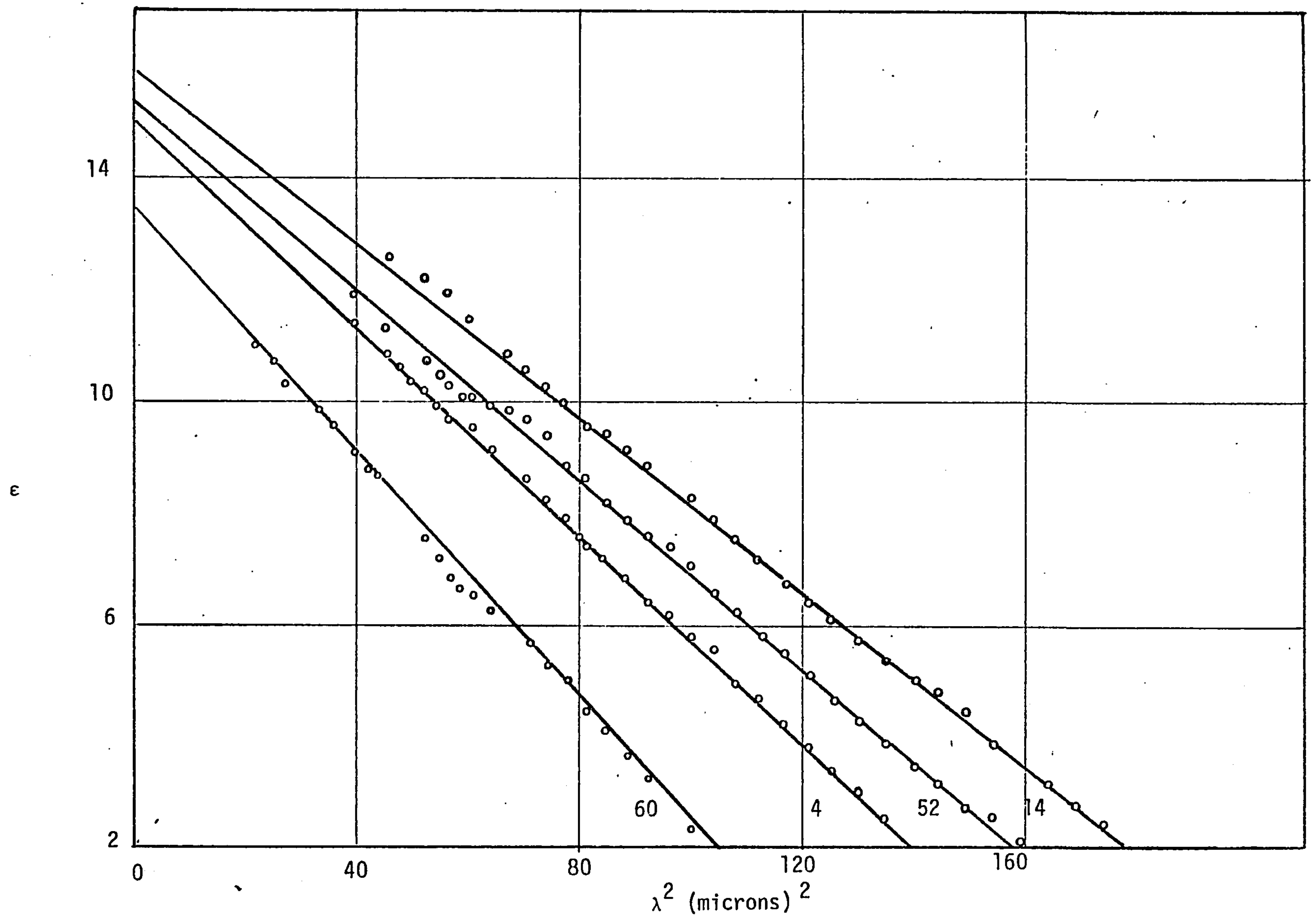

Fig. (4:16) Typical graphs of ε vs λ^2 for $InAs_xSb_{(1-x)}$ alloys

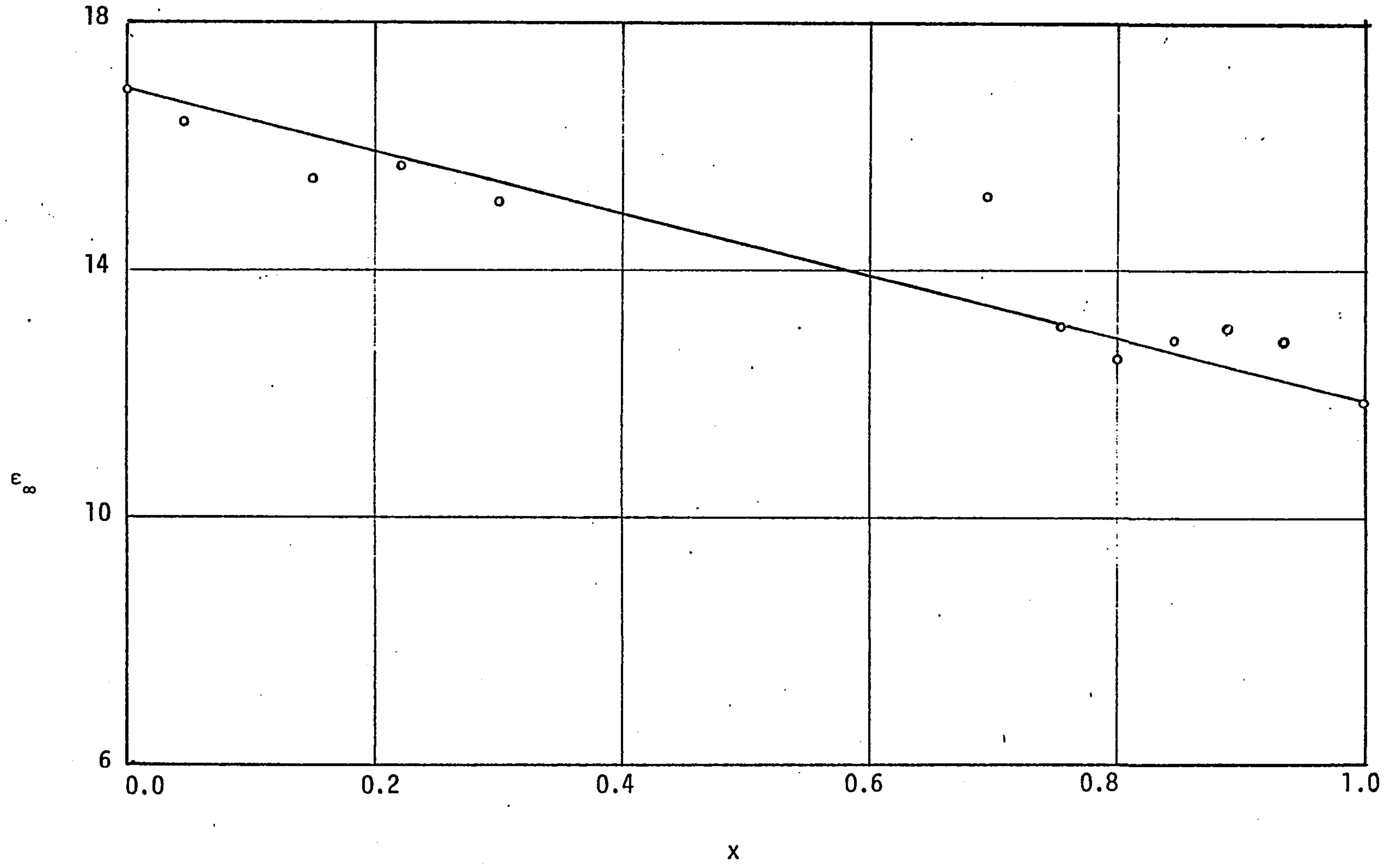

Fig. (4:17) Variation of ε_∞ with composition for $InAs_xSb_{(1-x)}$ alloys

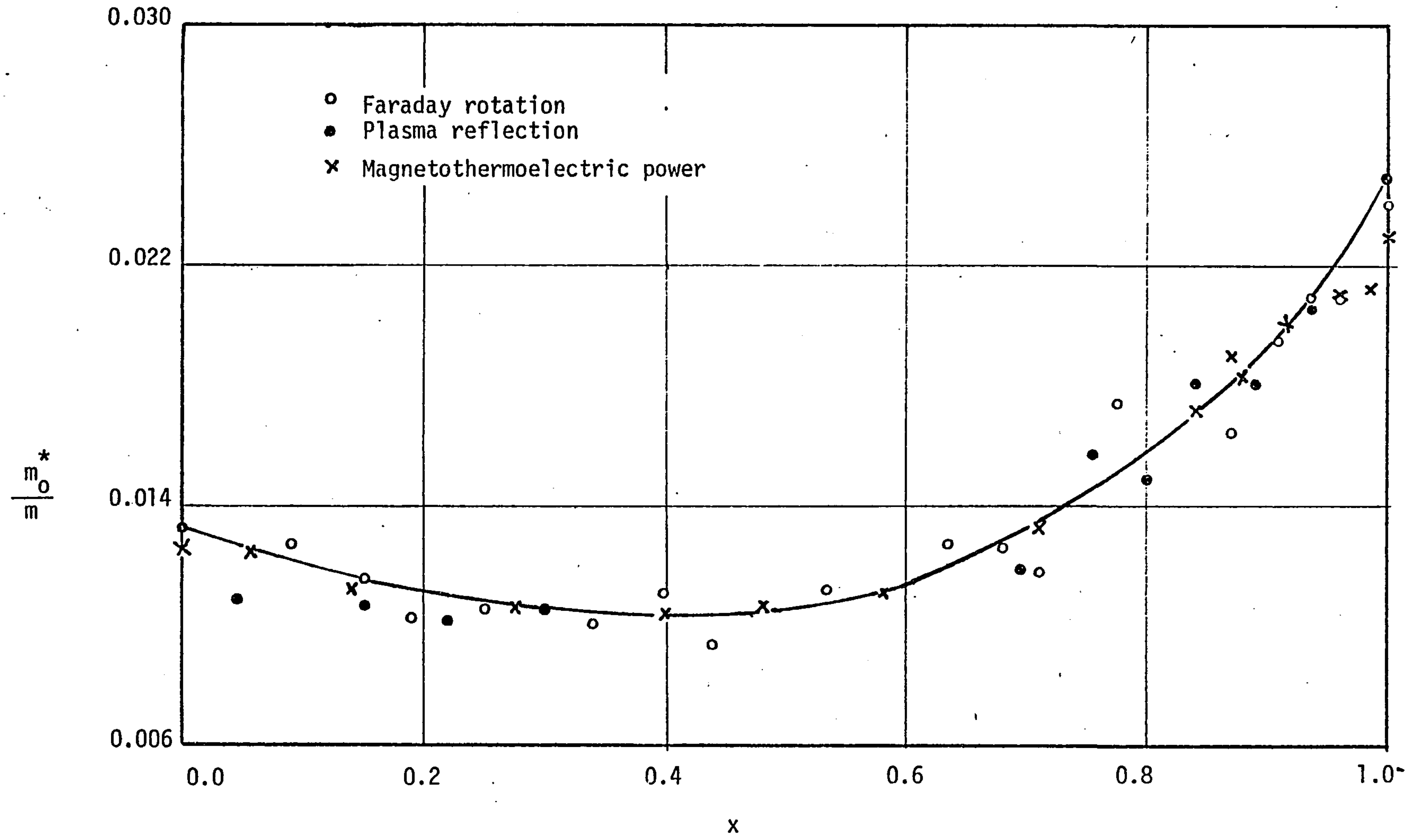

Fig. (4:18) Variation of m_o^*/m with composition for $InAs_xSb_{(1-x)}$ alloys

Ingot	Code No of Specimen	Distance along the ingot (cms)	x	Thickness (mm)	n $(\times 10^{24}/m^3)$	slope $(\times 10^{-2}/m^2)$
-	InSb	-	0.000	0.389	6.278	10.120
T.F.C-6'	14	3.75	0.045	0.686	3.977	7.882
T.F.C-6'	13	3.05	0.15	0.698	4.229	7.750
T.F.C-7	52	3.05	0.22	0.397	4.981	8.556
T.F.C-6'	4	2.5	0.30	0.597	6.019	9.348
T.F.C-7	48	2.65	0.695	0.596	7.165	11.290
T.F.C-6'	11	2.25	0.755	0.665	7.922	11.240
T.F.C-6'	10	2.15	0.80	0.570	8.423	12.650
T.F.C-7	60	2.1	0.84	0.539	7.515	10.980
T.F.C-7	40	1.60	0.89	0.415	5.322	9.085
T.F.C-6'	15	0.75	0.935	0.515	3.612	6.736
-	InAs	-	1.000	-	12.030	15.455

Table (4,8) Experimental data for $InAs_xSb_{(1-x)}$alloys

Code No of Specimen	x	ε_∞	E_0^* (ev)	$\frac{m^*}{m}$	$\frac{m_0^*}{m}$	E_F (ev)
InSb	0.000	16.9	0.205	0.05564	0.0133	0.3567
14	0.045	16.4	0.191	0.04526	0.0109	0.3236
13	0.15	15.5	0.164	0.04894	0.0107	0.3169
52	0.22	15.7	0.151	0.05222	0.0102	0.3375
4	0.30	15.1	0.141	0.05775	0.0105	0.3485
48	0.695	15.2	0.188	0.05693	0.0119	0.3895
11	0.755	13.1	0.218	0.06321	0.0158	0.3627
10	0.80	12.6	0.243	0.05973	0.01500	0.3997
60	0.84	12.9	0.265	0.06141	0.0182	0.3484
40	0.89	13.1	0.302	0.05254	0.0181	0.3132
15	0.935	12.9	0.343	0.0481	0.0260	0.249
InAs	1.000	11.9	0.397	0.06982	0.0250	0.4007

Table (4,9) computed values for $InAs_xSb_{(1-x)}$alloys

Code NO of Specimen	x	R_{min}	λ_{min} (microns)	τ ($x10^{-13}$sec)	ω_p ($x10^{14}$/sec)	μ_{opt} (m^2/Volt.sec)	σ ($x10^5 \Omega^{-1} \cdot m^{-1}$)
InSb	0.000	0.095	11.6	0.5195	1.5157	0.1642	1.7850
14	0.045	0.037	13.6	1.2180	1.3244	0.4734	3.1016
13	0.15	0.040	13.4	1.0716	1.3388	0.3851	2.6346
52	0.22	0.028	12.9	1.3225	1.3984	0.4455	3.5935
4	0.30	0.025	12.2	1.2881	1.4778	0.3924	3.7594
48	0.695	0.019	11.0	1.3810	1.6434	0.4267	5.0173
11	0.755	0.022	10.9	1.0689	1.6448	0.2975	3.3526
10	0.80	0.010	10.33	1.5274	1.7418	0.4498	5.1675
60	0.84	0.010	10.6	1.6075	1.6993	0.4605	5.2998
40	0.89	0.009	11.4	1.8617	1.5819	0.6233	5.4010
15	0.935	0.014	13.2	1.6594	1.3622	0.6069	3.5153
InAs	1.000	0.029	8.3	0.6175	2.1407	0.1558	2.9802

Table (4,10) computed values from plasma minimum for $InAs_xSb_{(1-x)}$alloys

4.9 Estimation of error in the effective mass values

There are two sources of errors to be considered. The first one is the error due to the various approximations made in the calculation and this is very difficult to estimate. It was assumed that Kane model, which neglects the Γ_{1c} ,Γ_{15c} interaction, can be used to represent the conduction band. The neglect of this interaction, according to Cardona (63C1), can lead to about 4% error in the bottom of the band effective mass values. Another error is due to the uncertanity in the value of E_0^*. In order to estimate the effect of E_0^* on the values of m_0^*/m, some test calculations can be made. InSb was chosen for this calculation, since this material has the smallest band gap and hence the effect on m_0^*/m due to the change in E_0^* should be the largest among all the alloys considered here. When 0.205 ev (the mean of room temperature and absolute zero values of the energy gap) was taken to be E_0^*, a value of 0.0133 was obtained for m_0^*/m. When the room temperature energy gap (0.18 ev) was taken to be E_0^*, the value of effective mass obtained was 0.0118. If a rough estimation is made based on this calculation, it may be easily seen that a 50% error in the choice of E_0^* can not make more than 5% error in the effective mass value.

The second source of error to be considered is the experimental error. Relative errors in the effective mass values may be estimated considering the error involved in the various measurements. The error in the measurement of carrier concentration may be estimated as follows. The measured quantities involved are Hall voltage V, magnetic field B, current I and thickness of the specimen t. The measurement accuracy involved in each of these quantities were approximately $\Delta V = \pm\ 0.1\%$, $\Delta B = \pm\ 0.1\%$, $\Delta I = \pm\ 0.1\%$ and $\Delta t = \pm\ 1\ \%$. Hence the total measurement accuracy in n is $\Delta n = \pm\ 1.3\%$. The relative error in the reflectivity measurements may be estimated from ε vs λ^2 graphs. Most of the experimental points for a sample were falling on a line. A typical sample T.F.A- 49 was chosen for the calculation of the error in the slope. Two lines were drawn ;the first one the best fit to the points and the second one a line as different as possible, but, still a satisfactory fit to the points. The slopes obtained were 5.31 and 5.57 m^{-2} respectively. Hence $\Delta S = \pm\ 0.26$. The values of n and E_0^* for this sample were $2.21 \times 10^{24}\ m^{-3}$ and 0.43 ev respectively. The following combinations of ΔS and Δn were taken. S, n ; $S + \Delta S, n + \Delta n$; $S + \Delta S$, $n - \Delta n$; $S - \Delta S$, $n + \Delta n$; $S - \Delta S$, $n - \Delta n$. The corresponding effective mass values obtained were 0.0261, 0.0260, 0.0252, 0.0270 and 0.0261. Hence the possible error in the effective mass value is given by m_0^*/m 0.0261 ± 0.0009. Thus it may be seen that approximately ± 4% experimental error may be expected in the effective mass values. It may be seen that the scatter of experimental points about the continous curve is within these limits.

CHAPTER V

SUMMARY AND CONCLUSIONS

5.1 Summary of Results

Preparation of alloys was part of all the projects undertaken. Homogeneous polycrystalline samples of the alloy systems $Ga_xIn_{(1-x)}Sb$ and $Ga_xIn_{(1-x)}As$ have been prepared over the complete composition range. Good materials of the alloy system $InAs_xSb_{(1-x)}$ have been produced, except the region $0.3 < x < 0.7$. $GaAs_xSb_{(1-x)}$ alloy system was found to be very difficult to prepare. However good alloy samples in the regions $0 < x < 0.34$ and $0.85 < x < 1.0$ have been successfully obtained.

From transmission measurements the room temperature optical energy gap variation in $Ga_xIn_{(1-x)}As$ alloys has been accurately determined. The optical energy gap variation for $GaAs_xSb_{(1-x)}$ alloys has been determined for the first time. For both the alloy systems the energy gap variation has been found to be concave and parabolic. The deviation of the energy gap variation from linearity is represented by the parameter C. The bowing parameter C is the sum of two parts, C_i due to the intrinsic or virtual crystal effect and C_e due to the extrinsic or the disorder effect. It has been found that the value of C for $Ga_xIn_{(1-x)}As$ alloys is 0.54 and that for $GaAs_xSb_{(1-x)}$ alloys is 1.16. These values compare with the values 0.56 and 1 respectively, calculated theoretically by Van Vechten and Bergstresser (69V3, 69V4). The energy gap variation of $GaAs_xSb_{(1-x)}$ alloys shows considerable deviation from linearity. It undergoes a minimum at $x = 0.2$ and the value at the minimum is 0.685 ev which is lower than the values for either compound. This type of variation is very similar to the energy gap variation in $InAs_xSb_{(1-x)}$ alloys.

Plasma reflection measurements were made on the alloy systems $Ga_xIn_{(1-x)}Sb$, $Ga_xIn_{(1-x)}As$ and $InAs_xSb_{(1-x)}$. All the reflection curves showed very sharp plasma minimum. The contribution of lattice reflection was considered. In all cases of degeneracy, it has been shown that a plot of ε vs λ^2, for wavelengths lower than the plasma minimum, would give a straight line and the intercept on the ε axis would give the value of ε_∞. For all the alloy systems the values of ε_∞ have been found to vary linearly between the values of the two compounds, with in the limits of experimental error. The effective mass values at the bottom of the (000) conduction band have been calculated from plasma reflection and Hall effect data. For sufficiently degenerate samples ($E_F >> KT$) the effective mass values at the Fermi level have been obtained. Then using the Kane model the bottom of the band effective mass values have been obtained. When the condition of full degeneracy is not satisfied no effective mass has been defined. The free carrier contribution to the dielectric constant in this case has been calculated in terms of the electron distribution in k-space. Assuming a Kane model for the conduction band the bottom of the band effective mass values have been calculated. It has been found that the variation of m_0^*/m with composition has a concave deviation from linearity for all the alloy systems. The virtual crystal and disorder effects of the alloy tend to predict this type of behaviour. The variation of m_0^*/m with composition for any of the alloy systems did not agree with the calculated values of Thompson and Woolley (64W2). This is mainly due to the choice of a constant value of $P^2 = 23$ ev for all the alloy systems, in the calculation. The present results for all the three alloy systems are in very good agreement with the experimental results of Faraday rotation and magnetothermoelectric power measurements.

Relaxation time, mobility and conductivity for all the samples have been calculated from the plasma minimum by the method suggested by Moss (68M1). The results are qualitatively good, but no attempt has been made to make any quatitative comparison with theory.

5.2 Suggestions for future work

In $As_xSb_{(1-x)}$ and $GaAs_xSb_{(1-x)}$ alloys in the middle region of composition could be prepared using a narrow Travelling Zone furnace. Attempts along this line are already underway in this laboratory. It is also worth trying some new method such as the solute build up method.

For $Ga_xIn_{(1-x)}Sb$ alloys no measurements were made in the range $0.85 < x < 1.0$, since the effect of electrons in the <111> minima makes interpretation of data very difficult. However, if measurements of Plasma reflection, Faraday rotation and Hall effect were made on the same specimen a combined analysis of the data using two band model can be made and accurate values of effective mass at the bottom of the (000) and <111> bands can be obtained. Thus a systematic investigation of the region $0.85 < x < 1.0$ can be made. It is also of interest to make plasma reflection measurements on all the alloy systems at low temperature and investigate the change in effective mass with temperature.

REFERENCES

F1 Faraday M., Expt. Res. in Elec. Series 4, 433 (1833)

B1 Braun F., Ann. Phys. Chem., 153, 566 (1874)

S1 Smith W., J. Soc. Tel. Engr., 2, 31 (1873)

H1 Hall E.H., Am. J. Math., 2, 287 (1879)

B2 Bardeen J., Brattain W.H., Phys. Rev., 75, 1208 (1949)

28B1 Bloch F., Zeit. Phys., 52, 555 (1928)

31K1 Kronig R., DEL. And Penny W. G., Proc. Roy. Soc., A 103, 499, (1931)

28S1 Sommerfeld A., Zeit. Phys., 47, 1 (1928)

31N1 Nordheim L., Ann. Physik (Leipzig), 9, 607, (1931)

33W1 Wigner E. and Seitz F., Phys. Rev., 43. 804 (1933)

35K1 Kramers H.A., Physica, 2, 483 (1935)

36M1 Mott N. and Jones H., "The Theory of the Properties of Metals and Alloys", Oxford (1936)

38M1 Muto T. Sci. Pap. Inst. Phys. Chem. Res. (Tokyo), 34, 377 (1938)

39S1 Stohr H., and Klemm W., Anorg Z., Allgem. Chem., 241, 305 (1939)

40H1 Herring C., Phys. Rev., 57, 1169 (1940)

50C1 Conwell E.M., Weisskopf V.F., Phys. Rev., 77, 388 (1950)

50E1 Erginsoy C., Phys. Rev., 79, 1013 (1950)

52D1 Dexter D.L., Seitz F., Phys. Rev., 86, 964 (1952)

52H1 Herman F., Phys. Rev., 88, 1210 (1952)

52H2 Hume-Rothey W., Christian J.W., Pearson W.B., "Metallurgical Equilibrium Diagrams"., Institute of Physics, London (1952)

52W1 Welker H.Z., Naturforsch., 7a, 744 (1952)

53H1 Howarth D.J., Sondheimer E.H., Proc. Phys. Sos., Ser. A 219, 53 (1953)

53P1 Pfann W.G. and Olson R.M. Phys. Rev., 89, 323 (1953)

53S1 Shih C. and Peretti E.A., J. Am. Chem. Soc., 75, 608 (1953)

53T1 Tanenbaum M. and Briggs H.B. Phys. Rev., 91, 1561 (1953)

54B1 Bonn M. and Huang K., "Dynamical theory of crystal lattices", Oxford University Press, London, P82 (1954)

54B2 Breckenridge R.G., Blunt R.F., Hosler W.R., Frederickse H.P.R., Becker J.H., Oshinsky W. Phys. Rev., 96, 571 (1954)

54B3 Burstein E., Phys. Rev., 93, 632 (1954)

54D1 Bebye P.P., Conwell E.M., Phys. Rev. 93, 693 (1954)

54H1 Herman F., Phys. Rev., 95, 847 (1954)

54H2 Herman F., Physica, 20, 801, (1954)

54H3 Hrostowski H.J. and Tanenbaum M., Physica 20, 1065 (1954)

54H4 Hrostowski H.J., Wheatley G.H., Flood W.F., Phys. Rev., 95, 1683 (1954)

54O1 Oswald F. and Schede R.Z., Naturforsch 9a, 611 (1954)

54S1 Slater J.C. and Koster G.F., Phys. Rev., 94, 1498 (1954)

54W1 Willardson R.K., Harman T.C. and Beer A.C. Phys. Rev., 96, 1512, (1954)

55B1 Brooks H., Advances in Electronics and Electron Phys. 7, 144, (1955)

55B2 Brooks H., Advances in Electronics Electron Phys., 8, 85 (1955)

55D1 Dresselhaus G., Phys. Rev., 100, 580 (1955)

55D2 Dresselhaus G., A.F.K.P., C. Kittel Phys. Rev., 98, 368 (1955)

55F1 Folberth O.G., Naturforsch Z., 10a, 502 (1955)

55G1 Goryunova N.A. and Fedorova N.A., Zhur. Tekh. Fiz., 25, 1339 (1955)

55H1 Herman F., Proc. Inst. Radio Engrs., 43, 1703 (1955)

55H2 Herring C., Bell System Tech. J., 34, 237 (1955)

55K1 Kaiser W., Fan H.Y., Phys. Rev., 98, 966 (1955)

55P1 Paramenter R.H., Phys. Rev., 97, 587 (1955)

55S1 Stern F., Talley, R.M., Phys. Rev. 100, 1638 (1955)

56B1 Barrie R., Proc. Phys. Soc. B69, 553 (1956)

56B2 Brooks A. Advances in Electronics Vol. 7, Academic Press, New York (1956)

56F1 Fan H.Y. Rept. Progr. Phys., 19, 207 (1956)

56F2 Furth H.P. and Wanick R.W., Phys. Rev., 104, 343, (1956)

56H1 Harrison W.A., Phys. Rev., 101, 903 (1956)

56P1 Parmenter R.H. Phys. Rev., 104, 22 (1956)

56P2 Pergola G.C.D. and Sette P. Phys. Rev., 104, 598 (1956)

56S1 Sclar N., Phys. Rev., 104, 1559 (1956)

56W1 Weiss H., Naturforsch Z. 11a, 131 (1956)

56W2 Welker H. And Weiss H., Solid State Phys., 3, 1 (1956)

56W3 Woolley J.C., Smith B.A., Lees D.G. Proc. Phys. Soc., 69B, 1339 (1956)

57B1 Blatt F.J., Solid State Phys. 4, 199 (1957)

57E1 Ehranreich H.J., Phys. Chem. Solids 2, 131 (1957)

57K1 Kane E.O.J. Phys. Chem. Solids, 1, 249 (1957)

57M1 Macfarlane G.G., McLean T.P., Ourrington J.E. and Roberts V. Phys. Rev. 108, 1377 (1957)

57W1 Woolley J.C., Swith B.A., Proc. Phys. Soc. 70B, 153 (1957)

57S1 Spitzer W.G. and Fan H.Y., Phys. Rev., 106, 882 (1957)

58M1 Macfarlane G.G., McLean T.P., Qurrington J.E. and Roberts V. Phys. Rev. 111, 1245 (1958)

58N1 Newman R., Phys. Rev., 111, 1518 (1958)

58P1 Phillips J.C., Phys. Rev., 112, 685 (1958)

58R1 Ramdas A.L., Fan H.Y., Bull. Am. Phys. Soc., 3, 121 (1958)

58S1 Stephen M.J. and Lidiard A.B., J. Phys. Chem. Solids, 9, 43 (1958)

58W1 Woolley J.C., Smith B.A., Proc. Phys. Soc., 72, 214 (1958)

58W2 Woolley J.C., Smith B.A., Proc. Phys. Soc., 72, 867 (1958)

59A1 Abrahams M.S., Braunstein R., and Rossi F.D., J. Phys. Chem. Solids. 10, 204 (1959)

59E1 Ehrenreich H., J. Phys. Chem. Solids., 8, 130 (1959)

59I1 Ivarov-Omskii V.1. and kolomiets B.T., Doklady Akad. Nauk S.S.S.R., 127, 135 (1959)

59M1 Moss T.S., Optical Properties of semiconductors, London, Butterworth Publications, p. 29 (1959)

59O1 Oswald F., Naturforsch Z., 14a, 374 (1959)

59S1 Smith R.A., Semiconductors, Cambridge University Press, p. 79 (1959)

59S2 Spitzer W.G. and Whelan J.M. Phys. Rev., 114, 59 (1959)

59S3 Stern F., Dixon J.R., J. Appl. Phys. 30, 268 (1959)

59T1 Takimoto N., J. Phys. Soc., Japan 14, 1142 (1959)

59W1 Walton A.K. and Moss T.S., J. Appl. Phys., 30, 951 (1959)

59W2 Woolley J.C., Evans S.A. and Gillet C.M. Proc. Phys. Soc., 76, 244 (1959)

59W3 Woolley J.C., Lees D.G., J. Less, Common Metals, 1, 122 (1959)

60A1 Abrahams M.S., Braunstein R., Rossi F.D., Properties of Elemental and Compound Semiconductors. Interscience Publishers New York, p. 275, Vol. 5 (1960)

60C1 Cardona, M., International Conference on Semiconductor Physics, Prague, P. 388, (1960)

60C2 Cardona M., Paul W. and Brooks H., Helv. Phys. Acta, 33, 329 (1960)

60J1 Jones H., "The Theory of Brillouin Zones and Electronic States in Crystals". North Holland (1960)

60K1 Kopec Z., Acta Phys. Polon., 19, 295, (1960)

60P1 Parmenter R.H., Progress in Semiconductors, Vol. 2,p. 3 (1960)

60S1 Stern F., Proc. Iner. Conf. Semiconductor Phys. Prague, p. 363 (1960)

60V1 Visvanathan S., Phys. Rev., 120, 376 (1960)

60W1 Woolley J.C., International Conference on Semiconductors' Prague p. 966 (1960)

60W2 Woolley J.C., Gillet C.M., J. Phys. Chem. Solids, 17, 34 (1960)

60W3 Woolley J.C., Gillet C.M., and Evans J.A., J. Phys. CHem. Solids, 16, 138, (1960)

60Z1 Ziman J.M., Electrons & Phonons, Oxford University Press, P. 514 (1960)

61B1 Becker W.M., Ramdas A.K., and Fan H.Y., J. Appl. Phys. Suppl. 32, 2094 (1961)

61C1 Cardona M., Phys. Rev., 121, 752, (1961)

61C2 Cardona M., Proceedings of the International Conference on Semiconductors, Prague, P. 388 (1961)

61C3 Cardona M., J. Phys. Chem. Solids, 17, 336 (1961)

61E1 Ehrenreich H., J. Appl. Phys.,32, 2155 (1961)

61G1 Gashimzade F.M., and Kesamanlay F.P., Soviet Phys.,Solid state, 3, 910 (1961)

61K1 Kolodziejezak, Acta. Phys. Polon, 20, 289 (1961)

61P1 Paul W., J. Appl. Phys. Suppl.,32, 2082 (1961)

61S1 Smith R.A., Semiconductors' Oxford University Press, P. 110 (1961)

61S2 Stambaugh E.P., Miller J.F. and Himes R.C., "Growth of Refractory III - V Compounds and Alloys from Solutions" in "Metallurgy of Elemental Compounds Semiconductors" Grubel R.O., editor. Interscience, New York, (1961)

61W1 Woolley J.C., and Evans J.A., Proc. Phys. Soc., 78, 35 (1961)

61W2 Woolley J.C., Gillet C.M., Evans J.A.,Proc. Phys. Soc.,77, 700 (1961)

62D1 Long D., J. Appl. Phys., 32, 2155 (1961)

62H1 Holonyak N. Jr., and Bevacqua S.F., Appl. Phys., Letters 1, 82 (1962)

62K1 Kolodziejezak J. and Kowalezyk R., Acta Phys. Polon, 21, 399 (1962)

62K2 Kolodziejezak J. and Sosnowski L., Acta Phys. Polon, 21, 399 (1962)

62S1 Smith S.D., Pidgeon C.R., Posser V., Proceedings of International Conference on Semiconductors, Exterer, p. 301 (1962)

62S2 Sturge M.D., Phys. Rev., 127, 768 (1962)

62T1 Trumbore F.A., Freeland P.E., and Mills A.D., J. Electrochem. Soc., 109, 7, 645 (1962)

62W1 Woolley J.C., Chapt. 1 "Preparation of III - V Compounds", Willardson and Goering, editors, Reinholt, (1962)

62Z1 Zawadzki W., Phys. Stat. Sol., 2, 385 (1962)

63A1 Allen J.W. and Hobdy J.W., Proc. Phys. Soc., 82, 315 (1963)

63B1 Bassani F., and Brust D., Phys. Rev., 131, 1524 (1963)

63B2 Bassani F. and Yoshimine M., Phys. Rev., 130, 20 (1963)

63B3 Beer A.C., Galvanomagnetic effects in Semiconductors, Suppl. 4, Solid State Physics, Acadamic Press, (1963)

63C1 Cardona M., Phys. Chem. Solids, 24, 1543 (1963)

63C2 Cardona M., Phys. Rev., 129, 69 (1963)

63H1 Holonyak N. Jr., Bevacqua S.F., Bielan C.V. and Lobowski S.J., Appl. Phys. Letters, 3, 47 (1963)

63K1 Ku S.M. and Black J.F., Solid State Electron, 6, 505 (1963)

63K2 Kudman I.L., Vieland, J. Phys. Chem., 3, 121 (1963)

63S1 Sirota N.N., and Makovetskaya, Report of the Acad. of Sc. of BSSR, 7, 4, 230 (1963)

64C1 Callaway J., "Energy Band Theory", N.Y. Acadamic Press (1964)

64K1 Korenblit L.L., Mashovets D.V., and Shalyt S.S., Sov. Phys. Solid State, 6, 438 (1964)

64L1 Lyden H.A., Phys. Rev., 134, 1106 (1964)

64M1 Madelung O., Physics of III - V Compounds, John Wiley & Sons, (1964)

64M2 Muller E.K., and Richards J.L., J. Appl. Phys.,35, 1233 (1964)

64P1 Piller H., Phys. of Semiconductors Proceedings, 7th International Conference, Paris, P. 297, (1964)

64P2 Potter R.F. and Kretschmar G.G., Infrared Physics,4, 57 (1964)

64P3 Potter R.F., and Stierwalt D.L., J. Appl.Phys. 35, 1233 (1964)

64S1 Spitzer W.G. and Mead C.A., Phys. Rev., 133, A872 (1964)

64W1 Woolley J.C., Blazey K.W., J. Electrochem. Soc. III, 951 (1964)

64W2 Woolley J.C. and Thompson A.G., Can. J. Phys.,42, 2030 (1964)

64W3 Woolley J.C. and Warner J., Can., J. Phys. 42, 1879 (1964)

65D1 Dismukes J., Ekstrom L., Trans. Met. Soc. AIME, 223, (1965)

65P1 Pilkuhn M., and Rupprecht H., J. Appl. Phys., 36, 684 (1965)

65R1 Riedl H.R., Dixon J.R., and Schoolar R.B., Solid State comm. 3, 323, (1965)

65S1 Straumanis M.E., and Kim C.D., J. Electrochem. Soc., 112, 1, 112 (1965)

66C1 Cardona M., Pollak F., Phys Rev.,142, 530 (1966)

66C2 Cardona M., Pollak F., Broerman J.G. Phys. Letters, 19, 236 (1966)

66C3 Cohen M.L. and Bergstresser, Phys. Rev., 141, 789 (1966)

66H1 Hockings E.F., Kudman I., Seidel T.E., Schmelz C.M., and Steigmeier E.F., J. Appl. Phys., 37. 2879 (1966)

66M1 Murray L.A., Rivera J.J., and Hoss P.A., J. Appl. Phys., 37, 4743 (1966)

66P1 Phillips J.C., The optical properties of Solids, Acadamic Press, P. 155 (1966)

66P2 Pollak F.H., Higgiwbotham C.W., Cardona M., Proceedings of International Conference on Semiconductors, Kayoto, p. 20, (1966) 66T1 Thompson A.G., Cardona M., Shaklee K.L., and Woolley J.C., Phys. Rev., 146, 601 (1966)

66T2 Thompson A.G., Ph.D. Thesies, Physics Department, University of Ottawa, (1966)

66W1 Willardson R.K., and Beer A.C., Physics of III-V Compounds Vol. I, II, III, Iv and V, (1966)

67K1 Kudman I., Seidel T.E., J. Appl. Phy., 38, 4379 (1967)

67R1 Riedl A., Dixon J.R., and Schoolar R.B., Phys. Rev., 162, 692 (1967)

67S1 Sham R.R., and Pruss T.V., Trans. Met Soc., AIME., 239, 1523 (1967)

67S2 Schumann P.A. and Phillips R.P., Solid State Electronics, 10 , 943 (1967)

67S3 Sirota N.N., and Bolvanovich E.I., Dok. Akad. Nauk, BSSR, 11, 6, 503 (1967)

67T1 Thompson A.G., Woolley J.C., Can., J. Phys., 45, 225 (1967)

67W1 Willardson R.K., Beer A.C., Semiconductors and Semimetals Vol. 3, p. 168 (1967)

68A1 Aubin M.J., and Woolley J.C., Can., J. Phys., 46, 1191 (1968)

68C1 Coderre W.M., and Woolley J.C., Can., J. Phys., 46, 1207 (1968)

68K1 Kudman I., and Ekstrom L., J. Appl. Phys., 39 , 3385 (1968)

68K2 Kwan C.C.Y., and Woolley J.C., Can., J. Phys., 46, 1669 (1968)

68L1 Liang C.Y., Piller H., and Stierwalt D.L., Appl. Phys. Letters, 12, 49 (1968)

68M1 Moss T.S., Hawkins T.D.F., and Burrell G.J., Proc. Phys. Soc., 1, 1435 (1968)

68B1 Brodsky M.A., and Lucovsky G., Phys. Rev. Letters, 21, 990 (1968)

68N1 Nesmelova I.M., Baryshev N. S. and Pyregov B.P., Sov. Phys. Semiconductors, 2 , 413 (1968)

68P1 Phillips J.C. 1 Phys. Rev. Letters, 20, 550 (1968)

68V1 Van Tongerloo E.H. and Woolley J.C., Can., J. Phys., 46, 1199 (1968)

68W1 Walton A.K. and Mishra V.K., Proc. Phys. Soc., 1, 533 (1968)

68W2 Williams E.W. and Rehn V., Phys. Rev., 172, 798 (1968)

68W3 Woolley J.C., Thomas M.B., Thompson A.G., Can., J. Phys., 46, 157 (1968)

69A1 Aubin M.J., Thomas M.B., Van Tongerloo E.H., and Woolley J.C., Can. J. Phys. 47, 631 (1969)

69C1 Claugh R.B., and Tietjen J.J., Trans. Met. Soc. AIME, 245, 583 (1969)

69C2 Coderre W.M., Ph. D. Thesies, Physics Department, University of Ottawa (1969)

69C3 Coderre W.M., and Woolley J.C., Can. J. Phys., To be published (1969)

69P1 Phillips T.C. and Van Vechten J.A., Phys. Rev. Letters, 22, 705 (1969)

69T1 Thomas M.B., Demars D. and Woolley J.C., Bull. of Can. Assoc. Phys. Vol. 25, No. 4 (1969)

69V1 Van Tongerloo E.H., and Woolley J.C., Can. J. Phys., 47, 241 (1969)

69V2 Van Vechten J.A., and Bergstresser T.K., To be published (1969)

69V3 Van Vechten J.A. and Bergstresser T.K., Phys. Rev., To be published (1969)

69V4 Van Vechten J.A. and Bergstresser T.K., (Private Communication) (1969)

69V5 Vishmubhatla S.S., Eyglument B., and Woolley J.C., Can. J. Phys., 47, 1661 (1969)

APPENDIX 1

```
C     PROGRAM TO CALCULATE THE EFFECTIVE MASS OF THE BOTTOM OF THE (000)
C     BAND FROM INFRARED REFLECTIVITY AND HALL EFFECT MEASUREMENTS
C     WITH OUT ANY ASSUMPTION REGARDING DEGENERACY
C     THE SLOPE INTEGRAL AND THE CARRIER CONCENTRATION INTEGRAL
C     ARE CALCULATED AS A FUNCTION OF THE FERMI LEVEL
C     ALL UNITS ARE M.K.S.
      DIMENSION CO(80),EF(80),EFMO(80),CONC(80),FEMO(80),EGS(80),
     1XFMO(80),SLOPE(80),AI1(80),AI2(80)
      READ(1,49) NSPEC,NMO
   49 FORMAT(2I3)
      READ(1,40)(CO(K),SLOPE(K),CONC(K),EGS(K),EF(K),K=1,NSPEC)
   40 FORMAT(5F15.6)
      READ(1,44)(EFMO(L),L=1,NMO)
   44 FORMAT(10F8.4)
      DO 125 L=1,NMO
  125 FEMO(L)=((1.0/EFMO(L))-1.00)
      AKT=0.02550
      ALPHA=3.8098E-20
      K=1
  105 DO 511 L=1,NMO
  511 XEMO(L)=EGS(K)*FEMO(L)
      L=1
      M=1
      N=1
      DELE=1.0E-03
      WRITE(3,43) EF(K),EGS(K),SLOPE(K)
   43 FORMAT(1H1,14HFERMI ENERGY =,F7.4,10X,21HADJUSTED ENERGY GAP =,F6.
     14,7HSLOPE=,E15.6/)
      WRITE(3,42)
   42 FORMAT(1H0,2X,11HCOMPOSITION,24X,15HEFFECTIVE MASS ,5X,12HCARRIER
     1CONC,5X,15HEFFECTIVE MASS //)
      WRITE(3,41)
   41 FORMAT(1H ,4X,9H(PERCENT),23X,17HAT BOTTOM OF BAND,3X,14H(PER METE
     1R**3),7X,10HCALCULATED//)
  102 EVEN1=0.000
      EVEN2=0.00
      ODD1=0.000
      ODD2=0.00
      AEE=EF(K)-5.0E-01
      IF(AEE.LT.0.0)AEE=0.0
      AEO=AEE+5.0E-04
      DO 100 I=1,500
      ENE=(AEE*(AEE+EGS(K)))
```

```
0034              ENO=(AFO*(AEO+EGS(K)))
0035              SE=(AEE-EF(K))/AKT
0036              SO=(AEO-EF(K))/AKT
0037              TE=EXP(SE)
0038              TO=EXP(SO)
0039              UE=1.00/TE
0040              UO=1.00/TO
0041              HE=2.0+TE+UE
0042              HO=2.0+TO+UO
0043              IF(M-1) 106,106,107
0044          106 RIE=(1+(FEMO(L))/((1+4*ENE/(EGS(K)**2))**0.5))
0045              RIO=(1+(FEMO(L))/((1+4*ENO/(EGS(K)**2))**0.5))
0046              F1E=((ENE**1.5)*(RIE))/HE
0047              F1O=((ENO**1.5)*(RIO))/HO
0048              EVEN1=EVEN1+F1E
0049              ODD1=ODD1+F1O
0050          107 IF(N-1) 108,108,109
0051          108 F2E=(ENE**1.5)/HE
0052              F2O=(ENO**1.5)/HO
0053              EVEN2=EVEN2+F2E
0054              ODD2=ODD2+F2O
0055          109 AEE=AEE+DELE
0056          100 AEO=AEO+DELE
0057              IF(M-2) 117,118,118
0058          117 AI1(L)=(DELE/6.0)*(4.0*EVEN1+2.0*ODD1)* (7.93871E+02)
                 1/((AKT*ALPHA**0.5)*XEMO(L)**1.5)
0059              IF(AI1(L)-SLOPE(K))110,111,111
0060          111 M=2
0061              IF(L-2) 118,116,116
0062          110 CONTINUE
0063          118 IF(N-2) 115,124,124
0064          115 AI2(L)=(DELE/6.0)*(4.0*EVEN2+2.0*ODD2) *3.3774E-02/((ALPHA**1.5)*
                 1AKT*XEMO(L)**1.5)
0065              IF(AI2(L)-CONC(K)) 500,112,112
0066          112 N=2
0067              GO TO 119
0068          500 WRITE(3,50) CO(K),EFMO(L),AI2(L),AI1(L)
0069           50 FORMAT(1X,E12.4,27X,E12.4,5X,E12.4,8X,E12.4)
0070              IF(L-NMO)120,101,101
0071          120 L=L+1
0072              GO TO 102
0073          116 SINTG=(EFMO(L)+(AI1(L)- SLOPE(K))*(EFMO(L)-EFMO(L-1))/(AI1(L-1)-
                 1AI1(L)))
```

```
0074                GO TO 118
0075            119 CNTG=(EFMO(L)+(AI2(L)-CONC(K))*(EFMO(L)-EFMO(L-1))/(AI2(L-1)-
                   1AI2(L)))
0076                GO TO 500
0077            124 IF(M-2) 500,122,122
0078            122 WRITE(3,121)SINTG,CNTG
0079            121 FORMAT(3X,44HEFFECTIVE MASS FOR EFFECTIVE MASS INTEGRAL =,E12.4,
                   110X,42HEFFECTIVE MASS FOR CARRIER CONCENTRATION =,E12.4//)
0080            101 IF(K-NSPEC)103,104,104
0081            103 K=K+1
0082                GO TO 105
0083            104 STOP
0084                END
```